# Structural Analysis of the 50S Ribosomal Stalk

**Dissertation**

zur Erlangung des Doktorgrades

der Mathematisch-Naturwissenschaftlichen Fakultäten

der Georg-August-Universität zu Göttingen

vorgelegt von

**Mihaela Ştefania Diaconu**

aus Bukarest, Rumänien

Göttingen 2006

D 7

Referent:      Prof. Dr. Ralf Ficner

Korreferent:  Prof. Dr. Oliver Einsle

Tag der mündlichen Prüfung: 05.07.2006

# **Table of contents**

# <u>Summary</u>

Protein biosynthesis represents a dynamic process that takes place on the ribosome and is driven by translation factors. Some of these factors are GTP binding proteins. They possess a limited inherent GTPase activity that is stimulated by interactions with the ribosome in a region located on the large ribosomal subunit (GTPase associated region). This site comprises several 23S rRNA elements (L10/L11 rRNA binding region and sarcin-ricin loop) and r-proteins, such as L6, L11, L14, and the L7/L12 stalk. The latter corresponds to an extended feature of the 50S ribosomal subunit, encompassing multiple copies of protein L12 that are linked to the ribosomal RNA *via* L10. Numerous lines of evidence indicated that L12 is essential for both translation factor binding and stimulation of their GTPase activities. Functionally, L12 can be divided into an N-terminal domain (NTD) responsible for dimerization and interaction with L10, a C-terminal domain (CTD) necessary for factor-related functions, and an intervening flexible hinge.

Crystallographic studies of 50S subunits and 70S ribosomes hitherto failed to disclose the structure of the L7/L12 stalk, most probably due to the high mobility of the L12 hinge region. Thus, a complex anticipated to exhibit less flexibility was designed. It encompassed L10 and the NTD of L12 from the hyperthermophilic bacterium *Thermotoga maritima*. In the three crystal structures obtained, L10 displayed a globular NTD connected by a flexible loop to a long C-terminal α-helix. The latter displayed different orientations relative to the L10 NTD in different crystal forms and harbored three consecutive binding sites for the L12 NTD dimers. Such a 1:6 (L10:L12) stoichiometry was unexpected, as a 1:4 ratio was well established in *E. coli*. The L12 NTDs formed dimers that fitted to a mode of dimerization reported for the protein in isolation, both in solution (Bocharov *et al.* 2004; Moens *et al.* 2005) and in crystalline environment (Wahl *et al.* 2000a). In the crystal structure of isolated *T. maritima* L12, the hinge region of one protomer exhibited an α-helical shape, folded onto the L12 NTDs of the dimer, while in *tma*L10:(L12 NTD)$_6$, the hinge was found replaced by the C-terminal α-helix of L10. Thus, it is likely that in complex with L10, the L12 hinges are flexible and unstructured, in agreement with several studies of this protein in solution.

In addition to obtaining the structure of *tma*L10:(L12 NTD)$_6$, attempts to solve the crystal structure of the full-length L10:L12 complex were also undertaken. While the

Summary

crystallization of the complex from the hyperthermophilic bacterium *Aquifex aeolicus* proved to be unsuccessful, the corresponding complex from *Thermotoga maritima* yielded crystals that diffracted to 3.5 Å. The structure could be solved by molecular replacement using the *tma*L10:(L12 NTD)$_6$ complex as a search model. No electron density could be detected for the L12 hinges and CTDs, consistent with a degradation of L12 during crystallization, as revealed by SDS-PAGE analysis of dissolved crystals. Comparisons of this structure to the three crystal structures obtained for *tma*L10:(L12 NTD)$_6$ revealed a fourth orientation of the L10 C-terminal α-helix-(L12 NTD)$_6$ element with respect to the L10 NTD, further supporting the notion of the presence of a flexible connection between these modules.

The *in situ* structure of an archaeal L10 NTD (a collaborative work with F. Schlünzen, J.M. Harms, Hamburg), enabled the positioning of the isolated *tma*L10:(L12 NTD)$_6$ complex on the 50S ribosomal subunit. The L10 NTD was found to constitute a separate folding unit, necessary and sufficient to anchor the *tma*L10:(L12 NTD)$_6$ complex on the L10/L11 rRNA binding region of the ribosome. The resulting model of a 50S subunit bearing a L10:(L12 NTD)$_6$ complex was confirmed by an excellent fitting into the cryo-EM envelop of an *E. coli* 70S:EF-G:GDP:fusidic acid complex (N. Fischer, H. Stark, Göttingen). Based on these data and on structures of isolated L12, it was envisioned that the stalk is organized into three structural and functional elements, that are connected by flexible regions: (i) the stalk base, formed by the L10/L11 rRNA binding region, L11 and the L10 NTD, serving as attachment site for peripheral components; (ii) the C-terminal α-helix of L10 in complex with L12 NTD dimers that constitute a movable platform carrying L12 hinges and CTDs; (iii) the highly mobile L12 CTDs attached to the mobile platform *via* the hinge regions. This arrangement was in agreement with L12 CTDs being active players in the dynamic functions of the stalk. Indeed, fast kinetic measurements using ribosomes with wild-type and mutant L12 (performed by U. Kothe, M.V. Rodnina, Witten; A.G. Tonevitski, Moscow) pinpointed L12 CTDs as initial interaction sites for translation factors, mediating their fast recruitment to the ribosome. These results also suggested that L12 CTDs activate GTP hydrolysis allosterically, a mechanism of action reminiscent of the regulators of G-protein signaling. Additionally, it can be hypothesized that L12 CTDs could either (i) remain bound to the factors' G-domains during their movement towards their ribosomal binding site or (ii) reach back to the ribosome-bound factors to stimulate their GTPase activities.

# Introduction

## I. Overview of the translation process

The fundamental principles underlying protein biosynthesis are common throughout all forms of life. They involve the translation of the genetic information contained in messenger RNA into a protein sequence by a multimegadalton ribonucleoprotein particle, the ribosome. Surprisingly, an *E. coli* cell can host up to 20,000 of such organelles that, in total, consume more than 80% of the cellular energy during protein synthesis. Consequently, such a high energy need requires a tight regulation. One level of control is exerted by translation factors, which cycle on and off the ribosome as they perform their function at defined stages of translation (Table 1). A number of factors exhibit GTP-binding properties and can thereby be considered as molecular switches.

| Translation phase | Prokaryotes | Eukaryotes |
|---|---|---|
| **Initiation** | IF1 | ~12 eIFs |
| | IF2 | |
| | IF3 | |
| **Elongation** | EF-Tu | EF1$\alpha$ |
| | EF-Ts | EF1$\beta$,$\gamma$,$\delta$ |
| | EF-G | EF2 |
| | | EF3 (fungi) |
| **Termination** | RF1 | eRF1 |
| | RF2 | - |
| | RF3 | eRF3 |
| **Ribosome recycling** | RRF | - |

**Table 1.** Prokaryotic and eukaryotic protein factors involved in different translation phases. Factor GTPases are depicted in red.

Translation follows the basic model sketched many years ago by Watson (Watson 1964) and consists of the following phases: initiation, elongation, termination and recycling.

## A. Initiation

The first phase of protein synthesis in prokaryotes, *the initiation* (Figure 1), begins with the formation of a complex between the small ribosomal subunit (30S) and the initiation factor 3 (IF3). The latter mainly acts to prevent the association of the two ribosomal subunits (30S and 50S) (Gualerzi and Pon 1990). Additionally, IF3 monitors the correct binding of the mRNA and the initiator tRNA (a tRNA carrying formylmethionine or fMet-tRNA$_f^{Met}$) to the 30S subunit (Hartz *et al.* 1989). The mRNA is anchored to the 30S subunit through a complementary base pairing between its Shine-Dalgarno sequence (ribosomal binding site) located upstream of the AUG start codon, and the 3'-terminal sequence of the 16S rRNA (anti Shine-Dalgarno sequence; ASD) (Shine and Dalgarno 1974). Consequently, the AUG start codon is positioned at the partial P site of the 30S subunit. Next, IF1 joins the complex and is believed to indirectly guide the initiator tRNA to the P site (Carter *et al.* 2001). The resulting complex formed between the mRNA, 30S subunit, IF1 and IF3, interacts with the initiator tRNA, whose anticodon is complementary to the mRNA start codon (Gualerzi and Pon 1990). Subsequently, in the absence of GTP, the GTPase protein IF2 connects to the initiator tRNA on the 30S subunit (Weiel and Hershey 1982). Upon GTP binding, IF2 triggers a rapid 50S subunit association to the initiation complex and thereby reconstitutes the 70S ribosome. The IF2 G-domain contacts a region termed the "factor binding site" of the 50S subunit (Moreno *et al.* 1999; La Teana *et al.* 2001; Allen *et al.* 2005). IF1 and IF3 display a very low affinity for the 70S particle (Maitra *et al.* 1982) and rapidly dissociate from it, inducing a conformational rearrangement of the complex (Gualerzi and Pon 1990). Subunit association entails GTP hydrolysis by IF2, followed by its detachment from the 70S ribosome (Tomsic *et al.* 2000; Boelens and Gualerzi 2002). Curiously, IF2 dissociation is not a consequence of GTP hydrolysis (Tomsic *et al.* 2000).

## B. Elongation

The resulting 70S initiation complex enters the *elongation phase* (Figure 1). Elongation represents a cyclic process, which includes: the binding and selection of the aminoacyl-tRNA to be added, the peptidyl transferase reaction and the translocation.
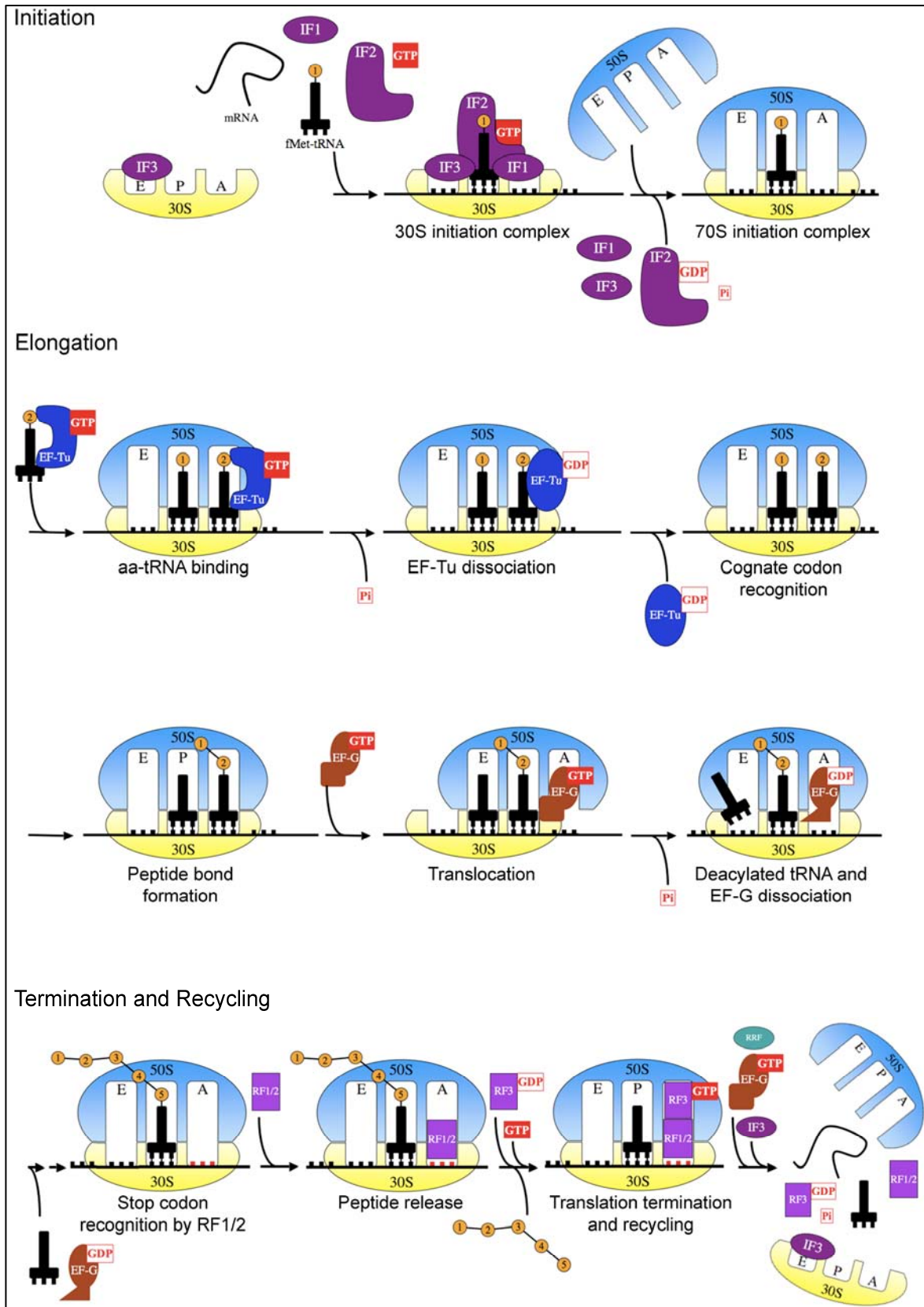
**Figure 1.** The prokaryotic translation. The genetic information encoded by the mRNA molecule is translated into a protein through a process comprising initiation, elongation of the peptide chain, termination and recycling of the translational apparatus elements (see main text for details).

Firstly, a ternary complex EF-Tu:GTP:aminoacyl-tRNA presents the second aminoacyl-tRNA (aa-tRNA), whose anticodon must form complementary base pairs with the mRNA codon, at the A site (decoding site) of the ribosome. Following the initial aa-tRNA binding, non-cognate complexes are immediately rejected, while the near-cognate (codon-anticodon complexes with one base pair mismatch) and cognate are recognized (Rodnina *et al.* 2002). Codon recognition has two important consequences: the first is the stabilization of the codon-anticodon interaction and the second, the stimulation of the GTP hydrolysis by EF-Tu. Upon the latter, EF-Tu undergoes extensive structural changes (Berchtold *et al.* 1993; Kjeldgaard *et al.* 1993; Polekhina *et al.* 1996). The resulting EF-Tu:GDP exhibits a very low affinity for the aminoacyl-tRNA and dissociates from the ribosome (Dell *et al.* 1990). The recycling of inactive EF-Tu:GDP complex to the active GTP complex is performed by EF-Ts, a guanine-nucleotide exchange factor (GEF) (Lucas-Lenard and Lipmann 1966). Interestingly, during the initial selection step, a near-cognate duplex is not rejected before GTP hydrolysis. However, it will be edited during a proofreading step, prior to the peptide bond formation (Rodnina *et al.* 2002).

Next, the peptidyl transferase reaction, characterized by the formation of a peptide bond between the peptidyl-tRNA from the P site and the aminoacyl-tRNA accommodated in the A site, occurs. The peptide chain is transferred to the A site aa-tRNA, leaving a deacylated tRNA in the P site. This reaction takes place on the 50S subunit (in the peptidyl transferase center, PTC) (Kaziro 1978) and is catalyzed by 23S rRNA elements (Noller *et al.* 1992; Nissen *et al.* 2000a). Recently, it has been hypothesized that, rather than catalyzing the reaction, rRNAs function as entropy traps, bringing reactants close enough to each other to allow the transpeptidase reaction (Sievers *et al.* 2004).

The last step of the elongation process, the translocation, results in the synchronous movement of the two tRNAs and mRNA by one codon (Wilson and Noller 1998). Precisely, the deacylated tRNA moves from the P to the E site and the peptidyl-tRNA, from the A to the P site, thus leaving the A site vacant for a new round of elongation. The process of translocation is catalyzed by the EF-G (Rodnina *et al.* 1997). Three models for the translocation mechanism have been proposed. In a first model, the translocation would occur before GTP hydrolysis (Inoue-Yokosawa *et al.* 1974), whereas a second suggests that the translocation would take place after the GTP is hydrolyzed (Rodnina *et al.* 1997). In a third model, the translocation would be initiated prior to GTP hydrolysis and completed afterwards (Zavialov *et al.* 2005). Concomitantly with the translocation process,

EF-G suffers extensive conformational changes, thereby inducing the tRNA:mRNA complex displacement. Using cryo-electron microscopy, it was established that, both EF-G binding and the subsequent GTP hydrolysis, lead to a ratchet-like movement of the 30S subunit relative to its 50S counterpart (Frank and Agrawal 2000). Upon tRNA-mRNA coordinated movement, the ribosome returns to its initial state. Finally, EF-G:GDP and E-site-deacylated tRNA dissociate from the ribosome. Interestingly, crystal structure comparisons of EF-G:GDP (Ævarsson *et al.* 1994; Czworkowski *et al.* 1994) with the EF-Tu:GTP:tRNA ternary complex (Nissen *et al.* 1995), as well as cryo-EM analysis (Stark *et al.* 1997b; Agrawal *et al.* 1998), revealed that both complexes adopt a similar shape when interacting with the ribosome, suggesting a molecular mimicry (reviewed in (Nyborg 1998; Kristensen *et al.* 2002)).

## C. Termination

The elongation cycle is repeated (with a rate of approximately 12 amino acids per second in bacteria (Gualerzi and Pon 1990)) until a *termination* codon appears in the A site (Figure 1, in red). The stop codon is then identified by a class-1 release factor (RF1 or RF2). RF1 recognizes UAA and UAG, whereas RF2 is specific for UAA and UGA (Kisselev and Buckingham 2000). Upon codon recognition, the peptide chain is hydrolyzed and released from the P site-tRNA. Cryo-electron microscopy results demonstrated that RF1/2 binds to the termination codon and, at the same time, contacts the peptidyl transferase center (Rawat *et al.* 2003; Rawat *et al.* 2006). However, it is not clear whether they are directly involved in the peptide chain release or indirectly induce this reaction by signaling the ribosome. Next, the class-2 release factor (RF3), a factor GTPase, induces the detachment of the class-1 RFs from the ribosome. Specifically, RF3 in a GDP-bound state contacts class-1 RFs, a GDP to GTP exchange occurs which subsequently triggers the RF1/2 release (Zavialov *et al.* 2001). Finally, the hydrolysis of RF3:GTP elicits its dissociation from the ribosome (Zavialov *et al.* 2001).

## D. Recycling

Following the release of the peptide chain, the ribosome, carrying the deacylated tRNA in the P site, and the mRNA are disassembled by a complex composed of the ribosome recycling factor (RRF), EF-G and GTP, through a GTP hydrolysis-dependent

process (Karimi *et al.* 1999). IF3 then binds to the 30S subunit and induces the release of the deacylated tRNA (Figure 1). The dissociated ribosomal subunits can now reenter a new round of protein synthesis.

## E. Action of antibiotics on the translation machinery

The translation machinery, especially the peptidyl transferase center and the decoding site, represent the target of numerous classes of antibiotics (briefly outlined in Table 2; reviewed in (Wilson *et al.* 2005)). Several antibiotics (e.g. thiostrepton, kirromycin) bind at defined locations on the ribosome, inhibit a specific conformation, and thereby impair further protein synthesis. An antibiotic that directly interacts with a translation factor is fusidic acid. It prevents EF-G dissociation from the ribosome upon GTP hydrolysis, thus blocking further rounds of elongation. The above mentioned properties of antibiotics were extensively exploited in cryo-electron microscopy studies (Stark *et al.* 1997b; Agrawal *et al.* 1999; Stark *et al.* 2000; Stark *et al.* 2002; Valle *et al.* 2003a). In this way, different phases of translation could be analyzed by stalling the ribosome in a specific conformation.

| Antibiotic | Effect |
|---|---|
| Tetracyclin | Inhibits aminoacyl-tRNA A-site binding |
| Streptomycin | Induces misreading |
| Kirromycin | Blocks EF-Tu after GTP hydrolysis |
| Chloramphenicol | Inhibits peptidyl transferase |
| Thiostrepton | Inhibits translocation |
| Fusidic acid | Induces arrest in the posttranslocational phase |
| Erythromycin | Inhibits peptide elongation |
| Puromycin | Inhibits peptide release |

**Table 2.** Antibiotic action on prokaryotic translation.

A number of antibiotics inhibit bacterial translation with sufficient selectivity to be suitable for antibacterial therapy. Hence, it is clear that a detailed structural knowledge of the protein synthesis mechanism represents a valuable source of information in biomedical research, providing tools for the design of new drugs aiming at impairing the proliferation of resistant pathogens.

# II. The ribosome

A further understanding of the processes underlying protein synthesis is correlated with a thorough characterization of the molecular mechanisms by which ribosomes exert their function. Remarkable contributions in deciphering the ribosome and its ligands were made in the last decade by two major advances, namely cryo-electron microscopy and X-ray crystallography.

## A. Components of the ribosome

Ribosomes were first identified by Palade as "small particulate components of the cytoplasm" (Palade 1955). Next, they were characterized as particles detected by ultracentrifugation of cell lysates and designated according to their rates of sedimentation: 70S for bacterial ribosomes and 80S for ribosomes of eukaryotic cells (Taylor *et al.* 1967). All ribosomes consist of two subunits of unequal size: the small (30S in bacteria and 40S in eukaryotes) and the large (50S and 60S, respectively) subunits. Both encompass several ribosomal RNAs (rRNAs) and numerous proteins (r-proteins), the latter being named S or L, depending on their location on the small or large subunit, respectively (Table 3).

| Prokaryotes (*E. coli*) | | | |
|---|---|---|---|
| **Characteristics** | **Ribosome** | **Small Subunit** | **Large Subunit** |
| **Size** | 70S (2.5 MDa) | 30S (0.9 MDa) | 50S (1.6 MDa) |
| **rRNAs** | | 16S rRNA (1542 Nt) | 23S rRNA (2904 Nt)<br>5S rRNA (120 Nt) |
| **Proteins** | | 21 Proteins | 36 Proteins |
| **Eukaryotes (Mammals)** | | | |
| **Characteristics** | **Ribosome** | **Small Subunit** | **Large Subunit** |
| **Size** | 80S (4.2 MDa) | 40S (1.4 MDa) | 60S (2.8 MDa) |
| **rRNAs** | | 18S rRNA (1874 Nt) | 28S rRNA (4718 Nt)<br>5.8S rRNA (160 Nt)<br>5S rRNA (120 Nt) |
| **Proteins** | | 33 Proteins | 49 Proteins |

**Table 3.** Composition of the prokaryotic and eukaryotic ribosomes.

Eukaryotic ribosomes are larger and present an increased protein content as compared to their prokaryotic counterparts. The primary sequences of both rRNA and r-

proteins of *E. coli* ribosomes were completely elucidated more than two decades ago (Brosius *et al.* 1980).

The 30S exhibits the following landmarks: the head, representing one third of volume, connected by a neck to the rest of the components, the shoulder, the platform, and the body with a spur (toe). The 50S subunit has a "crown" appearance: a hemispherical body with three protrusions, namely the L1 protuberance, the central protuberance (displaying 5S rRNA) and the L7/L12 stalk (Figure 2). The subunits are associated via multiple bridges, mostly between rRNA elements (Yusupov *et al.* 2001). Between them lies an internal cavity, containing three binding sites for tRNAs, designated the A (acceptor site of the **A**minoacylated tRNA), P (**P**eptydil-tRNA site), and E (**E**xit for deacylated tRNA) sites, respectively.
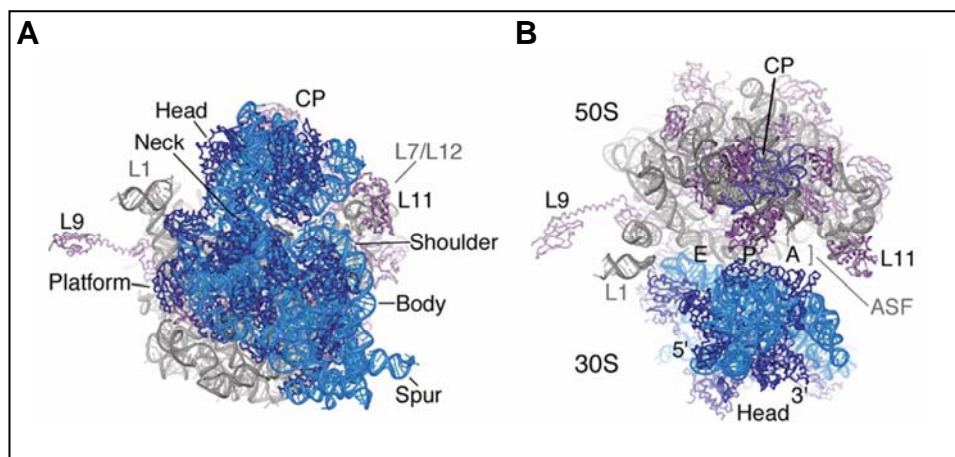


**Figure 2.** Structure of the intact *E. coli* 70S ribosome. (**A**) View from the solvent side of the 30S subunit. rRNA and proteins in the 30S subunit are colored in light blue and dark blue, respectively. 23S rRNA and proteins in the 50S subunit are in gray and magenta, respectively. 30S features include head, neck, platform, body, shoulder, and spur. 50S features encompass L1 (protein L1/rRNA arm), CP (central protuberance), ASF (A-site finger, labeled in (B)), and L11 (protein L11/rRNA arm). The approximate location of proteins L7/L12 and the tip of the ASF, not observed in the structure, are labeled in gray. (**B**) View rotated 90° on the horizontal axis compared to (A). Letters indicate the approximate location of the aminoacyl (A), peptidyl (P), and exit (E) tRNA binding sites at the subunit interface. The 5' to 3' direction of mRNA, which threads around the neck region of the 30S subunit, is also indicated (reproduced from Schuwirth *et al.*, 2005; PDB accession codes: 2AVY, 2AW4).

The bacterial rRNA, accounting for two thirds of the ribosomal mass, comprises one rRNA form (16S rRNA) in the small subunit and two types of rRNA (23S rRNA and 5S rRNA, respectively) in the large subunit (Wittmann *et al.* 1982). As the tRNA, it has been established that the rRNA forms characteristic secondary structures (organized in four domains in 16S rRNA and six domains in 23S rRNA) by complementary base pairing

(Gutell 1996), which further fold into distinct three-dimensional structures (Ban *et al.* 2000; Wimberly *et al.* 2000).

Ribosomal proteins are present in one copy each per ribosome, with the exception of L7/L12, displaying four copies in *E. coli* (Subramanian 1975). Generally, the net charge of the ribosomal proteins is basic, in order to neutralize the negative rRNA backbone (Klein *et al.* 2004). The proteins appear unevenly distributed within the ribosome: the inter-subunit sides are poor in proteins (only the S12 protein is found at the decoding center) (Brodersen *et al.* 2002), whereas at the mRNA entry site (Yusupova *et al.* 2001), the factor binding site (Ban *et al.* 1999) and the exit of the polypeptide tunnel (Klein *et al.* 2004), proteins are present in higher number and some have been identified as active players in these processes.

## B. Functional significance of the ribosomal elements

Ribonucleoprotein particles, later recognized as ribosomes, were shown to participate in protein synthesis approximately fifty years ago (Littlefield *et al.* 1955). Subsequently, the reconstitution of the small and large subunits *in vitro* using their intrinsic components, yielded functionally active ribosomes in protein synthesis (Traub and Nomura 1968; Nierhaus and Dohme 1974). Despite these discoveries, the attribution of specific functions to certain ribosomal components has been a matter of debate: at first, ribosomal proteins were seen as key players in protein synthesis, whereas rRNAs were thought to exert a scaffolding role. However, in 1992, Noller and coworkers clearly demonstrated that the rRNA from the large ribosomal subunit (stripped of almost all of its proteins) was able to catalyze peptide bonds (Noller *et al.* 1992). This discovery, produced a shift of paradigm that supported the implication of rRNAs in several ribosomal functions, including potential catalytic properties at the peptidyl transferase center ("the ribosome is a ribozyme": (Nissen *et al.* 2000a)), an interaction with mRNA during the initiation and translocation of protein synthesis, or its predominance at the decoding site (discussed by (Steitz and Moore 2003)). Notably, the corresponding rRNA elements were found highly conserved throughout kingdoms.

The current view reconciles both above mentioned notions: the rRNA is prevalently detected at active sites, but is assisted, both structurally and functionally, by r-proteins. Most probably evolved to replace an inefficient rRNA, numerous ribosomal proteins

synergically cooperate with rRNAs in order to promote the translation (Draper and Reynaldo 1999; Wilson and Nierhaus 2005). Consistently, several ribosomal proteins were found essential in some translational processes, i.e. S12 in decoding, L11 and L7/L12 in the interaction with translation factors. Thus, it can be concluded that in order to fulfill crucial functions, such as mRNA decoding, peptide bond formation, tRNA and mRNA translocation, or folding of the nascent polypeptide, a dynamic interplay occurs between the different ribosomal constituents. Moreover, in response to substrate binding (tRNAs, mRNA) and factor interaction, the ribosome changes its structure and takes an active part in all the steps of translation.

## C. Insights into the ribosome structure

By enabling the visualization of the ribosome at atomic resolution, X-ray crystallography proved to be extremely valuable for the interpretation of different steps underlying protein synthesis (discussed in (Al-Karadaghi *et al.* 2000; Nissen *et al.* 2000b; Ramakrishnan 2002; Nilsson and Nissen 2005; Ogle and Ramakrishnan 2005)). This project was promoted in 1980, with the first attempts to crystallize *Bacillus stearothermophilus* ribosomes (Yonath *et al.* 1980), and significantly improved within the last decade.

Recently, crystal structures of isolated ribosomal subunits revealed new insights into the organization of the translational machinery. Several structures of the 30S subunit from a thermophilic bacterium were determined at 5.5 Å (Clemons *et al.* 1999), 4.5 Å (Tocilj *et al.* 1999), 3.3 Å (Schluenzen *et al.* 2000) and 3.05 Å (Wimberly *et al.* 2000) resolution. In recent crystal structures of the small ribosomal subunit, all the ordered rRNAs (accounting for 99% of the 16S rRNA) were traced in the electron density, along with 20 associated proteins.

Of equal importance were the structures of the 50S subunit, obtained from a mesophilic bacterium at 3.1 Å resolution (Harms *et al.* 2001) and from an archaeon at 5 Å (Ban *et al.* 1999). A major breakthrough was the 2.4 Å resolution of the large ribosomal subunit, the first high-resolution structure of a ribosomal subunit (Ban *et al.* 2000). It comprises most of the 50S subunit, including a detailed structure of the peptidyl transferase center and several components of the translation factor binding site.

Furthermore, it strongly supports the notion that rRNA is responsible for the peptide bond formation, since the closest protein to the peptidyl transferase center is 18Å away.

In addition, high-resolution structures of ribosomal subunits in complex with numerous ligands and translation factors (Nissen *et al.* 2000a; Schmeing *et al.* 2002) or antibiotics (Brodersen *et al.* 2000; Carter *et al.* 2000; Pioletti *et al.* 2001; Schlunzen *et al.* 2001) were determined. Complexes of ribosomes with translation factors revealed some of the conformational rearrangements that the ribosome undergoes in response to their interaction. The 30S:IF1 complex revealed the location of IF1 at the A site of the 30S subunit (Carter *et al.* 2001). Studies performed by Ogle and coworkers on the 30S subunit in complex with mRNA and tRNA showed that the decoding center is built by parts of helices 18, 34, 44 of 16S rRNA. Importantly, residues responsible for monitoring the quality of codon-anticodon interactions were pinpointed. Thus, helix 44, through its A1493 and A1492, contacts the $1^{st}$ and the $2^{nd}$ position of the codon-anticodon duplex, whereas the $3^{rd}$ position is monitored less stringently by a contact from G530 (Ogle *et al.* 2001).

In parallel, the crystal structure of the 70S ribosome in complex with mRNA and tRNA from *Thermus thermophilus*, first at 7.8 Å (Cate *et al.* 1999), and subsequently at 5.5 Å resolution (Yusupov *et al.* 2001) was solved. Separate ribosomal proteins and rRNA components, for which high-resolution structures had been obtained in early X-Ray crystallographic and NMR studies, could then be recognized at these resolutions and modeled into the electron density. The resulting models revealed the relative orientations of tRNAs within the ribosome, providing new insights into the decoding phase. They also unraveled the path of the mRNA throughout the 30S subunit and the bridges formed between the two subunits. Recently, two structures of the 70S ribosome from *Escherichia coli* at 9 Å (Vila-Sanjurjo *et al.* 2003) and at 3.5 Å resolution (Schuwirth *et al.* 2005) were reported. They provided a detailed view of the interface between the small and large ribosomal subunits and the conformation of the peptidyl transferase center in the context of the intact ribosome. They also suggested a model for the final movements of mRNA and tRNAs during translocation. *E. coli* structures are of great importance, as most of the genetic, biochemical and biophysical data are available from this organism.

Taken together, these structural studies highlighted the roles of individual ribosomal subunits in translation. The small ribosomal subunit plays a crucial role in decoding and validating the accuracy of the codon-anticodon base pairing. The large subunit participates to the peptide bond formation. Additionally, it contains a region that

was identified as a common translation factor GTPase binding domain. While both processes underlying decoding and reaction at the peptidyl transferase center were clarified by several approaches, including crystallography, the mechanisms of factor GTPases binding to the ribosome are still not entirely understood.

## D. Modulators of the ribosomal activity

### 1. Requirement of GTPase activity by EF-Tu and EF-G for translation

As described previously, the ribosome orchestrates protein synthesis, playing crucial roles in: (i) decoding, (ii) peptide bond formation, and (iii) translocation of the tRNAs and mRNA. Remarkably, it was shown that the ribosome is able to fulfill these functions by itself (Gavrilova *et al.* 1976). Indeed, with an appropriate mRNA matrix and aminoacylated-tRNAs, the ribosome is capable to synthesize peptide chains in the absence of elongation factors and GTP, performing a residual translation. Moreover, EF-G-independent translocation occurs spontaneously *in vitro*, suggesting that this phenomenon resides entirely within the structure of the ribosome (Spirin 1985). However, it was also established that the elongation factor-free translation is inaccurate and does not meet the cell requirements. Therefore, in order to exert its function at physiological rates, the ribosome needs to associate with elongation factors (EF-Tu and EF-G), that act as catalysers improving its intrinsic properties.

### 2. GTP hydrolysis represents the driving force of translation

The high speed and fidelity of protein synthesis *in vivo* is achieved at the expense of energy consumption. This energy is provided by the hydrolysis of GTP coupled to EF-Tu and EF-G. Similarly, GTPase activity is also required for the function of IF2 and RF3 (Bourne *et al.* 1991).

The role of GTP hydrolysis by IF2, known to bind to the initiator tRNA on the 30S ribosomal subunit and to trigger subunit association, remains unclear. In contrast, GTPase activity by EF-Tu is better characterized and is coupled to the A-site aa-tRNA binding and correct codon-anticodon interaction (Pape *et al.* 1998). Through conformational changes, GTP hydrolysis elicits the dissociation of EF-Tu from the ribosome. The mechanism of GTP hydrolysis by EF-G is not clearly elucidated. Kinetic studies suggested that EF-G is a motor protein that, upon rapid GTPase reaction, drives the translocation (Rodnina *et al.*

1997). A different model suggested that GTP hydrolysis by EF-G is not required for translocation, but for the release of EF-G (Inoue-Yokosawa *et al.* 1974); a similar observation was made for RF3, responsible for detaching the decoding release factors 1 and 2 from the ribosome (Zavialov *et al.* 2001).

### 3. Ribosomal GTPases act as molecular switches

**G**uanine **N**ucleotide-**B**inding **P**roteins (GNBPs) cycle between the GTP- and GDP-bound states (Vetter and Wittinghofer 2001) (Figure 3). The transition from the GDP to the GTP-bound forms was shown to occur spontaneously *in vitro*. However, *in vivo*, this reaction is accelerated by **G**uanine nucleotide-**E**xchange **F**actors (GEFs). The GEF forms a complex with the GDP-bound protein, causing the dissociation of GDP. The resulting complex can then bind GTP and thereby, promotes the release of GEF. The selective binding of GTP instead of GDP is favored by the high cellular GTP/GDP ratio (Sprang 1997). In contrast, the conversion from the GTP to the GDP-bound states is an irreversible hydrolysis reaction (guanosine triphosphatase (GTPase) reaction). It is also intrinsically very slow, but can be accelerated by **G**TPase-**A**ctivating **P**roteins (GAPs).
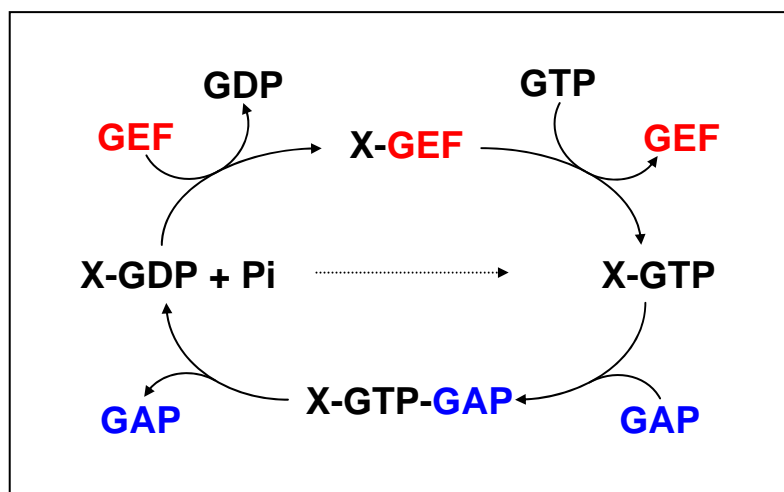


**Figure 3.** The mechanism of GTP/GDP cycling of guanine nucleotide-binding proteins. A GDP-bound protein exchanges its GDP for GEF, which in turn will be replaced by GTP. GTP-bound proteins hydrolyze GTP in a GAP-dependent mechanism (see main text for details).

Translation factor GTPases are multi-domain proteins. One of them, namely the G-domain, is responsible for binding and hydrolyzing GTP. The structure of this domain is similar in all factor GTPases, comprising a β-sheet flanked by α-helices. Accordingly, the mechanism of GTP binding is universal: a conserved N/TKXD motif binds the nucleotide base, while the P loop (phosphate-binding loop) interacts with the β, γ-phosphates of the

nucleotide (Saraste *et al.* 1990). Structural studies showed that the switch apparatus itself is a conserved fundamental module, but that its regulators and effectors are quite diverse in structures and modes of interaction (Vetter and Wittinghofer 2001).

Two of the ribosomal GTPases, namely EF-Tu and RF3, were shown to conform to the canonical mechanism described for the GNBPs, while IF2 and EF-G seem to act differently. EF-Ts and the ribosome act as GEFs for EF-Tu and RF3, respectively, promoting their activation (Lucas-Lenard and Lipmann 1966; Zavialov *et al.* 2001). Unlike them, IF2 does not seem to discriminate between GTP and GDP, as it was shown to catalyze the initiation of translation in the presence of either nucleotide (Tomsic *et al.* 2000). The mechanism of nucleotide binding by EF-G, correlated to its function in translocation, is not entirely elucidated. The classical interpretation is that in solution, both GTP and GDP forms of EF-G are in equilibrium and it is not yet clear, which of these forms binds to the ribosome (Martemyanov *et al.* 2001; Hansson *et al.* 2005). Recently, it was hypothesized that the ribosome, in its pretranslocational state, would act as a GEF for EF-G:GDP (Zavialov *et al.* 2005). However, this hypothesis is challenged by the fact that EF-G:GDP has low affinity for the ribosome (Munishkin and Wool 1997). Kinetic analyses revealed that the binding of EF-G:GTP to the pretranslocation complex triggers rapid GTP hydrolysis. The energy of this process is used to drive the translocation. Thus, EF-G is in a GDP-bound conformation throughout the translocation and dissociates from the ribosome after this process is completed (Rodnina *et al.* 1997).

Based on these observations, it can be concluded that ribosomal GTPases act as molecular switches, cycling between their GTP- and GDP-bound states on the ribosome. They bind GTP and upon GTP hydrolysis undergo conformational changes. The structural changes modulate affinities of the factors for a particular functional state or for a ligand molecule they carry and thus, allow the entry into the next translation phase or the next step of the elongation cycle.

## E. The GAP function of the ribosome

Translation factor-GTPases possess an intrinsic GTP hydrolysis activity in the presence of an appropriate physicochemical environment, but it does not meet the requirements of an efficient translational apparatus (De Vendittis *et al.* 1986). Importantly, this low intrinsic GTPase activity is stimulated by the presence of the empty ribosome

(Kawakita *et al.* 1974). The amount of GTP hydrolyzed by EF-G in one minute was about three orders of magnitude higher in the presence of the *E. coli* ribosomes (Masullo *et al.* 1989). Furthermore, GTPase activity was augmented in the presence of tRNA-bound ribosome (Chinali and Parmeggiani 1982) and further increased when both elongation factors interacted with the ribosome (Mesters *et al.* 1994). Thus, in addition to its multiple functions during translation, the ribosome also induces an increase in factor GTP hydrolysis by several orders of magnitude and thereby possesses a GAP function.

Biochemical analyses have defined a region of the large ribosomal subunit, whose elements act as GAPs for EF-Tu, EF-G, IF2 and RF3. This region encompasses several rRNA and r-protein elements, namely the sarcin-ricin loop, L10/L11 binding region, proteins L6, L11, L14 and the L7/L12 stalk. The latter corresponds to an extended feature of the 50S ribosomal body, comprising multiple copies of protein L7/L12, which are linked to the ribosomal rRNA through protein L10. The entire region formed by rRNAs and r-proteins can be collectively termed the **G**TPase **A**ssociated **R**egion (GAR) or factor-binding site (Wimberly *et al.* 1999) (Figure 4).
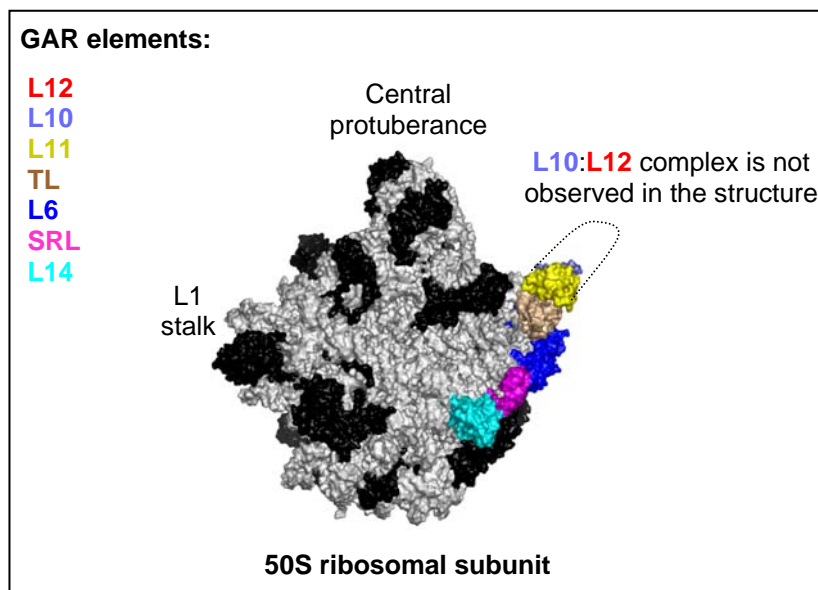


**Figure 4.** The GTPase associated region (GAR or factor binding site) of the large ribosomal subunit. 50S is depicted with its major landmarks: the central protuberance, the L1 stalk and the L7/L12 stalk (lacking the peripheral elements of the L10:L12 complex); rRNAs are depicted in gray and r-proteins in black, respectively. Components of the GTPase associated region (GAR) are highlighted in different colors and denominated accordingly in the legend on the left; TL, thiostrepton loop or L10/L11 rRNA binding region; SRL, sarcin-ricin loop (adapted from (Ban *et al.* 2000), PDB accession code 1FFK).

Initially, the complex of L11 protein with its corresponding rRNA binding region of the 23S rRNA (L11-rRNA region) was defined as the **G**TPase **A**ssociated **C**enter

(GAC). However, there is no uniform terminology of GAC in the literature, as it was also used to define, both the L11-rRNA region and the neighboring sarcin-ricin loop.

The GTPase associated region (GAR) acts as a ribosomal GAP. From the analysis of other GAP family members, three putative models emerge, to account for the GAP ribosomal function (reviewed in (Vetter and Wittinghofer 1999)):

- model 1: as for RasGAP and RhoGAP, the ribosome may provide a catalytic arginine residue ("arginine finger") to the GTPases' active sites and thereby stabilize their GTP transition state, leading to an increase in the rate of GTP hydrolysis (Noel 1997)

- model 2: as for RGSs (regulators of G protein signaling), the ribosome may bind to the switch regions of the factor GTPases and stabilize the GTPase transition state (Hunt *et al.* 1996)

- model 3: as for ARFGAP, the ribosome may enhance GTP hydrolysis by interacting with distant regions of the nucleotide binding site (Goldberg 1999)

Despite the definition of a ribosomal region capable of assuming the GAP function, the discrimination between either models remained so far unclear.

## 1. Sarcin-ricin loop, proteins L6 and L14

The Sarcin-Ricin Loop (SRL or stem-loop 95 or ribotoxin loop) is a universally conserved stem-loop structure, located in domain VI of the 23S rRNA around position 2660 (nucleotides 2645-2675 in *E. coli* 23S rRNA). The SRL is essential for the binding of elongation factors (Moazed *et al.* 1988) and IF2 (La Teana *et al.* 2001), and possibly acts as a stimulator of their GTPase activity. Additionally, it was shown that the SRL is the target of ribotoxins α-sarcin (Endo and Wool 1982) and ricin (Endo *et al.* 1987). The cleavage of a single covalent bond by either toxin inhibits the binding of EFs to the ribosome, thereby inactivating translation (Montanaro *et al.* 1975; Fernandez-Puentes and Vazquez 1977). Crystallographic data of the 50S ribosomal subunit (Ban *et al.* 1999; Ban *et al.* 2000) presented a detailed model of the structure of the translation factor-binding site. In these studies, the first element fitted into the electron density of the factor binding site was the SRL, which has a typical S-shaped structure (Szewczak and Moore 1995; Correll *et al.* 1998). Cross-linking (Leffers *et al.* 1988; Urlaub *et al.* 1995; Uchiumi *et al.* 1999) and immunoelectron microscopy (Walleczek *et al.* 1988) approaches provided information concerning other elements neighboring the SRL, namely proteins L6, L14 and the L7/L12 stalk. Notably, by docking the ternary complex (EF-Tu:GTP:tRNA) and EF-

G:GDP on the 50S subunit, interactions between the G domains and the GAR components were predicted (Ban *et al.* 1999). The C-terminal domain of protein L6 was found in the vicinity of both EF-G and EF-Tu G domains. Protein L14 was assumed to make extensive contacts with domains 2 and 3 of EF-G, EF-Tu and the acceptor stem of tRNA carried by EF-Tu (Ban *et al.* 1999). Additionally, G domains of both EF-Tu in the GTP conformation and EF-G in the GDP conformation seemed to contact the ribotoxin loop. Moreover, their switch regions, whose conformations are modified upon GTP hydrolysis, were found sandwiched between L14 and the SRL (Ban *et al.* 1999). The latter has a central position in the factor binding site, suggesting that it stimulates the GTPase activity of the ribosome-bound factors.

Supplementary evidence supporting these crystallographic data came from a cryo-EM map of EF-G bound to the 70S ribosome (Wriggers *et al.* 2000) that showed a direct contact between the G domain of the factor and sarcin-ricin loop. Moreover, a 13 Å cryo-EM three-dimensional reconstruction of the EF-Tu:GTP:aa-tRNA ternary complex stalled with kirromycin following GTP hydrolysis (Stark *et al.* 2002), depicted an extensive interaction between the G domain of EF-Tu and the SRL. This contact involves the switch regions of EF-Tu (nucleotide-binding pocket and the effector loop), implicating the SRL in the GTPase activation of this factor. IF2:GTP was visualized by cryo-electron microscopy in the proximity of the sarcin-ricin-loop. In contrast, IF2:GDP was found distant from the SRL and oriented toward protein L6 (Myasnikov *et al.* 2005). Interestingly, RF3 in its GTP-bound form adopted two conformations: in state-1, RF3 made only few contacts with the ribosome, predominantly with the 30S subunit; in state-2, RF3 was tightly bound to the ribosome and its G domain was oriented towards the factor binding site, suggesting an interaction similar to other factor GTPases (e.g. EFs) (Klaholz *et al.* 2004).

## 2. L11 protein and L10/L11 rRNA binding region

Protein L11 and L10:L12 complex interact in a mutually cooperative manner with a short sequence within domain II of 23S rRNA (L10/L11 rRNA binding region) (Beauclerk *et al.* 1984). L10:L12 elements form an elongated protuberance in the large ribosomal subunit, called the L7/L12 stalk. Early immunoelectron microscopy experiments placed protein L11 at the base of the L7/L12 stalk (Tate *et al.* 1984). The L10/L11 rRNA region neighbors the sarcin-ricin loop. Both rRNA elements display a high degree of

conservation throughout the kingdoms, suggestive of their important role in the translation process.

L11 interacts with a fragment of 58 nucleotides (1051-1108 in *E. coli*) within the L10/L11 rRNA region forming the L11:rRNA complex (Thompson *et al.* 1979; Schmidt *et al.* 1981). This complex is the target of a family of thiazole antibiotics, including thiostrepton and micrococcin. As a consequence, the L10/L11 rRNA sequence is often referred to as the **T**hiostrepton **L**oop (TL). These drugs bind irreversibly to the L11:rRNA complex and inhibit protein biosynthesis. The structure of thiostrepton was determined few decades ago (Hensens *et al.* 1983), but its exact orientation within the L11:rRNA complex is still unknown. However, based on structural and biochemical data, it was proposed that the thiostrepton/micrococcin-binding site is located in a "pocket" formed by the 1067/1095 region of the 23S rRNA and a proline-rich helix in the NTD of L11 (Wimberly *et al.* 1999). A proline 22 in the NTD of the L11 from bacteria, crucial for thiostrepton binding, is not conserved in eukaryotic counterparts, consistent with the natural resistance of the latter to thiazole antibiotics. Thus, the structural basis for the interaction of the L11:rRNA complex with these antibiotics (previously shown to be effective agents against the malaria parasite *Plasmodium falciparum*) is of great medical interest. The mechanism by which thiazoles arrest protein synthesis was studied in more detail for EF-G. Micrococcin inhibits a number of processes believed to involve the ribosomal A site while stimulating GTP hydrolysis by EF-G (Cundliffe and Thompson 1981). Thiostrepton was originally regarded as an inhibitor of GTP hydrolysis by EF-G (Pestka 1970). Later experiments showed that the drastically decreased GTPase activity of EF-G is an indirect effect of thiostrepton binding to the ribosome, which in turn reduces the affinity of EF-G for the ribosome (Cameron *et al.* 2002). Moreover, kinetic experiments demonstrated that thiostrepton does not prevent GTP hydrolysis by EF-G, but rather affects subsequent steps, such as inorganic phosphate and EF-G release (Rodnina *et al.* 1999). A possible explanation for this effect could be that thiostrepton prevents the mobile L11 NTD to undergo a conformational change required after GTP hydrolysis, thus blocking translation in this stage. Consistently, thiostrepton was used to visualize conformational changes occurring after GTP hydrolysis during translocation. Thus, it was seen that EF-G was trapped by thiostrepton at an earlier stage than fusidic acid, the latter preventing the EF-G:GDP dissociation from the ribosome (Stark *et al.* 2000).

The high-resolution structure of the L11:rRNA complex revealed a compact organization of the rRNA (Wimberly *et al.* 1999). Protein L11 consists of two globular domains connected by a short, proline-rich linker, which allows the independent movement of the NTD with respect to the CTD. These two domains are unequally associated with rRNA: the C-terminal domain (CTD) forms extensive tight contacts with the 58 nt fragment of the 23S rRNA, while the N-terminal domain (NTD) interacts weakly with this region. Contacts between the CTD of L11 and rRNA involve mainly the protein backbone and rRNA 2' OH moieties, suggesting a case of protein-RNA recognition based on shape complementarity.

The NTD region of L11 could not be visualized in the high-resolution map of the 50S subunit, or in several cryo-EM maps of the ribosome, most probably due to its flexibility (Ban *et al.* 2000). However, an intermediate resolution structure of the large ribosomal subunit placed the 58 nt-rRNA fragment and the CTD of L11 in the electron density and offered a convincing model for the location of the NTD (Ban *et al.* 1999). This hypothesis was further supported by a cryo-electron microscopy analysis of the GDP state-EF-G modeled onto the 70S ribosome, which ascertained the location of the L11-NTD in the electron density map (Agrawal *et al.* 2001). Noteworthy, this latter study also revealed that, following GTP hydrolysis, an **A**rc-**L**ike **C**onnection (ALC) is formed between the L11 NTD and the G' domain (a subdomain of the G domain) of EF-G. This thin bridge was noticed in both GDP state-EF-G and EF-Tu, but not in their GTP conformations, in several other cryo-EM studies (Stark *et al.* 1997b; Agrawal *et al.* 1998; Agrawal *et al.* 1999; Stark *et al.* 2000; Agrawal *et al.* 2001). In these reports, the G or G' domain of the GDP-state factors were found to contact a lobe positioned at the base of the stalk, which, as Agrawal and coworkers have inferred, implicates the N-terminal domain of protein L11.

The interaction of the L11:rRNA region with EF-Tu is less understood. Two similar cryo-EM studies of the kirromycin-stalled ternary complex (EF-Tu:GTP:tRNA) concluded that upon the cognate codon recognition, the tRNA interacts with the GTPase associated center and triggers GTP hydrolysis by EF-Tu (Stark *et al.* 2002; Valle *et al.* 2002). However, in these reports, different interpretations were made regarding the interaction between tRNA and GAC elements. The first study suggested an interaction between the tRNA and protein L11, whereas SRL would stimulate GTP hydrolysis. This observation portrayed protein L11 as a modulator of the GTPase rate, rather than a direct player in this process (Stark *et al.* 2002). Conversely, the second report assigned the tRNA

with an essential role in GTPase activation, interacting with the L11 rRNA binding region (Valle *et al.* 2002). It was envisioned that when a ternary complex binds the ribosome, the G-domain of EF-Tu contacts the SRL and the tRNA interacts with the L11 binding region of rRNA (around nucleotide 1067), which is in an "opened" conformation. Successful codon-anticodon base-pairing goes hand in hand with the interaction between the tRNA (T-loop) and the L11 binding lobe of rRNA, stabilizing it in a "closed conformation". This event is followed by GTP hydrolysis and by the transition of the rRNA to the initial "opened" conformation (Valle *et al.* 2003b).

### 3. L10:L12 complex

#### a. Characterization of the L10-L12 interaction

The most studied element of the stalk, but at the same time still puzzling, both in structure and function, is the L7/L12 protein (reviewed in (Gudkov 1997; Wahl and Moller 2002)). Together with protein L10, it builds a lateral protrusion on the large ribosomal subunit, termed the L7/L12 stalk (Figure 4). Indeed, early studies involving electron microscopic visualization of antibody-labeled ribosomal subunits, evidenced the presence of protein L7/L12 on the "rod-like appendage" (or stalk) of the 50S subunit (Boublik *et al.* 1976; Lake 1976; Strycharz *et al.* 1978; Kastner *et al.* 1981).

First considered as an individual protein, named L8, by means of two-dimensional gel electrophoresis (Kaltschmidt and Wittmann 1970), L10 and L7/L12 were further identified as distinct proteins forming a stable complex (Pettersson *et al.* 1976). The assignment L7/L12 resides in the occurrence, in different culture conditions, of two similar acidic protein populations, L12 and L7, the only difference between them being the N-terminal acetylation of L7 (Deusser 1972); for simplicity, in the following, the L7/L12 protein will be referred to as L12.

Both extraction from the ribosome or *in vitro* purification of the *E. coli* L10:L12 complex, yielded a pentameric complex formed by one copy of L10 and four copies L12, the latter being the only multicopy ribosomal protein (Terhorst *et al.* 1973; Hardy 1975; Subramanian 1975; Pettersson and Liljas 1979).

The L10:L12 complex is anchored on the large ribosomal subunit *via* protein L10. The L10 N-terminal domain (NTD) binds to a highly conserved region of the 23S rRNA (L10/L11 binding region), overlapping the binding site of protein L11 (Beauclerk *et al.* 1984; Egebjerg *et al.* 1990). In turn, four copies of protein L12 associate as two dimers

with the C-terminus of L10 (CTD). Terminal deletion variants of ribosomal protein L10 were constructed in order to define the binding sites of the two L12 dimers. Thus, it was determined that the deletion of the last ten amino acids of L10 results in the loss of one L12 dimer, while the deletion of the last 20 amino acids led to the loss of both dimers (Griaznova and Traut 2000) (Figure 5).
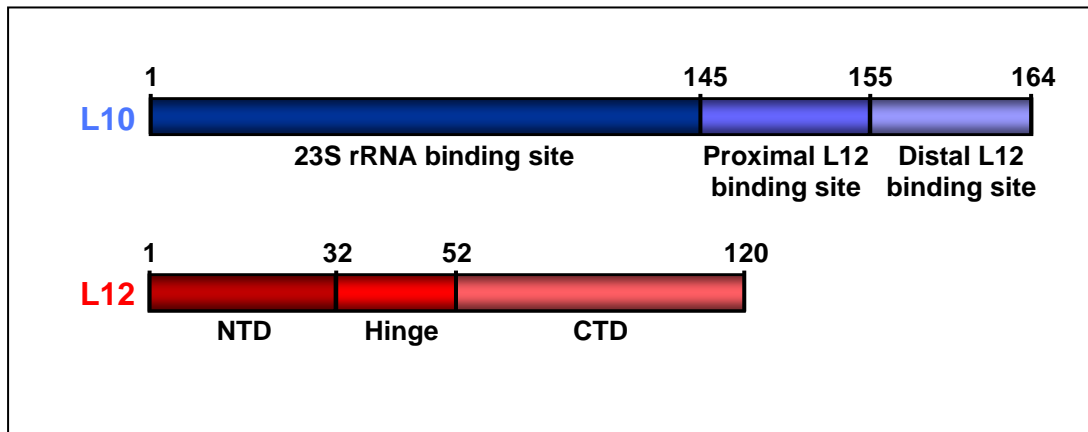


**Figure 5.** Organization of L10 and L12 proteins from *E. coli*. L10 binds to the 23S rRNA *via* its N-terminal part (residues 1-144), whereas the C-terminal part (residues 145-164) is responsible for the interaction with L12. One L12 protein encompasses three domains: a NTD (residues 1-31) connected to the CTD (residues 52-120) through a linker (hinge).

### b. Domain organization and dimerization mode of the L12 protein

Several biochemical, biophysical and structural data further deciphered the organization of the L12 protein. Three structurally distinct regions underlie L12 function: a N-terminal domain responsible for both dimerization and interaction with L10 (Gudkov and Behlke 1978; Gudkov *et al.* 1980), a C-terminal domain involved in factor binding and stimulation of their GTPase activity (Kischa *et al.* 1971), and a flexible hinge connecting both domains (Liljas and Gudkov 1987) (Figure 5). NMR studies envisioned that the NTD dimers of L12 interact in an antiparallel fashion, forming a four helix bundle (Bocharov *et al.* 1996). The CTDs have a globular aspect and exhibit on their surface several conserved residues (Liao and Dennis 1994) believed to represent the sites of interaction with translation factors (Wieden *et al.* 2001). The high-resolution crystal structure of the L12 C-terminal domain - the first structure of a ribosomal component - displays a split $\beta-\alpha-\beta$ motif, identified as an RNA recognition motif (RRM), although in this particular case no interaction with the rRNA was observed (Leijonmarck *et al.* 1980). Proton magnetic resonance studies portrayed the hinge region as highly mobile (Bushuev *et al.* 1989). The

importance of the hinge in translation was acknowledged by experiments with deletion mutants lacking this domain, which yielded ribosomes completely inactive (Oleinikov *et al.* 1993; Dey *et al.* 1995). In addition, it was hypothesized that the flexibility of the hinge may cause independent movements of the L12 CTDs. Indeed, a cryo-EM structure of the 70S ribosome, displaying a nanogold labeled CTD of L12, localized this domain at different sites of the ribosome, such as the stalk base, the peptidyl transferase center or the head of the 30S subunit (Montesano-Roditis *et al.* 2001). The latter study was supported by cross linking (Dey *et al.* 1998) and NMR data (Mulder *et al.* 2004).

L12 proteins, both in solution or in complex with L10, form symmetrical dimers *via* their N-terminal domains (Gudkov and Behlke 1978). Various arrangements of the subunits in L12 dimers have been proposed, i.e. antiparallel (head-to-tail orientation) (Moller *et al.* 1972) or parallel (Liljas 1982). The latter model is favored by experiments in which the hydrogen peroxide oxidation of methionine residues present in the NTD caused the disruption of the dimer and failure of L10 binding (Gudkov *et al.* 1977). Taken together, these data support a model of a parallel dimer in which the CTDs are well separated from the NTDs via a highly mobile linker.

### c. Structures of the L12 protein

The crystal structure of the isolated L12 protein from *Thermotoga maritima* challenged the previous model of the association of L12 dimers, providing new exciting hypotheses concerning both domain organization and dimerization (Wahl *et al.* 2000a). The asymmetric unit comprised two full-length molecules and two proteolysed N-terminal fragments, forming a compact hetero-tetrameric structure. The structure exhibited contacts from each component part to every other, except for an interaction between the NTD fragments. Two dimerization modes were observed: *parallel*, between the two full-length monomers, which form a tight, symmetric "core dimer", and *antiparallel*, between each N-terminal domain of a full-length monomer and an N-terminal L12 fragment. The hinge was seen in two alternative conformations: an extended coil in the NTD fragments or a long α-helix that folds back on the N-terminal domain of the full-length molecule. The existence of both an antiparallel dimerization mode and an unstructured, extended hinge was shown for isolated *E. coli* L12 (*eco*L12) in solution by NMR (Bocharov *et al.* 2004) and for *T. maritima* L12 (*tma*L12) in solution by FRET experiments (Moens *et al.* 2005). The latter study also indicated that *tma*L12 proteins formed dimers in solution, which implied that

the tetrameric arrangement observed in the crystal structure does not represent the solution state of the protein. Thus, corroborating the observations made for, both L12 in solution and in the crystalline environment, the ribosome bound-L12 was assumed to display one monomer with an α-helical hinge, and one with an extended hinge, allowing the movement of the CTD (Chandra Sanyal and Liljas 2000; Bocharov *et al.* 2004; Mulder *et al.* 2004; Moens *et al.* 2005).

### d. Different locations of the L12 protein on the ribosome

In the past two decades, several hypotheses were made regarding the orientation of L12 molecules within the ribosome. Thus, it was shown that one dimer per particle was sufficient to form a visible stalk (Moller *et al.* 1983), despite earlier studies using polyclonal antibodies that suggested that both dimers were present in the stalk (Tokimatsu *et al.* 1981).

By chemical cross-linking studies it was proposed that a dimer could reach the EF-Tu binding site on the 30S subunit (Dey *et al.* 1998). Additionally, three possible alternative locations of the dimer on the 50S subunit were inferred: (i) accounting for the stalk protrusion (ii) bent at the base of the stalk, near the EF-G binding site; (iii) extended far across the body of the 50S subunit, as the CTD of L12 was shown to be engaged in interactions with L2 and L5. The latter location can be refuted, since this site could only be reached by a twice longer L12 dimer (Wahl and Moller 2002).

### e. Phylogenetic comparison

Similar L10:L12 complexes are also present in archaeal and eukaryotic ribosomes (reviewed in (Gonzalo and Reboud 2003)). Both archaeal (aL10 or L10E) and eukaryotic (P0) L10 are longer than their bacterial counterparts. In archaea, there is only one form of the L12-like protein. In eukaryotes, the bacterial L12 is replaced by two proteins, P1 and P2 (Wood 1991), which form further subgroups in yeast (Shimmin *et al.* 1989) and by three proteins in plants (P1, P2, P3) (Szick *et al.* 1998). Dimers of both P1 and P2 are anchored to the ribosome via P0. The mechanism by which L12-like proteins exert their function on the ribosome is different: while bacterial proteins seemed permanently associated to core particles, P-proteins (post-translational **P**hosphorilated proteins) were found interchangeable between ribosome-bound and cytoplasmic non-phosphorilated pools (Kopke *et al.* 1992).

The bacterial stalk proteins do not have a detectable sequence homology to the eukaryotic and archaeal counterparts, which, on the other hand, are clearly homologous to each other (Liljas 1991). The replacement of the L10:L12 complex in *E. coli* ribosomes with the rat P protein complex changed its specificity from prokaryotic elongation factor (EF-G) binding to eukaryotic EF-2-dependent GTPase activity (Uchiumi *et al.* 1999). However, the latter study suggested that the rRNA-L10 protein association seems to be conserved across kingdoms, consistent with several other functional hybrid ribosomes reported: yeast cores reconstituted with *E. coli* L12 (Sanchez-Madrid *et al.* 1981) and *vice versa*, (Wool and Stöffler 1974), as well as *E. coli* ribosomes reconstituted with an archaeal P complex (Nomura *et al.* 2006)).

### f. Translation factor-related functions

An interesting property of both L10:L12 complex or isolated L12, allowing thorough studies of their functions, is represented by their selective extraction from the ribosome following a specific high salt/ethanol treatment (Kischa *et al.* 1971; Pettersson and Kurland 1980). The subsequent addition of these proteins to the depleted core particles, results in functional ribosomes. Thus, it was noticed that a severely impaired GTPase activity by EF-G in L12-depleted ribosomes, was rescued by addition of the purified protein (Kischa *et al.* 1971). Similar effects were seen for the other soluble factor GTPases EF-Tu, IF2, RF3 (reviewed in (Brot and Weissbach 1981)). The same observations were made with ribosomes depleted of the entire pentameric complex (Hamel *et al.* 1972). Based on these investigations, it was suggested that L12 is directly involved in translation factor GTPases binding and stimulation of their GTP hydrolysis (Kischa *et al.* 1971; Fakunding *et al.* 1973; Brot *et al.* 1974). Numerous other studies, including site-directed mutagenesis, limited proteolysis, crosslinking or structural approaches supported this hypothesis (Gudkov 1997; Wahl and Moller 2002).

Noteworthy, factor binding was evidenced not only for the ribosome-bound L12, but also for the protein in isolation. However, in the latter case, a different outcome was observed for elongation factor-dependent GTP-hydrolysis: while EF-G-dependent GTP hydrolysis was strongly stimulated by L12 (Savelsbergh *et al.* 2000), no GTPase activity by EF-Tu was detected, indicating that additional ribosomal components are required for this purpose (Piepenburg *et al.* 2000). Accordingly, recent rapid kinetics and mutagenesis experiments evidenced that the ribosome-bound L12 promotes EF-Tu binding (Kothe *et al.*

2004). Furthermore, comparisons of L12 CTD and EF-Ts (the guanine-nucleotide exchange factor of EF-Tu) structures revealed that the L12 CTD interacts with helix D of EF-Tu (Wieden *et al.* 2001); consistently, the corresponding region of the L12 CTD was found essential for the initial binding of EF-Tu to the ribosome (Kothe *et al.* 2004).

## III. Rationales

Numerous components of the GTPase associated region (GAR) have been ascribed in the recent crystal structures of the bacterial ribosome (Figure 4). However, the structure of L10:L12, a protein complex shown to be instrumental in translation, has long remained elusive. Several lines of evidence have demonstrated that this complex suffers major rearrangements as a result of its interactions with elongation factors during protein synthesis. The difficulty of disclosing electron density corresponding to this region most probably stems from its inherent conformational dynamics and potential heterogeneity. Thus, the L10:L12 structure was found disordered or absent even in high-resolution crystal structures of 50S ribosomal subunit (Ban *et al.* 2000) (Figure 4) or of entire ribosomes (Schuwirth *et al.* 2005) (Figure 2).

In a crystal structure of the 70S ribosome (Yusupov *et al.* 2001), one of the L12 dimers was tentatively modeled within the electron density in its compact arrangement, as previously described for L12 in isolation (Wahl *et al.* 2000a). However, this ribosome structure did not attribute any electron density for the second dimer of L12 or for the L10 protein. Two helices of the latter were defined in a high-resolution structure of the large ribosomal subunit (Ban *et al.* 2000). They correspond to residues located at the N-terminal part of L10 that interact with a secondary structure motif, called the K-turn (Klein *et al.* 2001). Hence, at the moment, there is no crystal structure describing a full L10:L12 complex and its location on the ribosome.

Cryo-EM studies evidenced that the G domains of elongation factors in their GDP-like conformation form a bridge with the base of the stalk (Figure 6A, C) (Stark *et al.* 1997b; Agrawal *et al.* 2001), which was not observed in their GTP-bound states (Figure 6B) (Agrawal *et al.* 1999). Moreover, the G domains of other factor GTPases, such as IF2 (Allen *et al.* 2005) and RF3 (Klaholz *et al.* 2004) seem to interact with several components of the GTPase associated region (GAR) in a site delineated by the sarcin-ricin loop and the

stalk. However, for protein L12, a central element of the GAR, it is not clear how it participates in GTP hydrolysis, since a contact between L12 and elongation factors, or other components of the ribosome that could trigger this process was not evidenced in previous structures or cryo-EM studies.
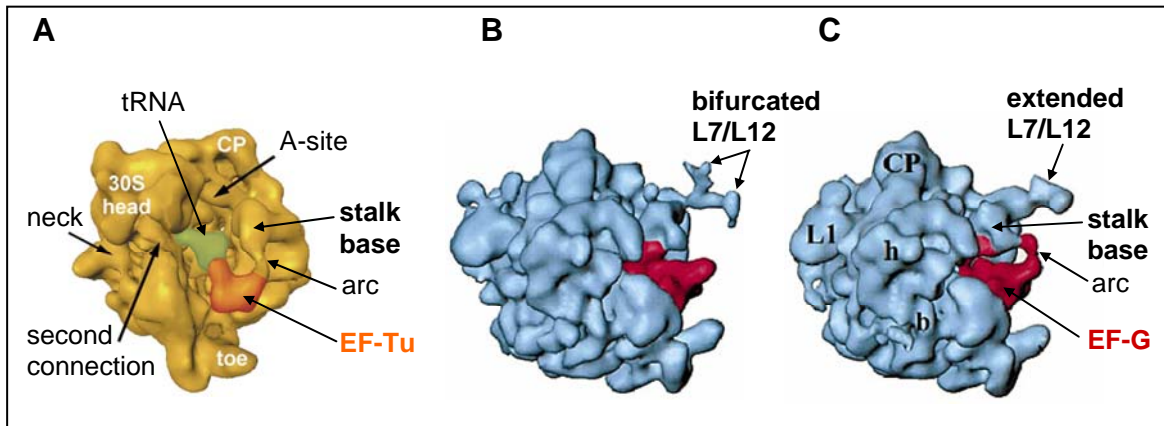


**Figure 6.** Visualization of the L7/L12 stalk by cryo-electron microscopy and single particle reconstruction at several main steps of the elongation cycle. (**A**) Ternary complex (EF-Tu:Phe:tRNA) kirromycin-locked at the A site (reproduced from Stark et al., 1997). The main landmarks of the 30S (head, neck, toe) and of the 50S subunit (central protuberance, CP) are evidenced. The stalk base forms an arc-like connection with EF-Tu. (**B**) EF-G (dark red) is bound to the ribosome in complex with a non-hydrolysable GTP analog. In this particular step, the L7/L12 stalk elements accounting for the L10:L12 protein complex adopt a bifurcated shape (reproduced from Agrawal et al., 1999). (**C**) EF-G is bound to the ribosome in the presence of fusidic acid, in a GDP-like conformation. Main landmarks of the 30S subunit: head (h), body (b) and 50S subunit: central protuberance (CP), L1 protuberance (L1), are depicted. Contrary to (B), here the stalk elements accounting for the L10:L12 complex are seen in an extended conformation. Similarly to (A), an arc-like connection is observed between the G'-domain of EF-G and the stalk base (reproduced from Agrawal et al., 1999).

In the 70S:EF-G:GDP:fusidic acid complex (Figure 6C), an extended lateral protrusion was observed, which became bifurcated in the GTP state of the same complex (Figure 6B) (Agrawal *et al.* 1999) and presumably represented the L10:L12 complex. However, these elements cannot be reliably interpreted without an atomic structure of the L10:L12 complex. Therefore, a crystallographic study of this complex is required to disclose the L10 protein structure and to understand how it distinguishes and accommodates two L12 dimers in its asymmetric sequence (Wahl and Moller 2002). In addition, this structure could reveal how this complex is anchored on the ribosome, what is the *in situ* orientation of the L12 dimers (particularly, how many copies of L12 form the extended stalk) and which parts of this complex are flexible when bound to the ribosome. The L10:L12 complex structure could be regarded as one of the last pieces to be discovered in the jigsaw puzzle of the ribosome and its deciphering would aid to further understand the complex molecular mechanism of translation.

Here, a high-resolution crystal structure of the L10 protein in complex with the N-terminal domain of L12 from the hyperthermophilic bacterium *Thermotoga maritima*, in three different crystal forms, is reported. Attempts to solve the structure of the full-length L10:L12 protein complex were also made. The fitting of the resulting L10:L12 NTD complex *in situ* on the 50S ribosomal subunit is discussed. The morphology and dynamics of the L7/L12 stalk region, as seen in electron microscopic reconstructions of ribosomes is reinterpreted. Together with structures of the isolated L12, a complete atomic model of the stalk is devised. Based on this model, structure-function relationships were established.

# Materials and Methods

## I. Molecular cloning

### A. Genomic DNA preparation

*T. maritima* MSB8 cells were purchased from DSMZ (Braunschweig) and their genomic DNA was isolated by phenol-chloroform extraction. Briefly, cells were resuspended in TE buffer (10 mM Tris-HCl, 1 mM EDTA, pH 8.0) and mixed with one volume of phenol (Roth, Karlsruhe). After centrifugation, one volume of chloroform (Roth) was added to the upper phase and re-centrifuged. The DNA content in the resulting upper phase was extracted by precipitation with 3 volumes of 100% ethanol containing 10% of 3 M sodium acetate pH 5.5, and was subsequently placed at −80°C for 20 min. Following 30 min centrifugation, the DNA pellet was washed with 70% ethanol and resuspended in 100 µl of water. The concentration, measured at $OD_{260}$ (Sambrook *et al.* 1989), was 97.5 ng/µl.

### B. PCR amplification

The DNA fragments encompassing the entire coding sequence of the proteins used in this work were amplified by PCR. For this purpose, primers (MWG Biotech, Ebersberg) were designed to introduce restriction enzyme sites compatible with those present in the multiple cloning site of the vectors used (Table 4). 4-9 bases were added at the 5' ends of these primers, to allow an optimal activity of the restriction endonucleases. The following describes a typical PCR reaction and a PCR cycling program employed for the amplification of the products generated in this work (the only variable was the annealing temperature, which was chosen based on the melting temperature of the primers).

| 50 µl PCR reaction mixture | | PCR program | | |
|---|---|---|---|---|
| 5.0 µl | 10x cloned *Pfu* buffer | 1 x | 94°C | 2 min |
| 5.0 µl | DNA sample (200 ng) | 35 x | 94°C | 1 min |
| 1.0 µl | 5' primer (50 pmol/µl) | | 55°C | 1 min |
| 1.0 µl | 3' primer (50 pmol/µl) | | 72°C | 3 min |
| 5.0 µl | DMSO | 1 x | 72°C | 5 min |
| 2.0 µl | dNTP (25 mM each) | hold temperature at 4°C | | |
| 29.0 µl | $H_2O$ | | | |
| 2.0 µl | *Pfu* polymerase (5 U/µl) (NEB) | | | |

| Gene product | Sequence (5' → 3') | Restriction enzyme | Vector |
|---|---|---|---|
| *aae*L10 | F: CGATGCCATGGCTGAATTTGACAAGGAAGCTTAC | NcoI | pETM-CoEx |
| | R: CGACGGTACCTTACTGACCTCCTTTAGATTTTTCTTC | Acc65I | |
| *aae*L12 | F: CGATGCCATGGCAACTTTAACTATTGACGAG | NcoI | pETM-CoEx |
| | R: CGACGGTACCTTACTTGAGCTCGACTTCCGCTC | Acc65I | |
| *tma*L10 | F: CGTACGTCTCACATGCTGACCAGGCAACAGAAAG | BsmBI | pETM-ZZ |
| | R: CGACGGTACCTCATTCAGATTTTTTCTCTTAATAGC | Acc65I | |
| *tma*L12 CTD | F: GCTGTACAGCATATGACAGAGTTTGACGTCGTTTTG | NdeI | pETM22b(+) |
| | R: CTAATTGGATCCTTACTTCAGTTCCACTTCAGCACC | BamHI | |
| *tma*L12 CTD | F: GATACGTCTCACATGACAGAGTTTGACGTCGTTTTG | BsmBI | pETM-11 |
| | R: CTGAACTATGGTACCTTACTTCAGTTCCACTTCAGC | Acc65I | |
| *tma*EF-Tu (Gd) | F: GTTGTACAGCATATGGCGAAGGAAAAATTTGTGAGAAC | NdeI | pETM22b(+) |
| | R: CTCAGTGGATCCTTAATCAGGAATGTAGTTATCCATAG | BamHI | |
| *tma*EF-Tu (Gd) | F: GTATCACCATGGCGAAGGAAAAATTTGTGAGAAC | NcoI | pETM-11 |
| | R: CGTAGTGGTACCTTAATCAAGAATGTAGTTATCC | Acc65I | |
| *tma*L11 | F: GATTATCCATGGCAGAGAAAGTAGCGGCTCAG | NcoI | pETM-11 |
| | R: CCTGTCGGTACCTCAGTCCACTACTTCTATTC | Acc65I | |

**Table 4.** Oligonucleotide primers used for PCR amplification. The encoded gene product names, primers used, restriction sites inserted within the primers (also in red) and the vectors used for targeted cloning are indicated. For each primer pair, the forward primer is denominated F and the reverse R, respectively.


## C. Restriction digestion

Following PCR, the products of amplification were purified with the GFX purification kit (Amersham Biosciences, Freiburg) and subjected to digestion with appropriate restriction endonucleases, according to the manufacturer's instructions (New England Biolabs, Frankfurt). The enzymes used for restriction digestions of the various PCR products are mentioned in Table 4. In parallel, the vectors of interest were digested with compatible enzymes (Table 5). A general map of the pETM-series vectors is provided in the Suppl. Figure 1, Appendices.

| Vector | Source | Tag | Restriction enzymes |
|---|---|---|---|
| pETM-CoEx | EMBL (Heidelberg) | none | NcoI/Acc65I |
| pETM-11 | EMBL (Heidelberg) | N-terminal His$_6$ | NcoI/Acc65I |
| pETM-ZZ | EMBL (Heidelberg) | N-terminal His$_6$/ZZ double tag | NcoI/Acc65I |
| pET22b(+) | Novagen (Darmstadt) | none | NdeI/BamHI |

**Table 5.** Description of the vectors used in the cloning procedure. The vector names, their sources, the encoded tag (when present) and the restriction enzymes employed for directed cloning purpose are mentioned.

Digestions using appropriate restriction enzymes were performed as follows:

| 40 µl PCR product double digestion reaction | | 100 µl vector double digestion reaction | |
| --- | --- | --- | --- |
| 4 µl | 10X NEB buffer | 10 µl | 10X NEB buffer |
| x µl | DNA (2 µg) | x µl | vector (2 µg) |
| 1 µl | Enzyme 1 (10 U/µl) | 2 µl | Enzyme 1 (10 U/µl) |
| 1 µl | Enzyme 2 (10 U/µl) | 2 µl | Enzyme 2 (10 U/µl) |
| 1 µl | BSA (10 mg/ml) | 2 µl | BSA (10 mg/ml) |
| y µl | $H_2O$ | y µl | $H_2O$ |
| Incubation time: 4 h | | Incubation time: 4 h | |
| Incubation temperature: according to NEB | | Incubation temperature: according to NEB | |

## D. Ligation

The digested PCR products and vectors were separated on agarose gel and purified using the QIAquick gel extraction kit (Quiagen, Hilden) according to the manufacturer's instructions. Subsequently, the purified PCR products were ligated to the linearized vectors. For optimal ligation efficiency, a molar ratio insert:vector of 3:1 was employed. Ligation reactions were performed as follows:

| 10 µl ligation reaction | |
| --- | --- |
| 1 µl | 10X T4 DNA ligase buffer |
| x µl | linearized vector (100 ng) |
| y µl | DNA insert (300 ng) |
| z µl | $H_2O$ |
| 1 µl | T4 DNA ligase (2000 U/µl) (NEB) |
| Incubation conditions: 16°C, overnight | |

## E. Competent cells preparation by calcium chloride treatment

The resulting plasmids were transformed in *E. coli* competent cells by heat shock method. These cells were prepared from an *E. coli* DH5α strain (Invitrogen, USA) by calcium chloride treatment. Briefly, one colony of DH5α strain was inoculated in 5 ml Luria Bertani medium (LB, autoclaved prior usage at 121°C for 20 min, containing 10 g tryptone, 5 g yeast extract, 10 g NaCl and $ddH_2O$ up to 1 liter) and grown overnight at 37ºC. This pre-culture was inoculated in 50 ml LB medium. Cells were grown to mid-log phase ($OD_{595}$ of 0.7). Next, they were harvested for 10 min at 2000 rpm and resuspended in 25 ml of ice-cold 50 mM $CaCl_2$. After centrifugation for 10 min at 2000 rpm, cells were treated with 3 ml of ice-cold 50 mM $CaCl_2$ supplemented with 10% glycerol, aliquoted (100µl) and shock-frozen in liquid nitrogen.

## F. Transformation of *E. coli* cells by heat shock

Prior to transformation, a 100 µl aliquot of competent cells was thawed on ice. The ligation products were then added to competent cells. Next, this mixture was incubated on ice for 30 min, heat shocked at 42°C for 30 s and then retransferred for 2 min on ice. 900 µl of LB medium were added to the cells and the mixture was incubated at 37°C for 1h with gentle shaking. Finally, cells were spread onto LB plates (6 g agar in 400 ml LB broth, autoclaved at 121°C for 20 min, and subsequently supplemented to the appropriate antibiotic for selection) and incubated at 37°C overnight.

## G. Mini-preparation of plasmid DNA

From the resulting colonies, plasmid DNA was extracted using the QIAprep spin miniprep kit (Qiagen), according to the instructions of the manufacturer. Positive clones were identified by restriction mapping.

## H. DNA sequencing

The sequence accuracy of PCR products for each construct was confirmed by automated Sanger dideoxynucleotide sequencing (Sanger *et al.* 1977). The reactions and PCR cycling programs were established as follows:

| 20 µl sequencing reaction | | PCR program | | |
|---|---|---|---|---|
| 3.0 µl | sample (300 ng) | 1 x | 96°C | 1 min |
| 1.0 µl | sequencing primer (10 pmol/µl) | 25 x | 96°C | 30 s |
| 10.0 µl | $H_2O$ | | 55°C | 30 s |
| 6.0 µl | BigDye | | 60°C | 4 min |
| | | | hold temperature at 4°C | |

Following the temperature cycling, reactions were spun down briefly. To precipitate the samples, 15 µl 3 M sodium acetate pH 5.3, 65 µl $H_2O$ and 300 µl 100% ethanol were added and mixed. The samples were centrifuged at 13,000 rpm for 20 min at 15°C. The pellets were washed once with 750 µl 70% ethanol, air-dried and resuspended in 25 µl of template suppression reagent. The DNA was sequenced on an ABI PRISM 310 Genetic Analyzer (Applied Biosystems, Weiterstadt) by M. Killian or G. Dowe, MPI for Biophysical Chemistry, Göttingen.

The sequences obtained were verified by comparison with sequences published in the public database using the Vector NTI program (http://www.invitrogen.com/content.cfm?pageid=10373) and Blast 2 sequences program (http://www.ncbi.nlm.nih.gov/blast/bl2seq/wblast2.cgi).

## I. Site-directed mutagenesis

Several deletion constructs were produced using the QuickChange Site-Directed Mutagenesis Kit (Stratagene, Heidelberg) (Table 6). The resulting truncated constructs were verified by sequencing.

| Gene product | Sequence (5' → 3') / Mutagenized codon | Vector |
|---|---|---|
| *tma*L12 NTD | F: CTCGAAGACAAATTTGGATAGACTGCTGCTGCACCTGTG / 31 | pETM22b(+) |
| | R: CACAGGTGCAGCAGCAGTCTATCCAAATTTGTCTTCGAG | |
| *tma*L12 NTD/hinge | F: GCTGCCGGTGCCGCTCAGTAAGAAAAGACAGAGTTTGAC / 54 | pETM22b(+) |
| | R: GTCAAACTCTGTCTTTTCTTACTGAGCGGCACCGGCAGC | |
| *tma*L10$_{\Delta 2DBS}$ | F: GTGTGAAAGCTCCGATTACCTAGCTTGTGTTTGCATTGAGTGG / 154 | pETM-ZZ |
| | R: CCACTCAATGCAAACACAAGCTAGGTAATCGGAGCTTTCACAC | |
| *tma*L10$_{\Delta 1DBS}$ | F: GTTTGCATTGAGTGGTATTTTGTAGAATCTCGTGTATGTGCTCAATG / 164 | pETM-ZZ |
| | R: CATTGAGCACATACACGAGATTCTACAAAATACCACTCAATCCAAAC | |

**Table 6.** Oligonucleotide primers used for mutagenesis. The gene product names, primers used, STOP codon inserted within the primers (in red) and vectors used are indicated. In each primer pair, the forward primer is denominated F and the reverse R, respectively. The mutagenesis of *tma*L10:L12 NTD and *tma*L10:L12 NTD/hinge were performed using a previously described plasmid (Wahl *et al.* 2000b).

# II. Protein production

## A. Expression of native proteins

- ***aae*L10**, ***aae*L12**, ***tma*L12 CTD, *tma*EF-Tu(Gd)** (using pETM-11 for the latter two) were individually expressed in Rosetta(DE3) *E. coli* cell strain.

- ***eco*L10:L12** complex (from a biscistronic, pGEX-5x-3-based plasmid with sequential genes for GST-L10 and L12; this plasmid was kindly offered by M.V. Rodnina, Witten) was expressed in Rosetta(DE3) cell strain.

- ***tma*L10:L12**, ***tma*L10:L12 NTD**, ***tma*10:L12 NTD/hinge**, ***tma*L10$_{\Delta 1DBS}$:L12**, ***tma*L10$_{\Delta 2DBS}$:L12**, ***tma*L12 CTD** (based on pETM-11)**:EF-Tu** (based on pET22b(+)), ***tma*L12 CTD** (based on pET22b(+))**:EF-Tu** (based on pETM-11), ***tma*L10** (based on the pETM-ZZ)**:*eco*L12 (**based on pT7-6::rplL (Oleinikov *et al.* 1993)) were co-expressed after

co-transformation in Rosetta(DE3). For co-transformation, 1µl (0.5 µg/µl) of each plasmid was introduced in 100 µl Rosetta(DE3) cells, by heat-shock transformation procedure.

- ***tma*L11** was expressed in BL12(DE3) cell strain.

For expression purpose, *E. coli* cells from Rosetta(DE3) (Novagen, Darmstadt) and BL21(DE3) (Novagen) strains were prepared by calcium chloride treatment.

Following transformation, the cells were used to inoculate a starter culture of 100 ml LB supplemented with the appropriate antibiotics for selection. The antibiotics used in this study had the following concentrations: 30 µg/ml kanamycin (Boehringer, Mannheim), 34 µg/ml chloramphenicol (Boehringer) and 100 µg/ml ampicillin (Sigma, Deisenhofen). The starter culture was grown overnight at 37ºC. Next, the cells were harvested, resuspended in 12 ml fresh LB medium and distributed among 6 l LB medium supplemented with the required antibiotics. Cells were grown in 1 l shaking cultures at 37ºC and 200-250 rpm to mid-log phase ($OD_{595}$ of 0.7-0.8), induced by addition of 1 mM isopropyl-β-D-thiogalactopyranoside (Sigma) and harvested 4 h after induction. To avoid protease degradation of the overexpressed proteins, two Complete EDTA-free Protease Inhibitor Cocktail tablets (Roche, Mannheim) were added.

## B. Purification of native proteins

### 1. Purification of the *aae*L10:L12 complex

A crude cell extract was prepared by sonification on ice with a Branson (Danbury, USA) macrotip (50% pulsed, output 7) in lysis buffer (50 mM Tris-HCl, 50 mM NaCl, 5 mM DTT, 2 mM EDTA, pH 7.0, supplemented with lysozyme (Sigma)) and centrifuged for 45 min at 30,000 x g in a SA-600 rotor, run on a Sorvall centrifuge (Kendro, USA). The resulting S-100 fractions containing L10 and L12 overexpressed proteins were combined to reconstitute the *aae*L10:L12 complex. To ensure complex formation, combined cell lysates were incubated for 30 min at room temperature. Next, the complex was further purified by heat treatment at 90ºC. This purification step was rendered possible by the thermophilic properties of *Aquifex aeolicus* bacterium. Thus, most of *E. coli* proteins present in the cell lysate were denatured and precipitated through a centrifugation step at 30,000 x g for 20 min. The supernatant was loaded onto a HiTrap DEAE FF anion exchange column (Amersham Biosciences), which had been previously equilibrated with buffer A (50 mM Tris, 2 mM DTT, pH 7.0). The *aae*L10:L12 complex

was eluted with a linear gradient of buffer A and B (50 mM Tris, 500 mM LiCl or NaCl, 2 mM DTT, pH 7.0). As identified on a 15% SDS-PAGE (Laemmli 1970), the fractions containing the *aae*L10:L12 complex were pooled, concentrated to 2 ml (Millipore, Schwalbach) and loaded onto a HiLoad Superdex 75 (26/60) prep grade gel filtration column (Amersham Biosciences) run with Buffer C (10 mM, 50 mM LiCl or NaCl, 2 mM DTT, pH 7.0) to remove the uncomplexed protein and allow transfer to a buffer appropriate for crystallization. Thus, the fractions containing the complex were pooled, concentrated to 20 mg/ml and frozen in liquid nitrogen (KGV, Karlsruhe). The protein complex concentration was first measured by Bradford assay (Bradford 1976) and subsequently estimated using in-gel comparisons with proteins of known concentrations and according to (Wahl *et al.* 2000b). The authenticity of the purified complex was confirmed by mass spectrometry (performed by M. Raabe, U. Pleßmann, H. Urlaub, Research Group Mass Spectrometry, MPI for Biophysical Chemistry, Göttingen).

## 2. Purification of *tma*L10:L12, *tma*L10:L12 NTD, *tma*L10:L12 NTD/hinge, *tma*L10:*eco*L12, *tma*L10$_{\Delta2DBS}$, *tma*L12 CTD, *tma*EF-Tu(Gd) complexes

Unless otherwise specified, all purification steps were performed at 4ºC. The pellets obtained from 6 x 1 l culture were resuspended in 10 ml lysis buffer (20 mM Tris-HCl, 10 mM imidazole, 150 mM NaCl, 0.2% Igepal CA-630, 2 mM β-mercaptoethanol, pH 8.0, supplemented with Pefabloc SC (Biomol, Hamburg)). A crude cell extract was prepared by sonication. The cell lysate was cleared for 45 min at 30,000 x g. The resulting S-100 fraction was purified via affinity chromatography on Ni-NTA column (Quiagen). The proteins of interest bound to the Ni-NTA beads via their His$_6$-tags. The bound proteins were then washed with W1 (20 mM Tris, 10 mM imidazole, 150 mM NaCl, pH 8.0), W2 (20 mM Tris, 10 mM imidazole, 1 M NaCl, pH 8.0) and W3 (20 mM Tris, 30 mM imidazole, 150 mM NaCl, pH 8.0) buffers, to remove the *E. coli* proteins non-specifically attached to the beads. Next, the proteins were eluted with buffer A (20 mM Tris, 150 mM NaCl, 300 mM imidazole, pH 8.0) and brought into low-salt buffer B (20 mM Tris-HCl, 100 mM NaCl, pH 8.0) using PD-10 columns (Amersham Biosciences). The tags were removed by cleavage with tobacco etch virus protease (1 ml TEV protease (0,5 mg/ml) was incubated with the proteins resulting from 1 l culture for 2 h at RT and subsequently overnight 4°C) and the samples were re-purified on Ni-NTA beads to remove the TEV protease and the His$_6$ or His$_6$/ZZ tags. The flow-through was heated at 80°C for

20 min and centrifuged (30 min, 10,000 x g). This purification step was possible due to the thermophilic properties of this bacterium. Thus, most of the *E. coli* proteins present in the cell lysate were denatured and precipitated in a centrifugation step at 30,000 x g for 20 min. (The purification *via* heat denaturation was omitted for *tma*L10:*eco*L12, as the *eco*L12 protein is not stable above 65°C). The supernatant was concentrated and further purified by size exclusion chromatography (Superdex 75) with buffer C (10 mM Tris-HCl, 50 mM NaCl, 2 mM DTT, pH 8.0). Peak fractions corresponding to purified proteins or protein complexes were identified on SDS polyacrylamide gels (15 - 18%), pooled, concentrated to 8 - 10 mg/ml, frozen in liquid nitrogen and stored at −80ºC. The purity of the resulting preparations was estimated at >90% according to Coomassie blue-stained SDS gels. The authenticity of the purified products was confirmed by mass spectrometry.

### 3. Purification of the *eco*L10:L12 complex

The *eco*L10:L12 complex was isolated from a clarified lysate on glutathione affinity beads (Amersham Biosciences). Following several washing steps with 500 mM Tris pH 8.0, the complex was eluted with 10 mM reduced glutathione, 500 mM Tris pH 8.0. Subsequently, the protein complex was buffer exchanged in a low salt buffer 50 mM Tris, 100 mM NaCl, 5 mM $CaCl_2$, pH 8.0 (recommended for Factor Xa cleavage) with PD-10 columns. The GST tag was next removed by cleavage with 5 µl Factor Xa (2 U/µl; Novagen) for 20 h at 4°C and 3 h at RT on a head-over-tail rotor. This reaction was stopped by adjunction of 0.5 mM PMSF (Boehringer) for 1 h. The protein complex was further purified on a heparin column (HiTrap Heparin 5 ml; Amersham Biosciences) with a linear gradient of buffer A (20 mM Tris, 50 mM NaCl, 2 mM DTT pH 8.0) to buffer B (20 mM Tris, 500 mM NaCl, 2 mM DTT pH 8.0) and on a Superdex 75 size exclusion column (Amersham Biosciences) operated with 10 mM Tris, 50 mM NaCl, 2 mM DTT, pH 8.0. The fractions containing the *eco*L10:L12 complex were further concentrated (Millipore) to 10 mg/ml, frozen in liquid nitrogen and stored at −80ºC.

### 4. Purification of the *tma*L11 protein

The *tma*L11 protein was isolated from a clarified lysate on Ni-NTA affinity beads, washed and eluted as described in section II.B.2. Next, the protein was transferred in a low salt buffer containing 20 mM MES, 150 mM NaCl, pH 6.5 using PD-10 columns. Following the removal of the $His_6$-tag by TEV protease, the protein was heated at 80ºC for

20 min and centrifuged for 20 min at 10,000 x g. The supernatant was re-purified on Ni-NTA beads and subsequently buffer exchanged in 50 mM MES pH 6.5 with a HiTrap desalting column (Amersham Biosciences), concentrated to 1 ml and loaded onto a HiTrap CM cation exchange column. The protein was eluted with a linear gradient of buffer A (50 mM MES, 2 mM DTT, pH 6.5) and B (50 mM MES, 1 M NaCl, 2 mM DTT, pH 6.5). The peak fractions containing the purified protein were combined and buffer exchanged with PD-10 columns in buffer C (10 mM Tris, 50 mM NaCl, 2 mM DTT pH 7.0) for crystallization and in buffer D (20 mM $NaH_2PO_4$, $Na_2HPO_4$, 150 mM NaCl, 1 mM DTT, pH 7.0) for calorimetric studies.

### 5. Purification of TEV protease

This protein was expressed as a $His_6$-tagged protein in BL12(DE3)pLysS cells. A glycerol stock containing cells expressing TEV (Invitrogen) was used to inoculate 100 ml LB medium supplemented with 30 μg/ml kanamycin and 34 μg/ml chloramphenicol. The cells were grown overnight at 37°C. This pre-culture was used to inoculate 2 l of LB medium containing 30 μg/ml kanamycin. These cells were grown to mid-log phase. Prior induction, they were cooled at 25°C, induced by adjunction of 1 mM IPTG, grown at 25°C and 200 rpm and harvested 3 h post induction. The resulting pellet was resuspended in lysis buffer (20 mM Tris-HCl, 10 mM imidazole, 150 mM NaCl, 0.2% Igepal CA-630, 2 mM β-mercaptoethanol, pH 8.0). A crude cell extract from a 2 l of culture was prepared by sonification in lysis buffer and subsequently centrifuged at 30,000 x g for 45 min. The lysate was passed three times over a Ni-NTA column, washed with W1, W2, W3 (described in section II.B.2.) and eluted with 300 mM imidazole, 2 mM β-mercaptoethanol, 20% glycerol. Next, the protein was buffer exchanged in 20 mM Tris, 100 mM NaCl, 20% glycerol, 2 mM DTT, pH 8.0 using PD-10 columns. Subsequently, one volume of glycerol was added. The protease was then rapidly aliquoted to prevent degradation, flash-frozen in liquid nitrogen and stored at –80ºC.

## C. Expression of the selenomethionine-derivatized protein

The expression of the selenomethionine-containing *tma*L10:L12 NTD complex was performed using the methionine auxotrophic *E. coli* B834(DE3)pLysS (Novagen) strain according to (Budisa *et al.* 1995).

Following co-transformation with plasmids containing *tma*L10 and *tma*L12 NTD genes, cells were added to a starter culture of 100 ml minimal medium supplemented with the required antibiotics (30 µg/ml kanamycin, 34 µg/ml chloramphenicol and 100 µg/ml ampicillin) and grown overnight at 37°C. The minimal medium contained a salt solution (comprising NaCl, $(NH_4)_2SO_4$, $MgSO_4$, $CaSO_4x2H_2O$, $FeH_8N_2O_8S_2x6H_2O$ supplemented with 0.4% glucose, 10 mg/ml thiamine and 10 mg/ml biotin), a trace elements solution (containing 1 µg/ml of each $MnCl_2$, $CuSO_4x5H_2O$, $Na_2MoO_4$, $ZnSO_4$ compound) and a potassium phosphate solution containing 0.083 g/l of all amino acids except methionine. To the final composition of the minimal medium 0.3 mM selenomethionine was added. The overnight culture was harvested, resuspended into 12 ml of fresh minimal medium and subsequently distributed among 6 l culture. The cells were grown at 37°C, 250 rpm to mid-log phase, induced with 1 mM IPTG and harvested 8 h after induction.

## D. Purification of the selenomethionine-derivatized protein

The protocol of purification used was as described for the native *tma*L10:L12 NTD protein complex (section II.B.2.). The final preparation was concentrated to 8 mg/ml.

# III. Crystallization

## A. Principles of protein crystallography

The process of X-Ray crystallographic structure determination of a protein consists of: (i) crystal growth, (ii) data collection, (iii) solution of the phase problem, (iv) generation of the atomic model (model building), and (v) fitting the atomic model to the measured data (refinement) (Drenth 1994; Rodes 2000).

### 1. Crystal growth

The first essential step in determining the X-ray structure of a protein is to grow crystals to sufficient size and quality. A highly pure and concentrated protein (5 - 20 mg/ml) is dissolved in a suitable solvent from which it must be precipitated in a crystalline form. Crystallization occurs when the concentration of the protein in solution is greater than its limit of solubility (protein supersaturation). There are three stages of crystallization: nucleation, growth and cessation of growth.

Crystallization methods include: vapor diffusion, dialysis, microbatch, seeding etc. Among these methods, one of the most commonly used is vapor diffusion. In this approach, the initial reagent concentration in the droplet is lower than that in the reservoir. Over time, the reservoir will pull water from the droplet in a vapor phase, such that an equilibrium will occur between the drop and the reservoir. During this equilibration process, the sample is also concentrated, thereby increasing the supersaturation of the sample in the drop. Two vapor diffusion techniques are frequently employed: sitting drop and hanging drop. In the sitting drop technique (frequently employed in the present work), one places a small droplet of the sample mixed with crystallization reagent on a platform in vapor equilibration with the reagent (Figure 7). In the hanging drop technique, one places a small droplet of the sample mixed with the crystallization reagent on a siliconized glass cover slide inverted over the reservoir in vapor equilibration with the reagent.
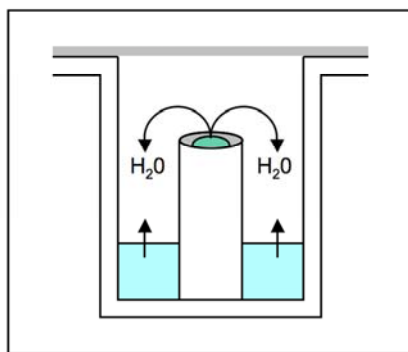


**Figure 7.** Sitting drop vapor diffusion technique. A drop composed of a mixture of sample and reservoir solution is placed in vapor equilibration with a liquid reservoir of reagent. In order to achieve equilibrium, the water leaves the droplet and eventually ends up in the reservoir. If the reservoir solution contains a volatile compound (e.g. alchool), the equilibrium will be reached through an interchange between both droplet and reservoir solutions.

## 2. Data collection

The resulting crystal is exposed to X-rays for structure determination, as the wavelength of X-rays is comparable to the interatomic distances of a crystal. The conventional X-ray sources are: (i) the sealed tube (in which X-rays are produced by bombarding a metal target, usually copper, with electrons produced by a heated filament and accelerated by an electric filed), (ii) the rotating anode, with a higher intensity, (iii) the synchrotron with a high intensity X-ray radiation and high tunability (allowing the selection of radiation with a wavelength of 1 Å or below). When a crystal is placed in the path of an X-ray beam, it diffracts the source beam into many discrete beams. The X-rays

are scattered exclusively by the electrons in the atoms. Each of the resulting beams will produce a distinct spot (reflection) on a detector. To collect a full set of reflections, it is necessary to rotate the crystal, in small steps, by an angle determined by its degree of symmetry. Each reflection is given co-ordinates *h*, *k*, *l* (reciprocal space coordinates) and an intensity. Because X-rays cannot be optically focused (they simply continue in a straight line when they enter most solids), each ray that caused a diffraction spot has to be traced back to the structure that diffracted it. To achieve this tracing, one needs to determine not only the position and intensity of each spot, but also the phase. Each diffracted ray from a crystal unit cell recorded by a reflection *hkl* is described by a structure factor *F(hkl)*. The latter represents a vector characterized by frequency (that of the X-ray source), amplitude *|F(hkl)|* (derived from the intensities of the spots) and phase *α(hkl)*. Following the diffraction pattern acquisition, an electron density map can be calculated, which is basically the image of the structure of interest. The calculation of the electron density ρ at every position x, y, z (real space coordinates) in the unit cell is done with a Fourier transform and is defined as:

$$\rho(xyz) = \frac{1}{V} \sum_h \sum_k \sum_l |F(hkl)| \exp[-2\pi i(hx + ky + lz) + i\alpha(hkl)]$$

where *V* is the unit cell volume and *i* represents the contribution of each atom.

Thus, to obtain the electron density throughout the unit cell, one needs to know the amplitude *|F(hkl)|* and the relative phase angles *α(hkl)*. The amplitude results from the diffraction data, as it is the square root of the measured intensity *I(hkl)*. However, the phase angles cannot be derived from the diffraction pattern.

### 3. Solution of the phase problem

Several methods have been developed in order to deduce phases for reflections, including Molecular Replacement (MR), Single Isomorphous Replacement (SIR), Multiple Isomorphous Replacement (MIR), Single-wavelength Anomalous Dispersion (SAD) and Multi-wavelength Anomalous Dispersion (MAD). Combinations of several of the above mentioned approaches, e.g. MIRAS (Multiple Isomorphous Replacement using Anomalous Scattering) and SIRAS (Single Isomorphous Replacement using Anomalous Scattering) proved to be useful for experimental phasing of a number of structures. Three of the most common methods to obtain phases are MIR, MAD and MR.

Multiple isomorphous replacement (MIR) represents a method of choice for determination of phases of a completely unknown structure. This method involves collection of data from crystals of the protein alone, and crystals soaked in various *heavy-atom compounds* (e.g. ions or ionic complexes of Hg, Pt, Au, Ta, U etc.). If heavy atoms bind specifically to the protein, their locations can be identified, and the phase problem can be solved from the difference in the structure factors between the protein and its heavy-atom derivatives (isomorphous differences). Frequently, more than one heavy atom derivative is necessary due to the ambiguity of the phase angle. In addition, heavy atoms absorb X-rays of a specified wavelength. As a result of this absorption, the Friedel law postulating that $|F(hkl)| = |F(-h-k-l)|$ and $\alpha(hkl) = -\alpha(-h-k-l)$ does not hold. The inequality of symmetry-related reflections is called anomalous dispersion. The measurement of the differences between Friedel pairs (termed Bijvoet differences) leads to an additional source of information from the heavy atom. Thus, MIR can make use of both isomorphous and Bijvoet differences.

Multi-wavelength anomalous dispersion (MAD) can be considered an ideal case of MIR because (i) scattering of *preexisting* atoms in the crystal is varied by changing the X-ray wavelength and (ii) only one crystal is measured, resulting in a perfect isomorphism. An example of an atom, which can be scattered by changing the X-ray wavelength, is selenium (this atom is introduced during the preparation of protein, by replacing the conventional methionine with selenomethionine). In this approach the wavelength is varied around the absorption edge of such an atom. At these wavelengths, there is significant variation in the real f' and imaginary components f'' of the anomalous scattering of these special atoms. The best is to select a peak wavelength ($\lambda 1$) where f'' has its maximum, inflection point ($\lambda 2$) where f' has it maximum and one or more remote points at which f' is substantially closer to zero than at the edge. However, the signal obtained from anomalous scattering is normally quite small (compared to conventional heavy atom phasing), therefore high occurrence of scatterers (a rule of thumb is one Se per 15-20 kD) and precise measurement of the signals are required.

Molecular replacement (MR) can be used when a good model for a reasonable portion of the structure in the crystal is known. As a rule of thumb, MR is straightforward if the known model and the unknown protein share approximately 40% sequence identity or if, for another reason, the two structures are expected to have a very similar fold of their polypeptide chain. Placement of the molecule in the target unit cell requires a rotation and

a translation step. In the rotation step, the spatial orientation of the known and the unknown molecule with respect to each other is determined, while in the next step, the translation needed to superimpose the now correctly oriented molecule onto the other molecule is calculated.

### 4. Model building

An interpretable electron density map can usually be produced after density modification and phase combination. Following these steps, the atoms can be traced in the electron density.

### 5. Structure refinement

Refinement is the process of adjusting the model to fit to a closer agreement between the calculated and the observed structure factors and is represented by the crystallographic R-factor. In addition to lowering the R-factor, the structural parameters should indicate a model that is chemically, stereochemically and conformationally reasonable.

## B. Crystallization experiments

Crystallization was performed on the in-house high-throughput facility, a nano drop robot (Cartesian Dispensing System MicroSys 4000XL, Genomic Solutions Ltd, UK). This apparatus was programmed to set up 100 nl-scale vapor diffusion sitting drop crystallization experiments in 96-well plates (containing 100 µl reservoir solutions). The process was controlled by a computer using AxSys software. An overview of the crystallization experiments performed with different protein complexes is provided in Table 7. The initial conditions that yielded crystals using the nano drop robot were subsequently scaled up to microliter range and refined by screening the effects of precipitant, additives and pH. Thus, droplets were set up by mixing 0.5 - 1 µl protein (8 - 20 mg/ml) with 1 µl reservoir and were equilibrated against 500 µl reservoir. The techniques used for the refinement of the crystallization conditions were: sitting drop (for most of the screens) and hanging drop vapor diffusion.

| Proteins | Conditions screened | Source | T °C | Crystal forms |
|---|---|---|---|---|
| *aae*L10:L12 | 288 | Hampton Research (USA)<br>Emerald BioStructures (USA)<br>Sodium malonate screen (made)<br>Ammonium sulfate screen (made) | 4, 20 | |
| *tma*L10:L12 | 1344 | Hampton Research<br>Emerald BioStructures<br>Sodium malonate screen<br>Ammonium sulfate screen<br>Nextal Biotechnologies (Canada) | 4, 20 | 1 |
| *tma*L10:L12 NTD | 384 | Hampton Research<br>Emerald BioStructures<br>Nextal Biotechnologies | 20 | 3 |
| *tma*L10$_{\Delta 2DBS}$:L12 | 288 | Hampton Research<br>Nextal Biotechnologies | 20 | |
| *tma*L12 CTD:EF-Tu(Gd):GMPPNP | 672 | Hampton Research<br>Nextal Biotechnologies | 20 | 1 |
| *tma*L12 CTD:EF-Tu(Gd):GDP | 672 | Hampton Research<br>Nextal Biotechnologies | 20 | |
| *tma*L12 CTD:EF-G:GMPPNP | 672 | Hampton Research<br>Nextal Biotechnologies | 20 | |
| *tma*L12 CTD:L11 | 1152 | Hampton Research<br>Nextal Biotechnologies | 20 | |

**Table 7.** High-throughput crystallization experiments with several protein complexes from *Thermotoga maritima* and *Aquifex aeolicus*.

- *tma*L10:L12 yielded needle-like crystals after 7 days at 20°C in several conditions containing PEG 3350 as a precipitant. After improvement, two conditions gave rise to single, large, needle-shaped crystals. The optimized reservoir formulations were:
- condition I (derived from Index screen condition 72, Hampton Research): 0.2 M NaCl, 0.1 M Tris pH 8.0, 20% PEG 3350 (also with pH ranging from 7.0 to 8.0);
- conditions II (derived from Index screen condition 80, Hampton Research): 0.4 M ammonium acetate, pH 7.2, 25% PEG 3350 (similar crystals were grown in the same conditions with pH ranging from 7.2-8.2).

*tma*L10:L12 crystals obtained from condition I and II could be directly frozen in a liquid nitrogen stream and subjected to diffraction data acquisition.

- Crystals of *tma*L10:L12 NTD appeared within a day at 20°C. Three crystal forms were obtained from the following conditions:

- crystal **Form I** (SeMet): 0.2 M ammonium acetate, 0.1 M Na-HEPES, pH 7.2, 42% MPD (from Index screen number 52, Hampton Research);

- crystal **Form II** (native): 0.2 M $MgCl_2$, 0.1 M imidazole, pH 8.0, 40% MPD (condition number 34 of Cryo I screen, Emerald BioStructures);

- crystal **Form III** (native): Na-acetate, pH 4.5, 50% ethylene glycol, 5 % PEG 1000 (final pH 5.1) (from Cryo I number 12, Emerald BioStructures).

All these crystals possessed a cryo-buffer in their reservoir solution and could be therefore directly frozen in a liquid nitrogen stream and subjected to data collection.

- The initial crystallization condition for the *tma*L12 CTD:EF-Tu(Gd):GMPPNP putative crystals was Classics number 69 (Nextal Biotechnologies). Larger crystals were obtained with 0.05 M $KH_2PO_4$, 25% PEG 8000. Further screening and testing of these crystals are ongoing.

## C. Data collection and processing

- Initially, crystals of *tma*L10:L12 were tested for their diffraction ability on the in-house source. Diffraction images were collected at 100K on a Mar345 image plate (MarResearch, Eppendorf) equipped with a copper rotating anode generator (Nonius, Solingen). However, these crystals did not diffract X-Rays to high resolution (7-7.5Å). The diffraction pattern extended to 3.5 Å for the crystals belonging to condition II and a complete data set was collected on a Mar225 CCD detector at Swiss Light Source synchrotron (Villigen, Switzerland). *tma*L10:L12 crystals belonged to the R32 space group.

- Data sets for all three crystal forms of *tma*L10:L12 NTD were collected at beamline BW6 (DESY, Hamburg) at 100K on a Mar-Research CCD detector. Anomalous data were recorded at four wavelengths around the selenium K-edge from a SeMet-derivatized crystal of Form I. The crystal Form I diffracted to 2.3 Å and belonged to the orthorhombic space group. The native *tma*L10:(L12 NTD)$_6$ complexes yielded an orthorhombic and a monoclinic crystal forms that diffracted to 2.1 Å and 1.9 Å resolution, respectively. All complexes contained one L10 molecule and six L12 NTD molecules in the asymmetric unit. The X-Ray data were indexed and integrated with DENZO and scaled with SCALEPACK (Otwinowski and Minor 1996).

### D. Phase generation, model building and refinement

- Using peak-, inflection point-, and high energy remote data of the SeMet MAD experiment on a crystal Form I of *tma*L10:L12 NTD, six selenium sites could be located and refined with Shelx D (Schneider and Sheldrick 2002). Initial phase calculations and solvent flattening to derive the hand of the heavy atom positions were carried out with Shelx E. The phases output from Shelx E were further refined with DM (Collaborative Computational Project, 1994), that generated a high quality electron density map. The chain autotracing was done with ARP/wARP (Morris *et al.* 2003). Model building was completed manually with MAIN (http://www-bmb.ijs.si/doc/index.html). The crystal Forms II and III were subsequently solved by molecular replacement (Collaborative Computational Project 1994) using the Form I structure coordinates. All three crystal forms were refined with CNS (Brunger *et al.* 1998) using simulated annealing, positional and temperature factor refinement protocols. The water molecules were placed automatically with CNS and checked manually in MAIN.

- *tma*L10:L12 structure was solved by molecular replacement using the crystal structure of *tma*L10:(L12 NTD)$_6$ as a search model. The L10 NTD and the L10 helix α8-(L12 NTD)$_6$ were used as separate parts. The structure did not reveal electron densities corresponding to the hinges and CTDs of L12.

### E. Structure analysis

The molecular geometry of the *tma*L10:L12 NTD structure was validated with PROCHECK (Laskowski *et al.* 1993). Figures were prepared with PyMol (http://pymol.sourceforge.net). The intermolecular contacts were analyzed using the Protein-Protein Interaction Server (http://www.biochem.ucl.ac.uk/bsm/PP/server/).

## IV. Stoichiometry of L10:L12 complexes

### A. Multiple sequence alignment

The sequence alignment of bacterial L10 proteins and of archaeal L10E, yeast P0 and human P0 proteins was performed with Clustlal_X (Thompson *et al.* 1997), using default parameters, and displayed with ALSCRIPT (Barton 1993).

### B. Multi-angle laser light scattering

For molar mass measurements, purified *tma*L10:L12, *tma*L10:L12 NTD, *tma*L10:L12 NTD/hinge, *tma*L10:*eco*L12, *aae*L10:L12, *eco*L10:L12 complexes (200 μl samples at 2 mg/ml in complex) were analyzed by asymmetric flow field-flow fractionation using an Eclipse F particle sizing system (Wyatt Technologies Corporation, USA), operated in phosphate buffered saline (PBS), pH 7.4 (for a number of samples the measurement was repeated with a buffer containing 10 mM Tris, 50 mM NaCl pH 8.0), at room temperature. Ultra pure BSA (2 mg/ml) was used as a control. The L10:L12 complexes eluted as single peaks and were analyzed by multi-angle laser light scattering on a 18-angle DAWN EOS light scattering detector (Wyatt Technologies), equipped with a 30 mW Gallium-arsenide 690 nm laser light source and on an Optilab DSP differential interferometric refractometer (these results are summarized as an application note at http://www.wyatt.com/literature/ribozymesubunits.pdf). Data were analyzed using Astra software (Wyatt Technologies).

## V. CD spectroscopy studies of *tma*L10:L12 complex

Circular dichroism (CD) is commonly used in denaturation experiments in which the CD signal of a protein is monitored while the protein is perturbed in some fashion (e.g. increasing temperature, chemical denaturation). *tma*L10:L12 (0.1 mg/ml) was measured in PBS, pH 7.4. The thermal melting profile (molar ellipticity values *versus* temperature) was monitored at 222 nm on a Jasco 720 spectropolarimeter (Gross-Umstadt) between 25°C and 85°C. The heating rate was 60°C/h.

## VI. Characterization of the interaction between *tma*L12 CTD and elongation factors using Biacore

Interaction studies between *tma*L12 CTD and *tma*EF-Tu(Gd) or *tma*EF-G were performed on a Biacore X (Sweden). Biacore system exploits the surface plasmon resonance (SPR) as a detection principle to monitor the interaction between biomolecules in real time. The minute amounts in mass concentrations at the surface of the sensor chip as a consequence of the association and dissociation between the molecules is measured as an SPR response,

and is displayed as a function of time on a graph known as sensorgram. The effects of EF-Tu(Gd), EF-Tu(Gd):GTP and EF-G on the binding to His$_6$-tagged L12 CTD (that had the ability to covalently bind to a Ni-NTA sensor chip) were evaluated. The buffer of the system was 10 mM HEPES, 150 mM NaCl, 0.005% Tween 20 pH 7.4 and was run at 10 µl/min. The EF-Tu(Gd):GTP complex was prepared in buffer A (50 mM Tris, 30 mM KCl, 1 mM MgCl$_2$, pH 7.6) as follows: EF-Tu (84 nmol) was incubated with 1 mM GTP, 3 mM phosphoenolpyruvate, 10 µg/ml pyruvate kinase for 15 min at 37°C. Except for the His$_6$-L12 CTD:EF-Tu(Gd):GTP interaction (where approximately 200 nM of both His$_6$-L12 CTD and EF-Tu(Gd):GTP were used), all the experiments were performed with a concentration of 100 nM for each protein.

## VII. Calorimetric analysis of the *tma*L11:L12 CTD complex

The interaction between *tma*L12 CTD and *tma*L11 proteins was quantitated by isothermal titration calorimetry in a microcalorimeter (MicroCal Inc., UK). Prior measurements, both proteins were buffer exchanged with PD-10 columns in 20 mM NaH$_2$PO$_4$/Na$_2$HPO$_4$, 150 mM NaCl, 1 mM DTT, pH 7.0 buffer and degassed. The solution of *tma*L12 CTD (135 µM, 2.5 ml) was thermally equilibrated against the reference cell containing buffer at 20°C. Next, 12 injections of a solution of *tma*L11 (1 mM, 500 ml) were performed, and the energy required to reestablish thermal equilibrium between the two cells after each addition was measured and plotted in microcalories per second. Integration yielded the enthalpy of complex formation in kilocalories per mole. The stoichiometry of complex formation was calculated using the manufacturer's software.

## VIII. Preparation of *Thermotoga maritima* ribosomes

Ribosomes from *T. maritima* MSB8 were prepared as described (Rodnina and Wintermeyer 1995), except for opening of the cells by a French press (*T. maritima* MSB8 cells were a kind gift from K.O. Stetter, Regensburg). 70S ribosomes were prepared as follows: frozen *T. maritima* MSB8 cells (50 g, wet weight) were opened by a French press (14000-16000 psi, the crude extract was passed twice onto the French press) in 100 ml of buffer A (20 mM Tris-HCl, pH 7.6, 100 mM NH$_4$Cl, 10 mM magnesium acetate, 0.5 mM EDTA, 3 mM β-mercaptoethanol containing DNase I (RNase-free; Boehringer) at 3

µg/ml). The S-30 fraction was layered in portions of 16 ml on 9 ml of 1.1 M sucrose in buffer B (20 mM Tris-HCl, pH 7.6, 0.5 M $NH_4Cl$, 10 mM magnesium acetate, 0.5 mM EDTA, 3 mM β-mercaptoethanol). After centrifugation for 16 h at 33,000 rpm in a Beckman Ti 50.2 rotor, ribosomes were washed by dissolving the pellets in 200 ml of the same buffer, incubating for 2 h, and sedimenting portions of 20 ml through 1.5 ml of 1.1 M sucrose in the same buffer (Ti 50.2, 6 h, 45,000 rpm). The washing step was repeated twice, and the final centrifugation was made in a Beckman SW-28 rotor for 20 h at 28,000 rpm. Pellets were resuspended in buffer C (10 mM Tris-HCl, pH 7.6, 60 mM $NH_4Cl$, 5 mM magnesium acetate, 0.25 mM EDTA, 3 mM β-mercaptoethanol) containing 5% sucrose. The 70S tight couples were isolated by zonal centrifugation in a Beckman Ti15 rotor (17 h, 28,000 rpm) on a convex exponential gradient from 10% to 37% sucrose (1.4 liters) in buffer C. The 70S peak was collected, and ribosomes were pelleted (Ti 50.2, 20 h, 45,000 rpm), resuspended in buffer D (50 mM Tris-HCl, pH 7.6, 70 mM $NH_4Cl$, 30 mM KCl, 7 mM $MgCl_2$, 1 mM DTT, 0.5 mM EDTA), frozen in small portions in liquid nitrogen, and stored at −80°C. Ribosome concentrations were determined from absorption measurements on the basis of 23 pmol/$A_{260}$ unit. Unless otherwise specified, all operations were performed at 4°C.

# IX. Measurement of the *Thermotoga maritima* ribosomal activity

To prepare a 70S initiation complex, 0.4 µM of 70S ribosomes were incubated with a mix of 0.68 µM *E. coli* initiation factors (IF1, IF2, IF3), 0.8 µM f[$H^3$]Met-tRNA$^{fMet}$ (3200 dpm/pmol), 0.8 µM of mRNA (Rodnina and Wintermeyer 1995), 1 mM GTP, and up to 150 µl buffer A  (50 mM Tris, 70 mM $NH_4Cl$, 30 mM $KCl_2$, 7 mM $MgCl_2$, pH 7.6). The reaction mixture was left at 37°C for 1 h. 25 µl of this reaction corresponding to 10 pmol of ribosomes were rapidly filtrated through a 0.45 µm nitrocellulose filter (Sartorius, Göttingen), pre-equilibrated with buffer A. Next, the filter was washed extensively with buffer A and subsequently dissolved in a scintillation cocktail QS361 (Zinsser, Frankfurt). To measure the amount of f[$H^3$]Met-tRNA bound to the ribosome, the $^3H$ radioactivity was monitored in a Packard 2500 scintillation counter. Activities of the ribosomes in partial reactions of initiation, as measured by nitrocellulose filtration, were 25.2% after 1 h.

# Results

## I. Expression screening of L10 and L12 proteins from different bacteria

In order to produce a full-length L10:L12 complex, genes coding for the respective proteins were subcloned either individually in different expression vectors, or in the co-expression vector pETM-CoEx (EMBL, Heidelberg).

The *rplJ* and *rplL* genes coding for L10 and L12 proteins, respectively, from several thermophilic bacteria (*Aquifex aeolicus*, *Thermus thermophilus* and *Thermotoga maritima*) were selected for this study. Although most detailed functional studies of the protein synthesis mechanisms were carried out in *E. coli*, proteins from thermophilic organisms were chosen for their high thermostability and increased resistance to proteases. In addition, they appeared more suitable for crystallization and structural studies. Indeed, high resolution structures of the bacterial ribosome (Schluenzen *et al.* 2000; Wimberly *et al.* 2000; Yusupov *et al.* 2001), individual ribosomal proteins (Liljas and Garber 1995) and translation factors (Berchtold *et al.* 1993; Ævarsson *et al.* 1994) were derived from thermophilic organisms. Of particular importance for this study was the crystal structure of the isolated protein L12 from *Thermotoga maritima*, which yielded high quality crystals (Wahl *et al.* 2000a; Wahl *et al.* 2000b), in contrast to its *E. coli* ortholog, which disintegrated in time and provided high quality crystals only for the C-terminal part (Liljas *et al.* 1978).

Four *E. coli* cell strains were used as hosts for the expression of L10 and L12 proteins: BL21(DE3), BL21(DE3)pLysS, BL21(DE3)CodonPlus-RIL and Rosetta(DE3). An expression screening aiming to characterize the best vectors and cell strains for L10 and L12 protein production was performed. Its outcome is presented in Table 8. Based on this data, only few constructs leading to optimal results were selected for subsequent protein production and crystallization (described in detail in sections II and III).

| vectors | aae | | | tth | | tma | |
|---|---|---|---|---|---|---|---|
| | L10 | L12 | L10:L12 | L10 | L12 | L10 | L12 |
| pETM-CoEx | + | + | + | - | + | - | + |
| pGEX6P1 | - | | | - | | - | |
| pETM-10 | | | | + | | + | |
| pETM-11 | | + | | + | | + | |
| pETM-20 | | | | + | | + | |
| pETM-30 | | | | + | | + | |
| pETM-ZZ | | | | + | | + | |

**Table 8.** Expression pattern of L10 and L12 proteins from several thermophilic organisms (*aae: Aquifex aeolicus*, *tth: Thermus thermophilus*, *tma: Thermotoga maritima*) in four different *E. coli* strains. The vectors used for gene expression are also indicated. (+) constructs leading to L10 and L12 expression in all four *E. coli* strains tested; (-) constructs that failed to yield any L10 or L12 activity in all four *E. coli* strains tested. In red are depicted the constructs which were further used for protein complex production and crystallization. Several clones of both *tth*L10 and *tma*L10 in pETM-series vectors were produced together with U. Reidt, Cellular Biochemistry/X-Ray Crystallography Department, MPI for Biophysical Chemistry, Göttingen.

# II. L10:L12 complex from *Aquifex aeolicus*

## A. Production of the protein complex

As outlined in Table 8, an optimal expression of L10 (*aae*L10) and L12 (*aae*L12) proteins from *Aquifex aeolicus* was achieved using pETM-CoEx vector in Rosetta(DE3) cell strain.

Both *aae*L10 and *aae*L12 proteins were independently produced without affinity tag and displayed high solubility and stability. To reconstitute the complex, cell lysates containing overexpressed *aae*L10 and *aae*L12 proteins were pooled and purified by heat treatment at 90°C. This approach simplified subsequent chromatographic procedures, as most of *E. coli* proteins were denatured and precipitated. A similar purification procedure using heat treatment at 90°C was reported for EF-G from the same bacterium, without precipitation of the target protein (Martemyanov *et al.* 2000). Next, the protein complex was further purified *via* anion exchange chromatography, eluting at approximately 300 mM NaCl from a DEAE column. The complex was subjected to size exclusion chromatography, concentrated, and used for crystallization trials. An overview of this purification procedure is presented in Figure 8.
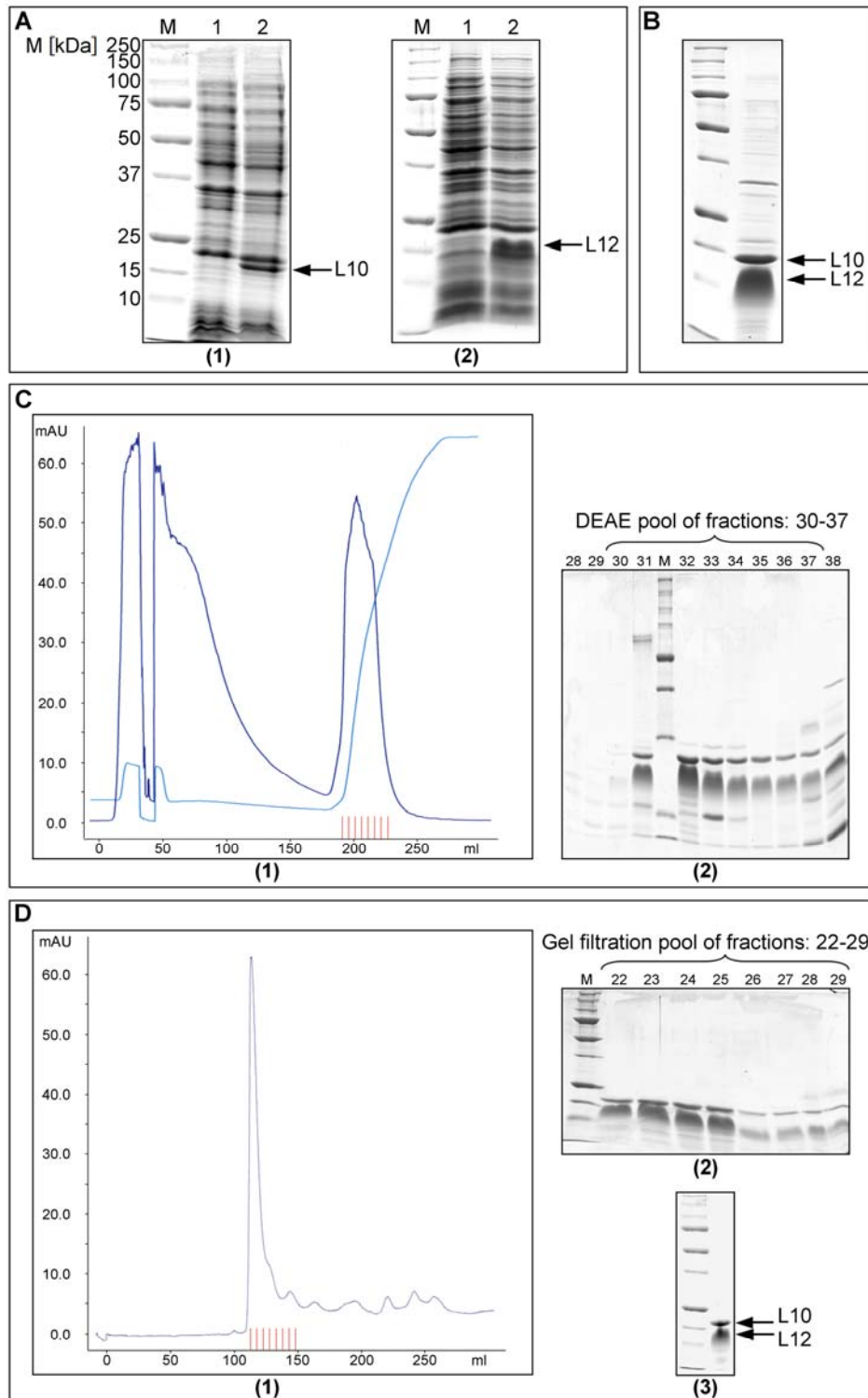
**Figure 8.** Expression and purification of L10:L12 protein complex from *A. aeolicus*. **(A)** (1) *aae*L10 expression. Prior induction (lane 1) and post induction (lane 2) phases are indicated. (2) *aae*L12 expression, labeling as for (1) **(B)** Reconstituted *aae*L10:L12 complex after heating at 90°C step. **(C)** Anion exchange chromatography. (1) Chromatogram representing the elution profile of the *aae*L10:L12 complex on a HiTrap DEAE column. On the x-coordinate is represented the volume [ml], whereas UV absorption at 280 nm [mAU] is provided on the ordinate. (2) Fractions containing purified *aae*L10:L12 complex (30-37) were subjected to gel filtration. **(D)** Size exclusion chromatography. (1) Chromatogram representing the elution profile of the *aae*L10:L12 complex on a HiLoad 26/60 Superdex 75 prep grade column. (2) Fractions containing the purified complex (22-29) were concentrated. (3) *aae*L10:L12, final preparation control.

## B. Validation of the complex formation

In isolation, the thermophilic archaeon *Sulfolobus solfataricus* L10 and L12 proteins were found to form a very stable complex, that could not be disrupted even using high concentrations of denaturation agents such as 6 M urea (Casiano *et al.* 1990). In the present work, the *aae*L10:L12 complex formation was ascertained by (i) differences in heat stability of the L10:L12 complex, as compared to its constituent proteins, and (ii) gel filtration. By heating individual *aae*L10 and *aae*L12 proteins to different temperatures ranging from 60 to 90°C, different abilities to withstand high temperatures were evidenced. The isolated *aae*L10 protein was unstable, rapidly precipitating above 70°C (Figure 9A). Moreover, attempts to purify L10 were not successful due to its loss during purifications steps (data not shown). Conversely, *aae*L12 protein was found very stable at all the tested temperatures (Figure 9B). This observation was in keeping with a previous experiment demonstrating the property of the sole L12 protein to retain some of its secondary structure elements even at extreme conditions of pH (its own pI is 4.9, suggesting a very acidic protein), temperature or 6 M guanidinium hydrochloride (Luer and Wong 1980). Remarkably, the *aae*L10:L12 complex was stable even at 90°C, suggestive for its formation and stability (Figure 8B). The stabilization of the secondary and tertiary structures of L10, only when complexed to L12, was also observed using calorimetry and CD spectroscopy for the *E. coli* counterparts (Gudkov *et al.* 1978).
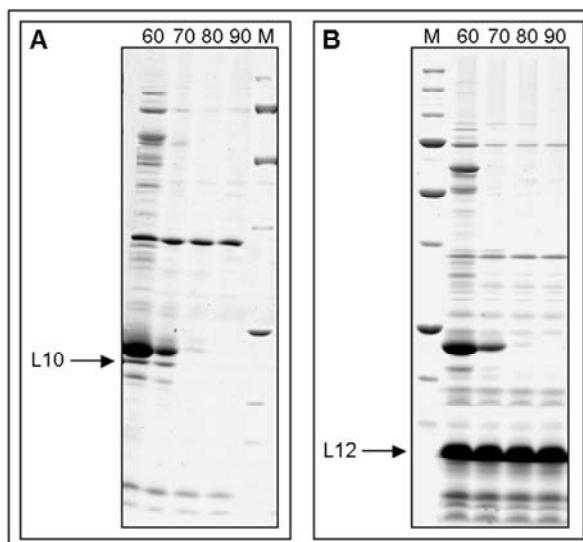


**Figure 9.** Heat treatment at 60, 70, 80, 90°C of S-100 fractions containing the overexpressed proteins L10 or L12, respectively. **(A)** Heat treatment of protein L10 indicates a denaturation above 70°C. **(B)** Conversely, L12 is stable at all the tested temperatures.

In line with heat denaturation experiments, the gel filtration profile (Figure 8D-1) showed an early elution, indicative for the complex formation, rather than individual *aae*L10 and *aae*L12, which are low-molecular weight r-proteins (22.5 and 13.5 kD, respectively), and therefore expected to exhibit a late elution.

### C. Crystallization trials

The *aae*L10:L12 protein complex (20 mg/ml) was subjected to crystallization by means of vapor diffusion. Mainly the sitting drop technique was employed. 288 conditions, covering a wide range of pH, precipitants and additives, were screened (Table 7). The protein was found stable in numerous conditions employed for crystallization. Both 4 and 20°C temperatures were tested. Despite these attempts, as well as usage of several protein concentrations or different ratios of protein:reservoir in the drop, crystallization of the *aae*L10:L12 complex proved to be unsuccessful.

## III. L10:L12 complex from *Thermotoga maritima*

As the previous approach did not lead to the crystallization of the *A. aeolicus* L10:L12 complex, attempts to crystallize the same complex from *T. maritima* were made.

It is important to notice that crystallization of a bacterial L10:L12 full-length complex was reported more than two decades ago, however without resulting in a successfully determined structure (Liljas and Newcomer 1981). Additionally, in numerous crystal structures or cryo-EM maps, no electron density corresponding to the L10:L12 complex was found. The difficulty of disclosing the structure of this complex could derive from its inherent flexibility, especially at the level of the hinge region of L12, connecting the NTD with the CTD. Hence, in parallel with the crystallization of the full-length *tma*L10:L12 complex, a strategy expected to limit the flexibility of *tma*L10:L12 was designed. A complex encompassing the full-length L10 and only the N-terminal domains of L12 (L12 NTDs) was generated (for a schematic representation of both L10 and L12 proteins, see Figure 5). Protein L12 was trimmed after residue G30 in a small loop connecting the NTD and the hinge, thereby removing the flexible part of the complex, namely the hinges carrying the CTDs.

## A. Production of protein complexes

### 1. Native *tma*L10:L12 and *tma*L10:L12 NTD complexes

*tma*L12 was obtained using a previously described clone (based on the pET22b(+) vector) (Wahl *et al.* 2000b), that allowed the protein production without affinity tag. To generate the *tma*L12 NTD, a stop codon was introduced after codon 30 in the above mentioned plasmid (Wahl *et al.* 2000b) (Table 6). *tma*L10 was cloned into the pETM-ZZ vector, which provides an N-terminal His$_6$/ZZ double tag (Table 8).

*tma*L10 and either full-length *tma*L12 or *tma*L12 NTD were co-expressed after co-transformation into *E. coli* Rosetta(DE3) cell strain. Both co-expressed *tma*L10:L12 and *tma*L10:L12 NTD complexes were purified *via* affinity chromatography on Nickel-Nitrilotriacetate (Ni-NTA) beads, through the His$_6$-tag attached to the *tma*L10 N-terminus. The protein complexes were eluted from the Ni-NTA resin in 300 mM imidazole. Following a buffer exchange step and the removal of the tag with tobacco etch virus (TEV) protease, the complexes were re-purified on Ni-NTA beads. Further heat treatment at 80°C and size exclusion chromatography yielded highly pure proteins. An overview of the *tma*L10:L12 and *tma*L10:L12 NTD expression and purification procedures is provided in Figure 10.

Due to its predominantly acidic amino acids composition (the calculated pI of *tma*L12 is 4.8), the 13.5 kD *tma*L12 protein migrated slower than expected on SDS-PAGE gels. The migration appeared to be concentration dependent: the more concentrated the protein, the slower the migration. In addition, *tma*L12 also lacks aromatic residues, in particular Tryptophan, resulting in a decreased absorbance at 280 nm. Similarly, protein concentration was found considerably underestimated by other conventional methods, e.g. Bradford assay. Indeed, previous quantitative amino acid analysis of this protein indicated a 6-7 fold increase in concentration as compared to a Bradford concentration determination (Wahl *et al.* 2000b). This information, as well as in-gel comparisons with proteins of known concentrations, allowed the concentration estimation of the L10:L12 complex.
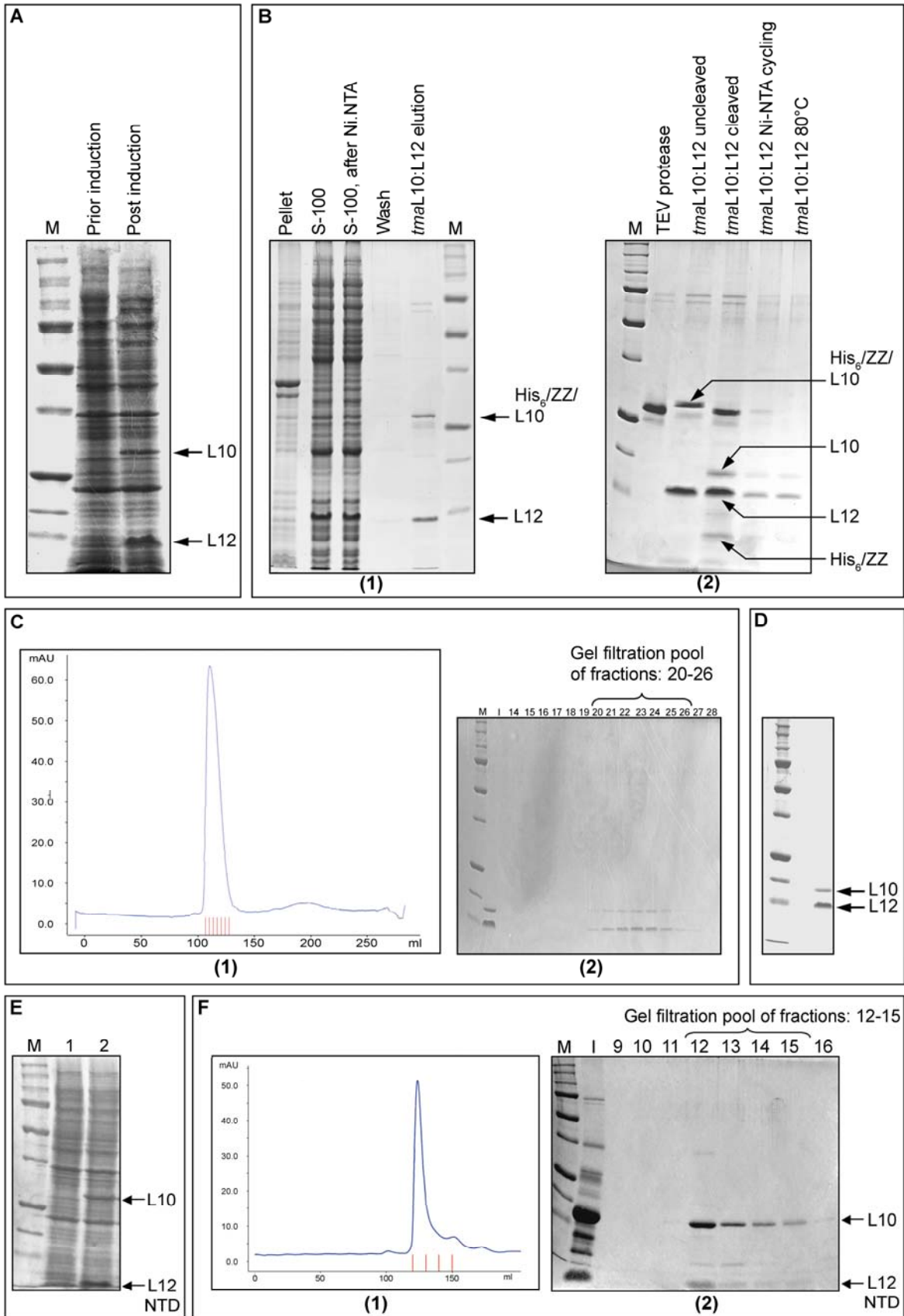
**Figure 10.** L10:L12 protein complex from *T. maritima*: expression and purification procedures. **(A)** *tma*L10:L12 complex co-expression. **(B)** (1) Purification *via* affinity chromatography on Ni-NTA beads: the pellet of the cell lysate exhibited minute amounts of the protein complex, indicative of its solubility; S-100 fraction representing the supernatant of the cell lysate and demonstrating the presence of the soluble protein complex; S-100 after Ni-NTA corresponds to the flow-through of the cell lysate passed onto Ni-NTA beads; wash represents the flow-through of the washing of Ni-NTA beads; *tma*L10:L12 elution corresponds to the elution of the protein complex from the Ni-NTA beads, demonstrating the presence of both His$_6$/ZZ/L10 and L12. (2) TEV protease control sample; TEV protease cleavage of the His$_6$/ZZ tags; *tma*L10:L12 Ni-NTA cycling: re-purification on Ni-NTA beads to remove His$_6$/ZZ tag and TEV protease; heating at 80°C of the protein complex **(C)** Size exclusion chromatography. (1) Chromatogram representing the elution profile of the *tma*L10:L12 complex on the Superdex 75 gel filtration column. (2) Fractions containing the purified complex (20-26) were further concentrated; I, input protein representing the complex before gel filtration. **(D)** *tma*L10:L12, final preparation. **(E)** *tma*L10:L12 NTD complex co-expression. Prior induction (lane 1) and post induction (lane 2) phases are indicated. **(F)** (1) Chromatogram representing the elution profile of the *tma*L10:L12 NTD complex on the Superdex 75 gel filtration column, as the last purification step. (2) Fractions containing the purified complex (12-15) were further concentrated and subjected to crystallization trials.

## 2. Selenomethionine-derivatized *tma*L10:L12 NTD complex

To allow structure solution by multiwavelength anomalous dispersion (MAD), a selenomethionine (SeMet) substituted complex was also produced. The *tma*L10 protein contains three methionines (N-terminal residue included) and *tma*L12 NTD possesses one N-terminal methionine. The selenomethionine-containing protein complex was expressed in the *E. coli* B834(DE3)pLysS strain. These cells, being methionine-auxotroph, can only incorporate the selenomethionine subsequently supplemented in the medium. The yield of expression was slightly lower as compared to the wild-type, which is often seen in SeMet-derivatized protein production. Subsequently, the complex was purified as described for the *tma*L10:L12 NTD native complex (see previous chapter), concentrated to approximately 8 mg/ml and subjected to crystallization.

## B. Thermostability of the *tma*L10:L12 complex

One of the purification steps of the *tma*L10:L12 complex consisted in heating at 80°C. In order to test the stability of the purified complex at this temperature, the potential modification in protein folding induced by temperature was monitored at 222 nm on a Jasco 720 spectropolarimeter. The protein complex was in a physiological buffer (PBS, pH 7.4). Previously, it was shown that the *tma*L12 protein exhibits a melting temperature of approximately 110°C at pH 7.5, compared to ~60°C for the highly homologous *E. coli* protein (Wahl *et al.* 2000b). Herein, due to instrument limitations, the data acquisition could not be performed above 85°C. However, the negative molar ellipticity recorded until

this temperature exhibited constant values, indicating no changes (e.g. denaturation) in the protein structure (Figure 11).
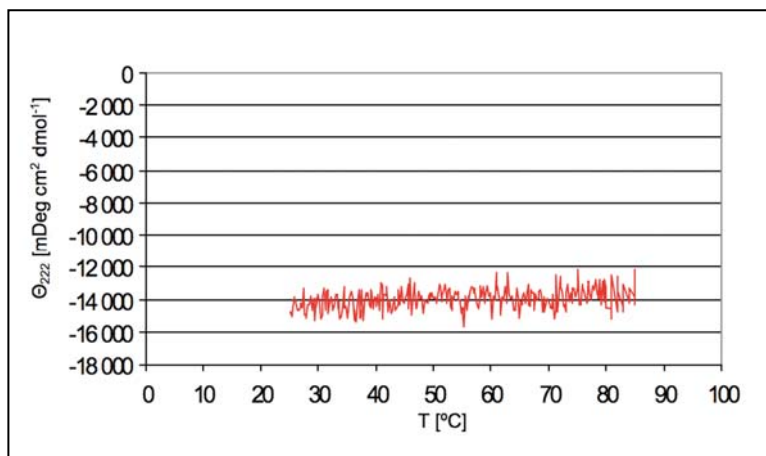


**Figure 11.** Thermal melting profile of the *tma*L10:L12 complex between 25 and 85°C. The molar ellipticity value was found constant with the temperature, consistent with an absence of modifications in the *tma*L10:L12 structure.

## C. Crystallization

### 1. *tma*L10:L12 crystals

In order to crystallize the *tma*L10:L12 complex, high-throughput crystallization was performed on the in-house vapor diffusion sitting drop dispensing apparatus. 1344 different conditions were screened using both sparse matrices and screens of ammonium sulfate and sodium malonate *versus* pH. Three-dimensional crystals appeared after 7 days in several conditions which contained PEG 3350 as precipitant. The screening was performed at both 4 and 20°C, but crystals grew better at 20°C. In all the cases, single or aggregated needle-shaped crystals appeared. After optimization of pH and buffers, two conditions gave rise to single crystals. Condition I contained 0.2 M NaCl, 0.1 M Tris pH 8.0, 20% PEG 3350 and condition II (Figure 12A) 0.4 M ammonium acetate, pH 7.2, 25% PEG 3350, respectively.

However, attempts to reproduce these crystals from complexes prepared with a higher concentration of protease inhibitors were not successful. This finding points to the notion that the initially obtained crystals did not encompass the full-length *tma*L10:L12 complex, but rather a trimmed variant, resulting from *in situ* proteolysis. Spontaneous cleavage was previously observed in the crystal structure of *T. maritima* L12 (Wahl *et al.* 2000a) and in crystallization trials of *E. coli* L12 (Liljas *et al.* 1978). Indeed, the full-

length L12 seemed to be quantitatively reduced as estimated by the SDS-PAGE gel examination of washed crystals dissolved in loading buffer. This result suggested that a part of the protein was degraded (Figure 12B).
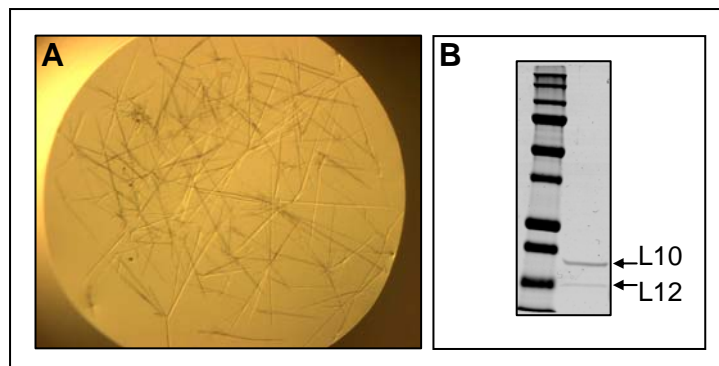


Figure 12. **(A)** The morphology of *tma*L10:L12 crystals. **(B)** *tma*L10:L12 crystals were repeatedly washed with reservoir solution in order to remove the non-crystallized protein from the drop, dissolved in loading buffer and subjected to SDS-PAGE. Note the weak amount of L12, suggesting a potential degradation due to proteolysis.

### 2. Three crystal forms of the *tma*L10:L12 NTD complex

The *tma*L10:L12 NTD complex, concentrated in a low salt buffer at 10 mg/ml, was subjected to crystallization by means of vapor diffusion. 384 different conditions were screened, using sparse matrices from Nextal Biotechnologies and Hampton Research. Several crystallization conditions with MPD and ethylene glycol as precipitants yielded single, small, needle-shaped crystals. They grew within a day at 20°C. One of these conditions, i.e. Cryo number 34 (Emerald BioStructures), gave three-dimensional crystals of excellent quality, which could be directly used for data collection. Subsequent buffer and pH optimization were required for some of the formulations, in order to produce single, large crystals. Next, the best conditions were probed for the selenium derivatized protein. After improvement steps, three crystals forms were used for data collection: one SeMet (**Form I**) (Figure 13A) and two native (**Forms II** and **III**) (Figure 13B, C). All the crystals, already cryo-protected from the reservoir solution, could be directly frozen in a liquid nitrogen stream.
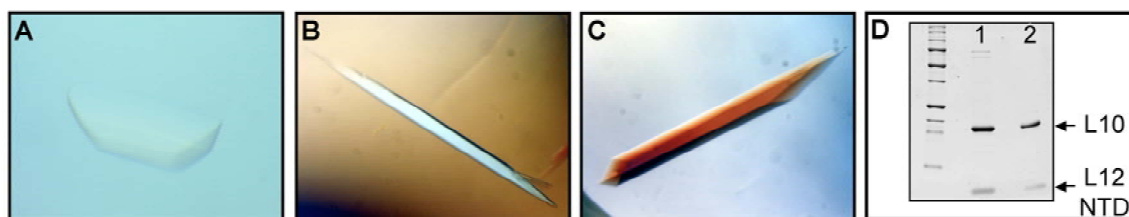
**Figure 13.** Crystal forms of *tma*L10:L12 NTD complex. **(A)** Crystal **Form I** (SeMet-derivative). **(B)** A needle-shaped crystal **Form II** (native), visualized in polarized light. **(C)** A needle-shaped crystal **Form III** (native), visualized in polarized light. **(D)** Protein (lane 1) and crystals of *tma*L10:L12 NTD dissolved in loading buffer (lane 2), subjected to SDS-PAGE and subsequently to mass spectrometry, for authentication.

## D. Data collection and processing

### 1. *tma*L10:L12 complex

Prior to the measurement of diffraction data, suitable crystals from conditions I and II were mounted with an adequately sized loop and directly frozen in a cold nitrogen stream. A complete data set of *tma*L10:L12 crystals was collected on a synchrotron (SLS, Villigen, Switzerland). These crystals diffracted to 3.5 Å and belonged to the primitive rhombohedral (R32) space group. The data collection statistics are summarized in Table 9.

| *Data collection* | |
| --- | --- |
| **Space group** | R32 |
| **Unit cell** (Å, °) | |
| a | 130.8 |
| b | 130.8 |
| c | 64 |
| α | 90 |
| β | 90 |
| γ | 120 |
| **Wavelength** (Å) | 1.05 |
| **Resolution** (Å) | 30.0-3.5 (3.6-3.5) |
| **Unique reflections** | 2728 (226) |
| **Redundancy** | 2.5 |
| **Completeness** (%) | 99.6 (99.1) |
| **I/σ(I)** | 12.8 (1.5) |
| **R$_{sym}$$^a$ (%)** | 10.2 (83.4) |

**Table 9.** Data collection statistics for the *tma*L10:L12 crystal. Values for the last 0.1Å between brackets.
$^a$R$_{sym}$(I) = $(\Sigma_{hkl}\Sigma_i[\,|\,I_i(hkl) - <I(hkl)>\,|\,]\,/\,\Sigma_{hkl}\Sigma_i[I_i(hkl)])$; $I_i$(hkl) – intensity of the i$^{th}$ measurement of hkl; $<I$(hkl)$>$ – average value of hkl for all i measurements.

### 2. *tma*L10:L12 NTD complexes

Data sets for all three crystal forms were collected on a synchrotron (DESY, Hamburg, Germany). Crystals of **Form I**, **II** and **III** diffracted to 2.3, 2.1 and 1.9 Å resolution, respectively. Anomalous data were recorded at four wavelengths (0.9793, 0.9795, 0.95, 1.05) around the selenium absorption-edge from a SeMet-derivatized crystal of **Form I**. The latter crystals belonged to an orthorhombic space group ($P2_12_12_1$) with unit cell dimensions of a=84.9 Å, b=84.9 Å, c=63.9 Å, $\alpha=\beta=\gamma=90°$. The native **Form II** and **III** crystals belonged to the orthorhombic ($P2_12_12_1$) and monoclinic ($P2_1$) space groups, respectively. Data statistics are summarized in Table 10.

| *Crystal Form* | I | | | | II | III |
|---|---|---|---|---|---|---|
| *Data collection* | Peak | Infl. Point | HE Remote[a] | LE Remote[a] | | |
| **Space group** | $P2_12_12_1$ | | | | $P2_12_12_1$ | $P2_1$ |
| **Unit cell** (Å, °) | | | | | | |
| a | 84.9 | | | | 45.0 | 43.4 |
| b | 84.9 | | | | 50.5 | 60.4 |
| c | 63.9 | | | | 179.1 | 83.4 |
| β | | | | | | 91.9 |
| **Wavelength** (Å) | 0.9793 | 0.9795 | 0.95 | 1.05 | 1.05 | 1.05 |
| **Resolution** (Å) | 99.0-2.62 | 99.0-2.62 | 99.0-2.55 | 30.0-2.2 | 30.0-2.1 | 30.0-1.9 |
| **Processing** | Anomalous | Anomalous | Anomalous | Normal | Normal | Normal |
| **Unique reflections** | 26365 | 26407 | 29005 | 24019 | 24199 | 34091 |
| **Redundancy** | 7.6 | 4.2 | 4.1 | 6.1 | 4.6 | 4.3 |
| **Completeness** (%) | 99.3 (97.5) | 99.3 (96.3) | 99.5 (98.6) | 99.4 (98.8) | 97.8 (96.7) | 99.8 (99.9) |
| **I/σ(I)** | 34.8 (5.3) | 24.6 (3.4) | 23.8 (8.4) | 27.6 (1.8) | 21.6 (2.6) | 35.4 (3.6) |
| **$R_{sym}$**[b] (%) | 6.2 (33.9) | 6.6 (36.0) | 6.9 (47.4) | 7.9 (56.1) | 9.6 (32.7) | 5.1 (21.7) |

**Table 10.** Data collection statistics for *tma*L10:(L12 NTD)$_6$ crystals. Values for the last 0.1Å between brackets. [a]HE – high energy; LE – low energy. [b]$R_{sym}(I) = (\Sigma_{hkl}\Sigma_i[\,|I_i(hkl) - <I(hkl)>\,|\,] / \Sigma_{hkl}\Sigma_i[I_i(hkl)])$; $I_i(hkl)$ – intensity of the ith measurement of hkl; $<I(hkl)>$ – average value of hkl for all i measurements

## E. Structure determination

### 1. *tma*L10:(L12 NTD)$_6$ complexes

The structure of **Form I** crystal could be solved by a four-wavelength Multiple Anomalous Diffraction (MAD) strategy (Table 11). Six selenium sites could be identified in the anomalous difference Fourier maps.

| *Phasing* | *Crystal Form I* | | |
|---|---|---|---|
| | **Peak** | **Infl. Point** | **HE Remote**[a] |
| **Resolution** (Å) | 20.0-2.62 | 20.0-2.62 | 20.0-2.55 |
| **Heavy atom sites** | 6 | 6 | 6 |
| **Correlation coefficients (CC)**[b] | | | |
| Overall | | | 0.39 |
| Map | | | 0.80 |
| Free | | | 0.62 |
| **FOM**[c] | | | 0.57 |

**Table 11.** Phasing statistics for the *tma*L10:(L12 NTD)$_6$ crystal **Form I**. [a]HE – high energy. [b]CC = $[\Sigma wE_oE_c\Sigma w - \Sigma wE_o\Sigma wE_c]/\{[\Sigma wE_o^2\Sigma_w - (\Sigma wE_o)^2]\ [\Sigma wE_c^2\Sigma w - (\Sigma wE_c)^2]\}^{\frac{1}{2}}$; $w$ – weight (see http://shelx.uni-ac.gwdg.de/SHELX/shelx_de.pdf for full definitions). [c]FOM = Figure of merit = $[\,|F(hkl)_{best}|\,]\,/\,|F(hkl)|$; $\mathbf{F}(hkl)_{best} = \Sigma_\alpha[P(\alpha)\mathbf{F}_{hkl}(\alpha)]\,/\,\Sigma_\alpha[P(\alpha)]$

Further density modification with DM (Collaborative Computational Project, 1994) generated a high quality electron density map (Figure 14), which could be partly interpreted by automated model building with ARP/wARP (Morris *et al.* 2003), and subsequently completed manually using MAIN (http://www-bmb.ijs.si/doc/index.html). Next, structures of the other two crystal forms were determined by molecular replacement using as a search model the structure derived from crystal **Form I**. In all three structures, the asymmetric unit contained one molecule of full length L10 complexed with three dimers of L12 NTD.
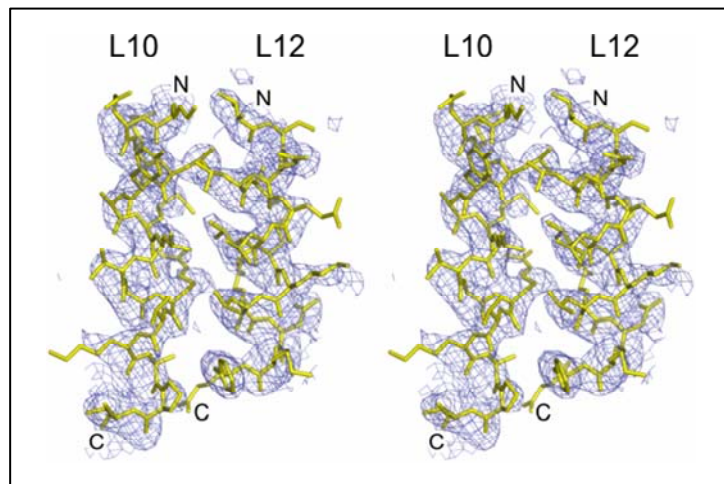
**Figure 14.** Stereo view of the experimental SeMet-MAD electron density map of the *tma*L10:(L12NTD)$_6$ after solvent flattening contoured at the 1σ level. The density covers part of L10 helix α8 in contact with an L12 NTD helix, which was chosen as a representative portion of the complex (data phased up to 2.5Å resolution). The final atomic model (of crystal Form I) is superimposed for comparison (yellow sticks).

### 2. *tma*L10:L12 complex

The structure of the *tma*L10:L12 complex was solved by molecular replacement, in which the L10 NTD and the L10 helix α8-(L12 NTD)$_6$ were used as separate parts (see structure description of the *tma*L10:(L12 NTD)$_6$ complex, section III.G.1.)

The resulting electron density did not reveal features beyond the Glycine 30 of L12. Electron density for the L12 hinge region and the CTD was missing. Therefore, this structure can be regarded as another *tma*L10:(L12 NTD)$_6$ truncated complex, in a different crystal form, which was generated by the spontaneous proteolysis of the full-length *tma*L10:L12 complex.

## F. Refinement and quality of the model of the *tma*L10:(L12 NTD)$_6$ crystal structures

Models were refined to comparable working and free R-factors. The refinement parameters are presented in Table 12. The crystal **Form I** was refined to 2.3 Å resolution, with an R-free value of 0.272. Similarly, crystals **Forms II** and **III** were refined with an R-free value of 0.286 and 0.274, respectively.

| *Refinement* | | | |
|---|---|---|---|
| *Crystal Form* | **I** | **II** | **III** |
| **Resolution** (Å) | 20.0-2.3 | 20.0-2.1 | 20.0-1.9 |
| **Model atoms** | | | |
| Protein | 2822 | 2807 | 2822 |
| Water oxygens | 223 | 322 | 413 |
| $R_{work}$[a] (%) | 22.2 | 21.2 | 22.6 |
| $R_{free}$[b] (%) | 27.2 | 28.6 | 27.4 |
| **RMSD**[e] **from ideality** | | | |
| Bond lengths (Å) | 0.006 | 0.006 | 0.007 |
| Bond angles (°) | 1.13 | 1.10 | 1.17 |
| Bonded B-factors (Å$^2$) | | | |
| Main chain | 1.6 | 3.0 | 1.5 |
| Side chain | 2.7 | 4.8 | 2.3 |
| **Wilson B-factor** (Å$^2$) | 47.4 | 36.7 | 39.8 |
| **Model B-factors** (Å$^2$) | | | |
| Protein | 63.7 | 50.1 | 52.2 |
| Water | 66.2 | 59.8 | 67.3 |
| $\phi/\psi$ (%) | | | |
| Core | 95.4 | 96.6 | 98.1 |
| Additionally allowed | 4.3 | 3.4 | 1.5 |
| Generally allowed | 0.3 | 0 | 0 |
| Disallowed | 0 | 0 | 0.3 |

**Table 12.** Refinement statistics for *tma*L10:(L12 NTD)$_6$ crystals. [a]$R_{work} = \Sigma_{hkl}[\,|\,|F_{obs}|\,-\,k\,|F_{calc}|\,|\,]\,/\,\Sigma_{hkl}[\,|F_{obs}|\,].$ [b]$R_{free} = \Sigma_{hkl\subset T}[\,|\,|F_{obs}|\,-\,k\,|F_{calc}|\,|\,]\,/\,\Sigma_{hkl\subset T}[\,|F_{obs}|\,]$; hkl$\subset$T – test set.

The Ramachandran plot of the crystal **Form I** is shown in Figure 15.
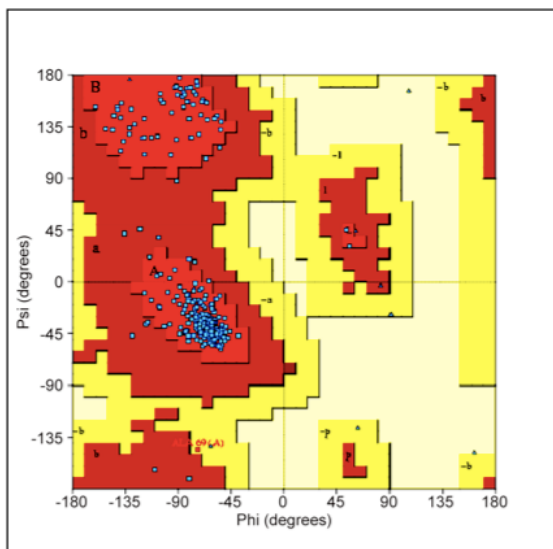


**Figure 15.** Ramachandran plot corresponding to the crystal **Form I** of *tma*L10:(L12 NTD)$_6$ structure, calculated with PROCHECK (Laskowski *et al.* 1993). The red area depicts the most favorable region, the dark red area is the additionally allowed region and the dark yellow area is the generously allowed region. The triangles symbolize glycines or prolines. More than 90% of the residues are in the most favorable region, indicating a satisfactory geometry of the model.

The model exhibits a good overall stereochemistry, with 95.4 % of the residues in the most favored region, 4.3 % in the additionally allowed region and one residue in the generously allowed region.

The structures were deposited in the Protein Data Bank (http://www.rscb.org/pdb), accession codes: 1ZAW (Crystal **Form I**), 1ZAX (Crystal **Form II**), 1ZAV (Crystal **Form III**).

## G. Crystal structure of the *tma*L10:(L12 NTD)$_6$ complex

### 1. Overall structure

In all three crystal structures of the *tma*L10:L12 NTD$_6$ complex, one molecule of full length L10 was found in complex with six copies of L12 NTD, the latter forming three dimers (Figure 16). Protein L10 displays a globular N-terminal domain, followed by a long C-terminal α-helix. A flexible loop connects these domains. The L10 NTD exhibits an α/β fold by which this protein is anchored to the 23S rRNA. The C-terminal helix (α8, K137-K174) of L10 is kinked twice, at residues P151 and G161, resulting in three ten-residue segments. Each segment associates with one L12 NTD dimer through a five-helix bundle. Thus, the L10-L12 interaction region is characterized by a repetition of three almost identical helix α8-L12 NTD dimer elements. The binding of L12 to the C-terminal portion of L10 is in agreement with early observations that L10 exhibits two functionally different regions: one for binding the 23S rRNA and one for binding L12 (Pettersson 1979).

Each L12 NTD molecule contains two α-helices connected by a short loop. Within each dimer, two L12 NTD molecules are entangled in an antiparallel fashion by extensive hydrophobic contacts, consistent with the previous observation that the N-terminal part of L12 is responsible for dimerization (Gudkov and Behlke 1978).
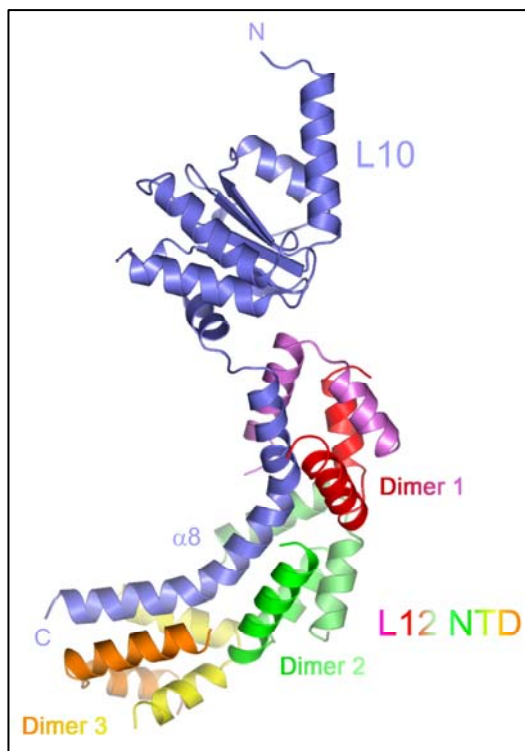
**Figure 16.** Overall structure of the *tma*L10:(L12 NTD)$_6$ complex showing the L10 NTD at the top and three L12 NTD dimers (protomers colored pink/red, light green/dark green, or yellow/orange, respectively) bound to the C-terminal helix α8 of L10 (blue) at the bottom.

## 2. Detailed insights into the L10-L12 interaction

Interfaces of the L12 NTD dimers with L10 bury about 1500 Å$^2$ of combined surface area each. The mode of interaction of the L12 NTD dimers with L10 is similar in each case and is dominated by hydrophobic contacts (Figure 17A). Precisely, 80% of the interface residues are hydrophobic. Shape complementarity and electrostatic interactions at the periphery, such as salt bridges, hydrogen bonds and bridging water molecules, register the L12 NTD dimers on L10 helix α8 (Figure 17B). Helix α8 of L10 presumably adopts a regular structure only upon interaction with L12, consistent with the observation that L10 in isolation exhibits a decreased stability (herein and (Gudkov *et al.* 1978)) Thus, resembling the architecture of other ribosomal proteins, which use long extensions for intimate interactions with rRNA (Ban *et al.* 2000), L10 employs a C-terminal extension to interact with another protein.
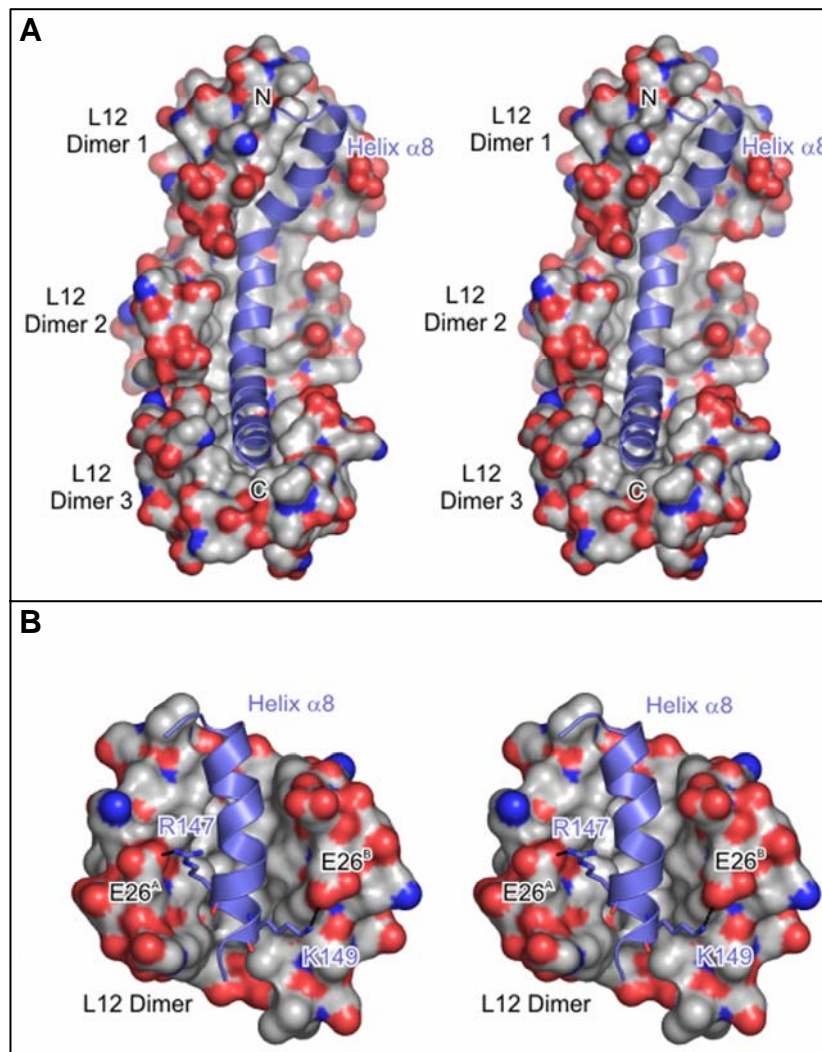
**Figure 17. (A)** Stereo view of the surface of the three neighboring L12 NTD dimers color-coded by atom type (carbon – gray, oxygen – red, nitrogen – blue) with the bound L10 helix α8 (blue ribbon). The image reveals the hydrophobic lining of the L10-binding groove (gray interior surface) and the deep burial of helix α8. **(B)** Stereo surface plot of one L12 NTD dimer, color-coded by atom type (carbon – gray, oxygen – red, nitrogen – blue) bound to a segment of L10 helix α8. Residues R147 and K149 of L10 engage in salt bridges with the carboxyl groups of E26 residues from the two L12 molecules (A and B) at the rim of the binding pocket.

Loops of adjacent L12 NTD dimers face each other and engage in four backbone-to-backbone hydrogen bonds via residues E11, L13, V15 and S16. Turns of L10 helix α8, which fall at the border of two adjacent L12 NTD dimers, are pried apart by inter-dimer contacts, leading to the two kinks of helix α8. Inter-dimer interactions support a rigid arrangement of the three L12 NTD dimers on helix α8 independent of the crystal environment.

In all six L12 NTDs a universally conserved phenylalanine (F29 in *T. maritima*), contacts L10 in a similar manner. Specifically, all six F29 residues stack on a hydrophobic

L10 residue: Y141, P151, I153, I162, L163, I173 (Figure 18 and Figure 22). These L10 residues delineate the borders of the three segments of helix α8, which carry the L12 NTD dimers. Consistently, F29 is important for the stabilization of the L12 NTD dimer onto the L10. This arrangement is in agreement with the observation that the corresponding residue of *E. coli* L12 (F30) is crucial for the interaction with L10 (Gudkov *et al.* 1982).
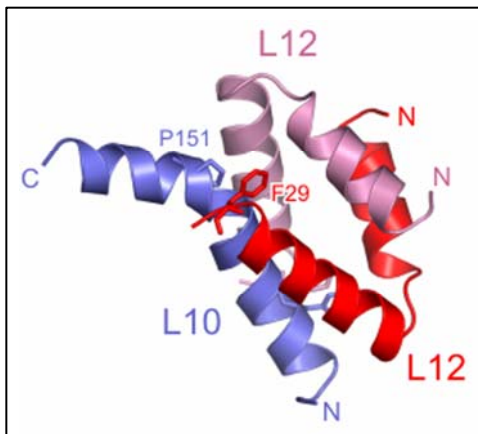


**Figure 18.** Diametric ribbon plots of an interaction of a *tma*L10 helix α8 section (blue) and a *tma*L12 NTD dimer (red and pink). All F29 residues of the six L12 NTD molecules stack onto hydrophobic residues (here Proline 151) from L10 helix α8 (interacting residues shown as sticks and labeled).

A recently characterized L12 point mutant (LL103; S15F in *eco*L12, T14F in *tma*L12) exhibited reduced affinity for L10 and led to reduced translational efficiency in mutant ribosomes (Nomura *et al.* 2003). In five of the six L12 molecules, T14 is not engaged in a direct contact to L10. Rather, its side chain hydroxyl stabilizes the tight turn between the L12 NTD helices by hydrogen bonding to the backbone nitrogen of E17. Only in the L12 molecule proximal to the L10 globular head, the T14 hydroxyl additionally engages in a hydrogen bond to the E119 carboxyl group of L10. Therefore, the present structures suggest that consequences of the LL103 mutation are mainly due to the role of T14 in the structural maintenance of the L12 NTD.

In *E. coli*, one L12 dimer is more tightly associated with L10 than the other (Wiggers *et al.* 1997). This observation agrees with the present structure where the proximal L12 NTD dimer in each of the three *tma*L10:(L12NTD)$_6$ complexes engages in interactions with the L10 NTD, which are not seen for the distal dimers. Specifically, the L12 NTD dimer proximal to the L10 NTD shows some contacts to the latter domain (e.g. T14(OG1)$_{L12}$ − E119(OE2)$_{L10}$; V15(N)$_{L12}$ − D91(OD2)$_{L10}$; E20(OE1)$_{L12}$ − K121(NZ)$_{L10}$)

which lead to the burial of an additional $570\text{Å}^2$ of combined surface area and thus, account for a stronger adhesion compared to the other two dimers.

### 3. A flexible point in L10

In the three crystal structures, L10 helix $\alpha8$-(L12 NTD)$_6$ elements adopt different orientations relative to the L10 NTD (Figure 19A). The $\alpha8$-(L12 NTD)$_6$ movement can be described as rotations around a pivot point, located in the beginning of an unstructured loop that connects the L10 NTD and helix $\alpha8$ (Figure 19A, close-up view). Different conformations observed are the result of different contacts between helix $\alpha8$ and the L10 NTD or between the L12 NTD dimers and the L10 NTD. Figure 19B shows several sets of salt bridges formed between these domains (e.g. E119 − K137, E129 − K133), which stabilize the structure in a certain conformation. These salt bridges surround hydrophobic interactions, by which a convex surface area on the first segment of helix $\alpha8$ bearing an L12 NTD dimer is inserted in to a concave surface area of the L10 NTD (Figure 19C). Moreover, in the R32 crystal structure derived from the *tma*L10:L12 complex after *in situ* proteolysis, the L10 helix $\alpha8$-(L12 NTD)$_6$ segment adopts yet another orientation relative to the L10 NTD, further supporting the notion that this region has a certain degree of flexibility.
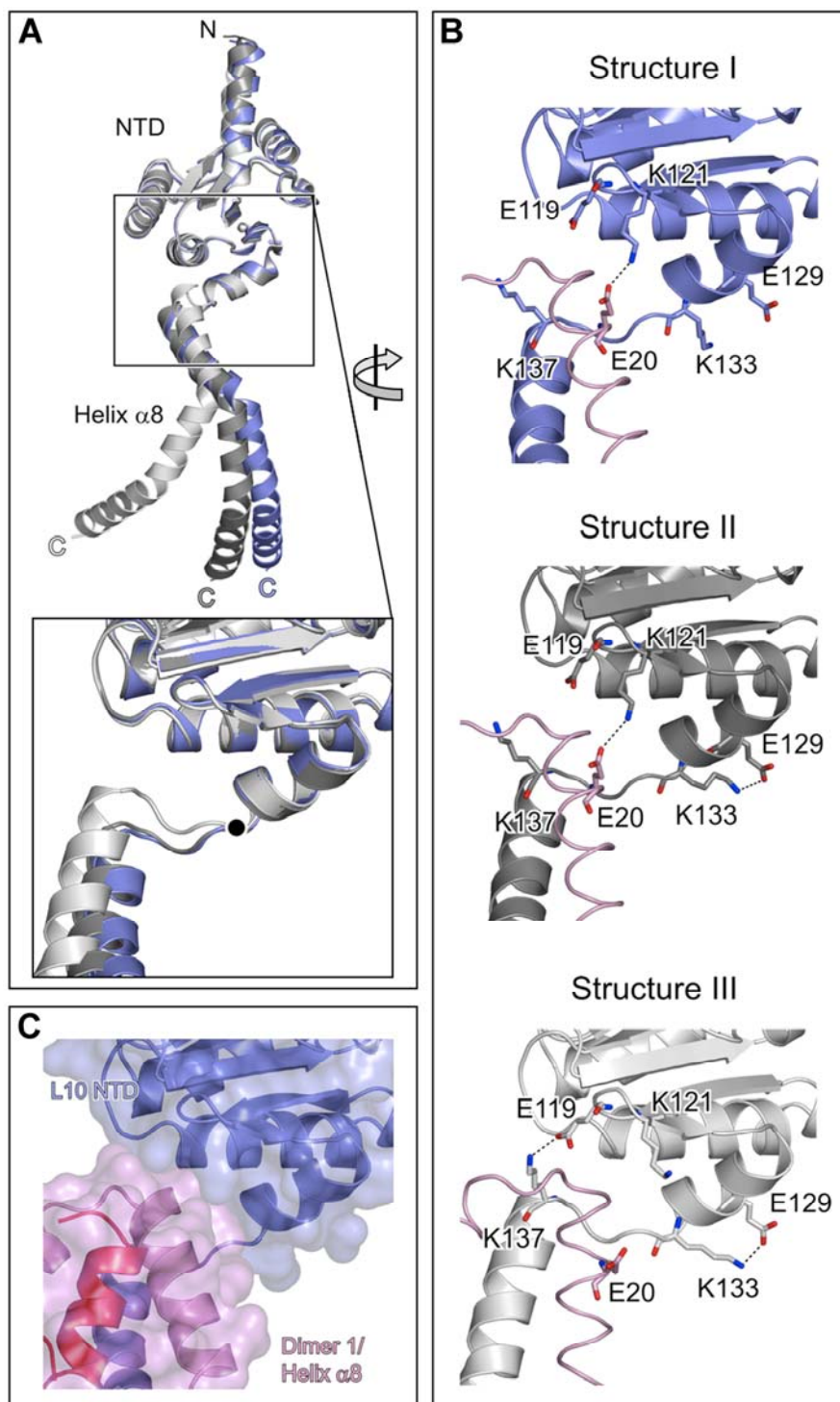
**Figure 19. (A)** Superposition of L10 from the three crystal structures (shown in blue, dark gray and light gray) aligned on their NTDs showing the flexible attachment of helix α8 to the L10 NTD. L12 NTD dimers have been omitted for clarity. In the close-up view (rotated 60° clockwise about the vertical axis) the black button identifies a pivot point around which helix α8 rotates relative to the NTD. **(B)** The same view on the three individual L10 molecules as in the close-up view with the proximal L12 NTD molecule shown as a pink tube. Coloring: Carbon – colored as the L10 molecules; oxygen – red; nitrogen – blue. Dashed lines indicate salt bridges between the L10 NTD and the flexible connector or helix α8 and between the L10 NTD and the proximal L12 NTD molecule, which stabilize the different conformations. **(C)** A convex surface area of the proximal L12 NTD dimer and the N-terminal part of L10 helix α8 (semitransparent pink surface) inserted into a concave surface area on the L10 NTD (semitransparent blue surface).

### 4. L12 dimerization mode

In the *tma*L10:(L12 NTD)$_6$ structures, two L12 NTD molecules forming a dimer face each other in an antiparallel fashion (Figure 16 , Figure 20).
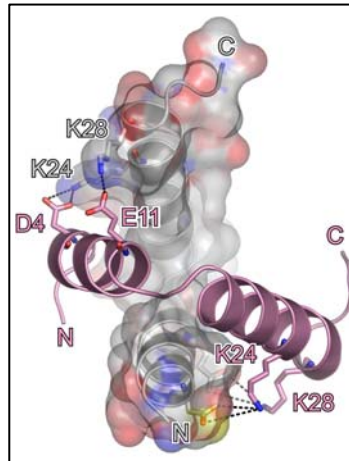


**Figure 20.** L12 NTD inter-dimer contacts. Stereo surface plot of one L12 NTD molecule, color-coded by atom type (carbon – gray, oxygen – red, nitrogen – blue) bound to the other NTD of L12 (pink ribbon) in an antiparallel fashion. The image reveals the prevalence of hydrophobic interactions between the two molecules (gray interior surface). Additionally, reciprocal salt bridges between Glu11 and Lys28 and between Asp4 and Lys24 are observed, strengthening inter-dimer interactions (Wahl *et al.* 2000a).

An identical dimerization mode (Figure 21A: between molecules I and III, as well as between molecules II and IV) was previously evidenced in the crystal structure of L12 in isolation (Wahl *et al.* 2000a). A second, parallel dimerization mode (Figure 21A: between molecules I and II) observed in the isolated L12 structure, is not seen in the present structures. Additionally, the N-terminal dimerization mode was previously proposed for both isolated *eco*L12 and *tma*L12 proteins in solution by NMR (Figure 21B; Bocharov *et al.* 2004) and FRET (Figure 21C; Moens *et al.* 2005) studies, respectively, and for *eco*L12 on the ribosome (Mulder *et al.* 2004).

In the *tma*L12 crystal structure, the hinge region of one L12 molecule folds back as an α-helix onto two interlaced L12 NTDs (Figure 21D). In the *tma*L10:(L12 NTD)$_6$ complex, the hinge is replaced by the ten-residue segments of L10 helix α8 (Figure 16, Figure 21E). This suggested that the α-helical hinge observed in the isolated *tma*L12 structure was in fact mimicking the L10 helix α8 of the *tma*L10:(L12 NTD)$_6$ complex.
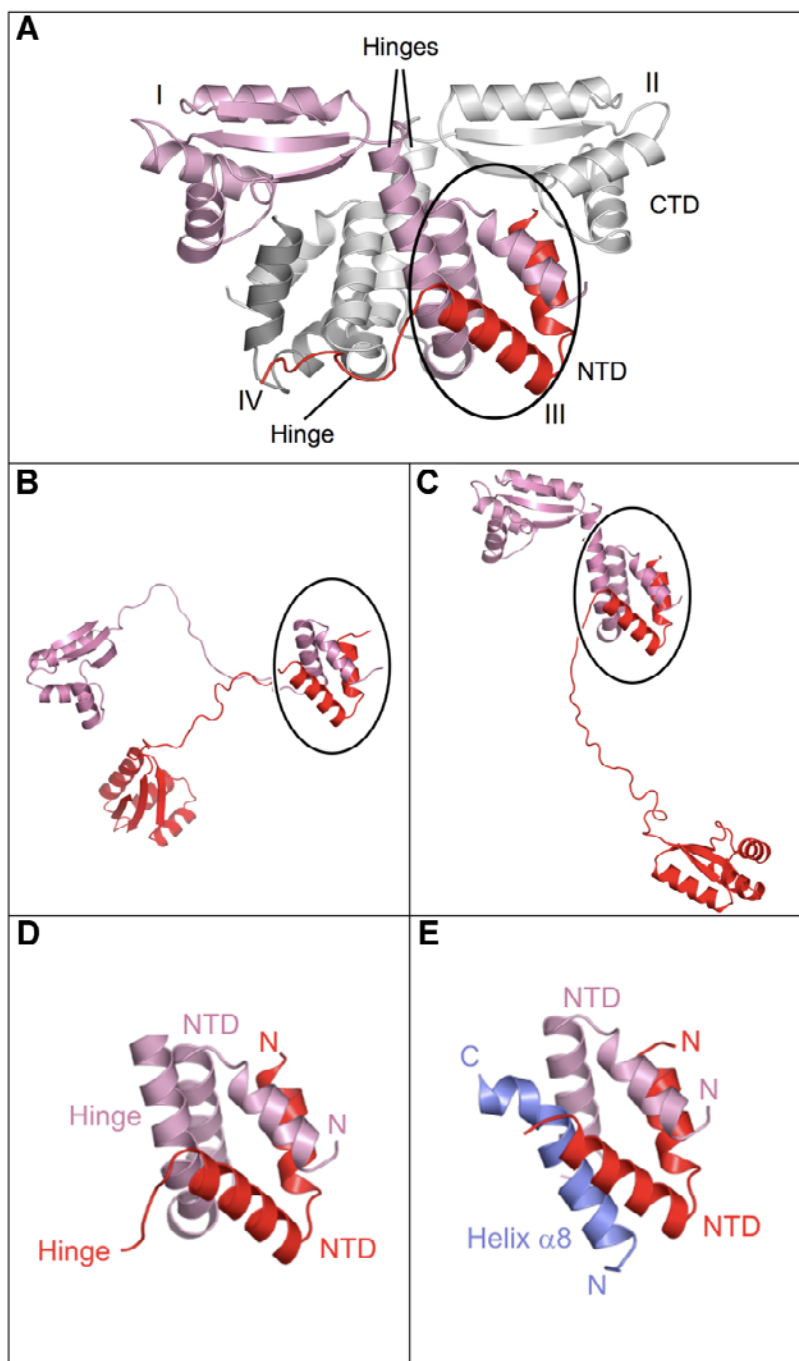
**Figure 21. (A)** Hetero-tetrameric arrangement in the crystal structure of isolated *tma*L12 (Wahl *et al.* 2000a) showing one type of dimerization (parallel) between two full-length molecules (molecules I and II) and another (N-terminal) between a full-length molecule and a N-terminal fragment (I and III or II and IV). **(B)** *eco*L12 conformation in solution: an N-terminal dimerization mode observed between L12 NTD molecules and random coil conformations of the L12 hinges (Bocharov *et al.* 2004). **(C)** Model proposed for *tma*L12 conformation in solution, deducted with FRET: a N-terminal dimerization mode is seen for the L12 NTD and hinges adopt both an extended and an α-helical conformation (Moens *et al.* 2005). This model is also in agreement with NMR data for ribosomal bound-*eco*L12 (Mulder *et al.* 2004). **(D)** Details of the interaction between a helical hinge (pink) in complex with the NTDs (red and pink) seen in the crystal structure of *tma*L12 in isolation (Wahl *et al.* 2000a). **(E)** One L12 NTD dimer (red and pink) of the present crystal structures in complex with its L10 binding region (blue). L10 helix α8 and the α-helical L12 hinge of isolated L12 (the latter depicted in (D)) bind in a similar fashion to the identically structured L12 NTD dimers.

### 5. Stoichiometry of the stalk proteins

The present crystal structures from the hyperthermophilic bacterium *T. maritima* revealed a 1:6 stoichiometry of the stalk proteins, namely one copy of the full-length L10 contacting six copies of L12 NTD. This stoichiometry was unexpected since in *E. coli* a ratio 1:4 (L10:L12) was well established (Terhorst *et al.* 1973; Hardy 1975; Subramanian 1975; Pettersson and Liljas 1979). However, the *T. maritima* L12 copy number was confirmed by several approaches: multiple sequence alignments, multi-angle laser light scattering and quantification of the ribosomal L12 by immunoblotting (the latter experiment was performed in collaboration with U. Kothe and M.V. Rodnina, Witten). Quantification of the L12 copy number by immunoblotting required functional *E. coli* and *T. maritima* ribosomes. To test the *T. maritima* ribosomes activity, a 70S initiation complex was prepared using available *E. coli* initiation factors (IF1, IF2, IF3), mRNA (Rodnina and Wintermeyer 1995) and f[H$^3$]Met-tRNA$^{fMet}$. The occupancy of the P-site was 25%, as determined by nitrocellulose filtration, suggesting active *T. maritima* ribosomes although orthologous initiation factors from *E. coli* were used (data not shown).

### a. Sequence alignment

Sequence comparisons showed that helix α8 in *eco*L10 is missing one of the ten-residue L12-binding sections compared to *T. maritima*, consistent with the notion that it can only accommodate two L12 dimers. In contrast, some other bacteria exhibit a similar length and partitioning in L10 helix α8 as *T. maritima* and are expected to maintain a L10:(L12)$_6$ complex (Figure 22, see Suppl. Figure 2, Appendices, for a complete denomination of all amino acids).
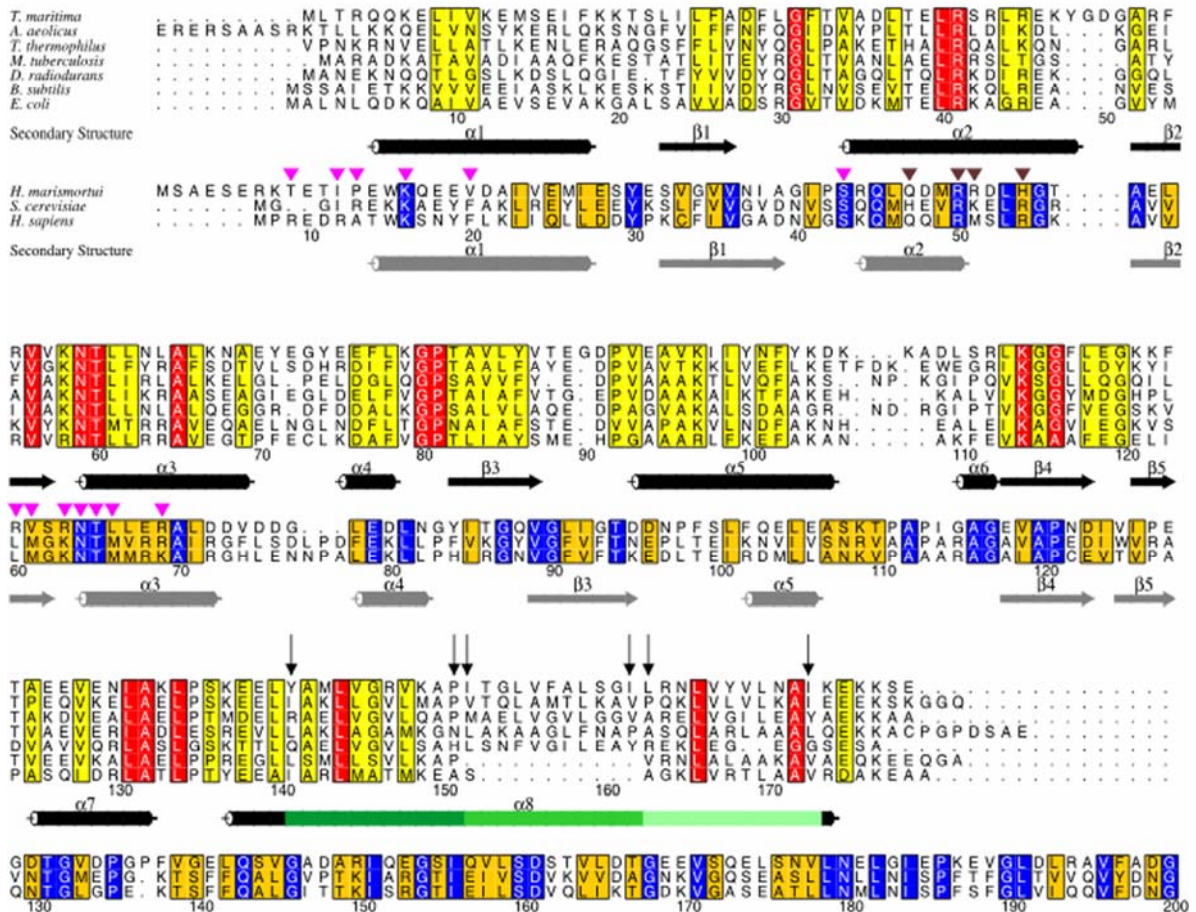
**Figure 22.** Sequence alignment of bacterial L10 proteins and of archaebacterial (*H. marismortui*) *hma*L10E, yeast P0 and human P0 proteins. Secondary structure elements of *tma*L10 and *hma*L10E, as revealed in the present crystal structures, are indicated below each alignment block (black and gray, respectively). Sequence numberings below the blocks correspond to *tma*L10 and *hma*L10E, respectively. Within the bacterial L10 sequences, highly conserved amino acids are color-coded in red, intermediately conserved positions in yellow. In the L10E/P0 block, identical residues are shown in blue, conserved residues in orange. Residues of *hma*L10E that interact directly with 23S rRNA are labeled with a magenta triangle. Residues that contact protein L11 are labeled with a brown triangle. The three segments of helix α8 in *tma*L10 that associate with L12 NTD dimers are indicated by different shades of green. Some bacteria (e.g. *T. maritima*) contain three ten-residue segments of L10, consistent with the accommodation of three L12 dimers, whereas other bacteria (e.g. *E. coli*) lack one ten-residue segment of L10, leading to the accommodation of only two dimers of L12. Above this segments, arrows indicate hydrophobic residues of L10 (Y141 and P152, I153 and I162, L163 and I173), which stack with the F29 side chains from the L12 NTD.

### b. Multi-Angle Laser Light Scattering

In order to confirm the L12 copy number in *T. maritima* L10:L12 complex, both recombinant full-length *tma*L10:L12 and *eco*L10:L12 complexes were produced and subjected to molecular mass measurements by means of Multi-Angle Laser Light Scattering (MALLS). In addition, *aae*L10:L12, *tma*L10:L12 NTD, *tma*L10:L12 NTD/hinge, *tma*L10:*eco*L12 complexes were investigated.

The production of the L10:L12 complex from *E. coli*, was achieved using a biscistronic plasmid (based on pGEX-5x-3 vector), with sequential genes for GST-L10 and

L12 (provided by M.V. Rodnina, Witten). *eco*L10:L12 complex was expressed in *E. coli* Rosetta(DE3) cells and further purified *via* glutathione affinity chromatography. Next, the GST tag of *eco*L10 was removed by Factor Xa cleavage. Subsequent purification on both heparin and size exclusion columns yielded a highly pure complex (Figure 23A). *tma*L10:L12 NTD/hinge was co-expressed after co-transformation in Rosetta(DE3) strain. The construct L12 NTD/hinge was designed by introducing a stop codon after codon 53 (corresponding to the end of the hinge region) in the same plasmid used for expression of full-length *tma*L12 (Wahl *et al.* 2000b). The purification of the resulting complex was employed as described for *tma*L10:L12 and *tma*L10:L12 NTD (Figure 23B). The *tma*L10:*eco*L12 complex was obtained from the plasmid pETM-ZZ containing the gene for His$_6$-L10 and the plasmid pT7-6::rplL, comprising the *eco*L12 gene without any affinity tag (Oleinikov *et al.* 1993). Following co-transformation and co-expression, the resulting protein complex was purified by Ni-NTA affinity chromatography and size exclusion, as described for the *tma*L10:(L12 NTD)$_6$, with the exception of heating at 80°C. The latter step was omitted, as the *eco*L12 is not thermostable beyond ~65°C (Figure 23C). The purity of all the resulting complexes was estimated at >90% according to Coomassie blue-stained SDS gels.
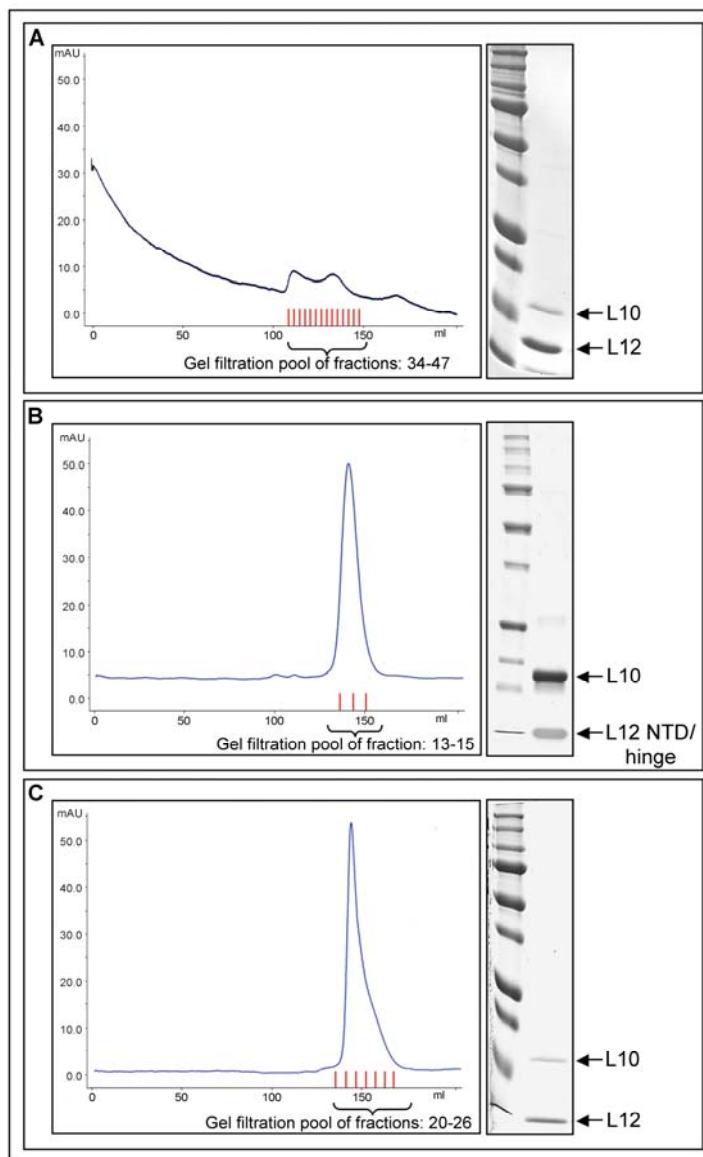
**Figure 23. (A)** *eco*L10:L12 protein complex. Chromatogram representing the elution profile of the *eco*L10:L12 complex on the Superdex 75 26/60 prep grade gel filtration column, as a last step of the purification process. Fractions 34 - 47 were pooled and concentrated to 10 mg/ml. The *eco*L10:L12 complex, final preparation, representing a complex between 17.6 kD L10 and 12.2 kD L12 proteins is also depicted. **(B)** *tma*L10:L12 NTD/hinge protein complex. Elution profile of the gel filtration, as a last step of the complex purification. Fractions 13-15 were combined and concentrated to 10 mg/ml. The final preparation, representing a complex between the 20.3 kD L10 protein and the 6 kD L12 NTD/hinge fragments is shown. **(C)** *tma*L10:*eco*L12 protein complex. Size exclusion chromatography of the complex, as a last step of the complex purification. Fractions containing the complex (20-26) were further concentrated to 10 mg/ml. The final preparation representing a complex between the 20.3 kD *tma*L10 and the 12.2 kD *eco*L12 proteins is depicted.

Purified proteins were subsequently analyzed by multi-angle laser light scattering and refractive index detection to measure their molecular weight. All measurements were performed at room temperature. An equal amount of protein (concentration of 2 mg/ml) was used for all the measurements. The mobile phase of the system was PBS, pH 7.4.

Ultra pure BSA was used as a control. Shortly after its solubilization, this protein forms monomers and, to a lesser extent, dimers and trimers, which were identified by MALLS measurement as three different peaks (marked in Figure 24A, and clearly distinguished by plotting molar mass *versus* volume in Figure 25A).
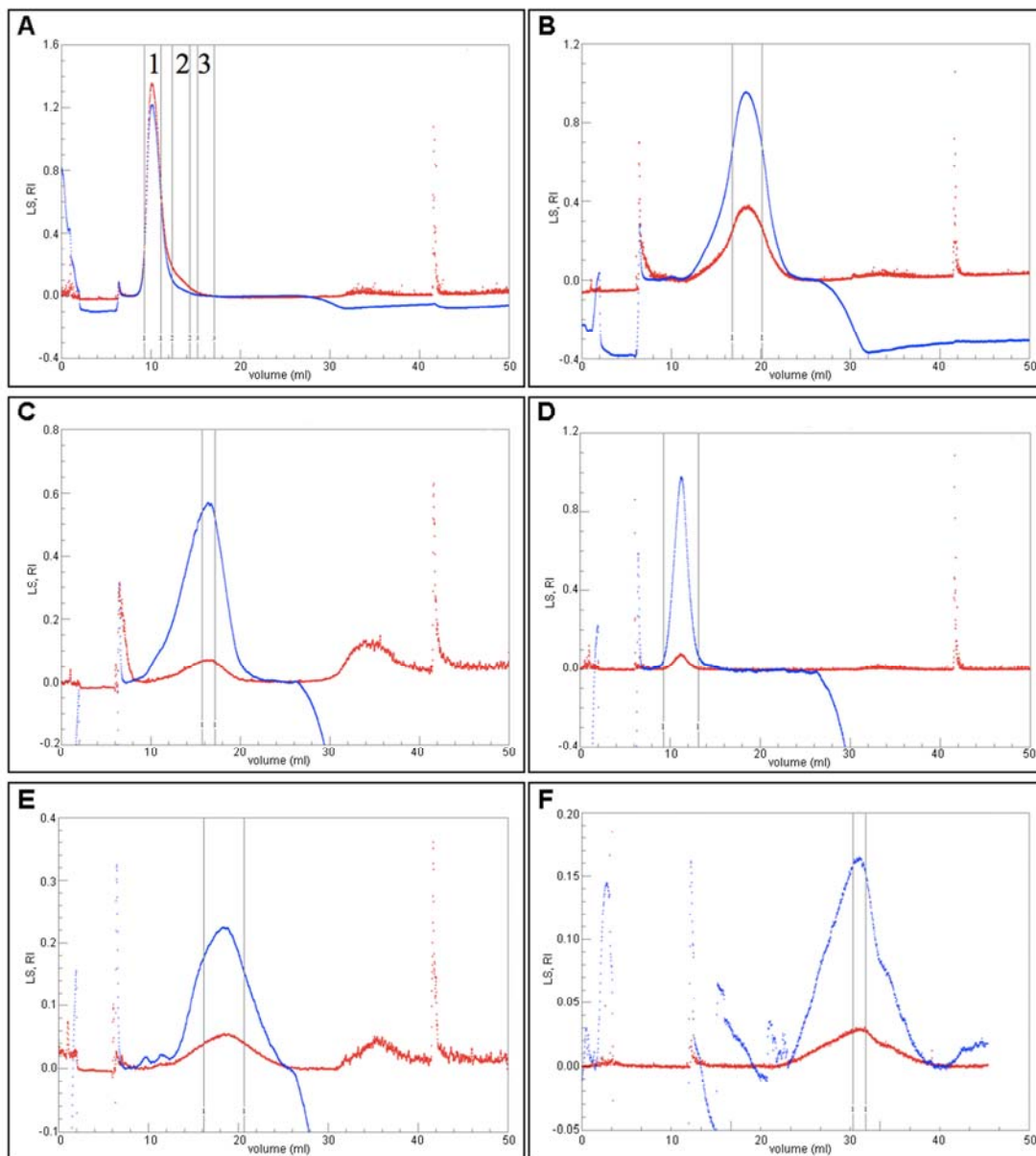


**Figure 24.** Light Scattering (LS: signal of the 90° light scattering detector, red curve) and Refractive Index (RI, blue curve) values of BSA or L10:L12 complexes are normalized and plotted versus volume [ml] in a flow field-flow fractionation chromatography. The peak area selected for mass measurement is delimited by parallel lines. **(A)** BSA elution profile. A major peak corresponds to the monomer state of the protein. At the shoulder of this peak, two additional peaks correspond to dimer and trimer states, respectively; the latter two peaks are too small to be distinguished in this graphic, however, the molar masses corresponding to these peaks are clearly evidenced in a plot of molar mass *versus* volume in Figure 25A. **(B-F)** Elution profiles of L10:L12 complexes from several bacteria. All the complexes eluted as single peaks. (B) *tma*L10:(L12)₆; (C) *tma*L10:(L12 NTD)₆; (D) *tma*L10:(L12 NTD/hinge)₆; (E) *aae*L10:(L12)₆; (F) *eco*L10:(L12)₄.

All the L10:L12 complexes eluted as single peaks (Figure 24B-F, Figure 25A). Molar mass determinations of L10:L12 complexes are summarized in Table 13. Multi-angle laser light scattering indicated a molecular mass of 101.3 ($\pm$ 1.5) kD for the $tma$L10:(L12)$_6$ complex, in excellent agreement with the predicted mass of 102.6 kD for a heptametric complex (Figure 25A). A recombinant full-length $eco$L10:(L12)$_4$ complex showed a mass of 69.7 ($\pm$ 2.3) kD as compared to 66.3 kD calculated for a pentameric composition (Figure 25A). The latter result is in line with the previously reported L12 copy number on the ribosome. Moreover, data obtained for $tma$L10:L12 and $eco$L10:L12 complexes were similar to those obtained from the quantification of the L12 copy number on $E.\ coli$ and $T.\ maritima$ ribosomes by immunoblotting (U. Kothe, M.V. Rodnina, Witten).

| | | | L10:L12 Stoichiometry | | |
|---|---|---|---|---|---|
| Protein Complex | Theor. Mass (kD) | Exp. Mass (kD) | MALLS | Crystal | Radioact. |
| $tma$L10:L12 | 102.6 | 101.3 ± 1.5 | 1:6 | | |
| $tma$L10:L12 NTD | 40.9 | [b]44.6 ± 17 | 1:6 | 1:6 | |
| $tma$L10:L12 NTD/hinge | 56.3 | 54.6 ± 7 | 1:6 | | |
| $aae$L10:L12 | 103.9 | [b]102.3 ±15 | 1:6 | | |
| $eco$L10:L12 | [a]66.3 | 69.7 ± 2.3 | 1:4 | | [c]1:4 |

**Table 13.** Size determination of L10:L12 complexes from different bacteria. [a]The $eco$L10:(L12)$_4$ molar mass, was previously determined by mass spectrometry as 66.3 kD (Hanson $et\ al.$ 2003). [b]The molar mass was calculated applying the $smoothing$ option (excluding extreme molar mass values) of the program used for data analysis. Initial values of the $tma$L10:L12 NTD and $aae$L10:L12 were 54 and 117 kD, respectively. [c]Quantification of the L12 copy number on the $E.\ coli$ ribosome using labeled amino acids (Subramanian 1975).

Additionally, both $tma$L10:L12 NTD and $tma$L10:L12 NTD/hinge size determinations confirmed the occurrence of the heptametric complex in $T.\ maritima$, exhibiting experimental molar masses close to the predicted values (Figure 25A). The $tma$L10/$eco$L12 molar mass could not be determined, despite several buffer, protein concentration and system parameters variations. The mass measurement suggested a potential aggregation of this complex. However, a peculiar conformation of this hybrid complex in the tested solutions could also have impaired the proper mass determination by means of MALLS. Interestingly, $aae$L10:L12 yielded a molar mass corresponding to a heptametric complex (Figure 25A). This result suggested that in some bacteria (presumably comprising all thermophilic bacteria) the L10:L12 complex exhibits a 1:6 stoichiometry (Table 13). Supporting evidence came from a recent report, which identified

by tandem mass spectrometry the occurrence of L10:(L12)$_6$ complexes on ribosomes of thermophilic bacteria (Ilag *et al.* 2005).
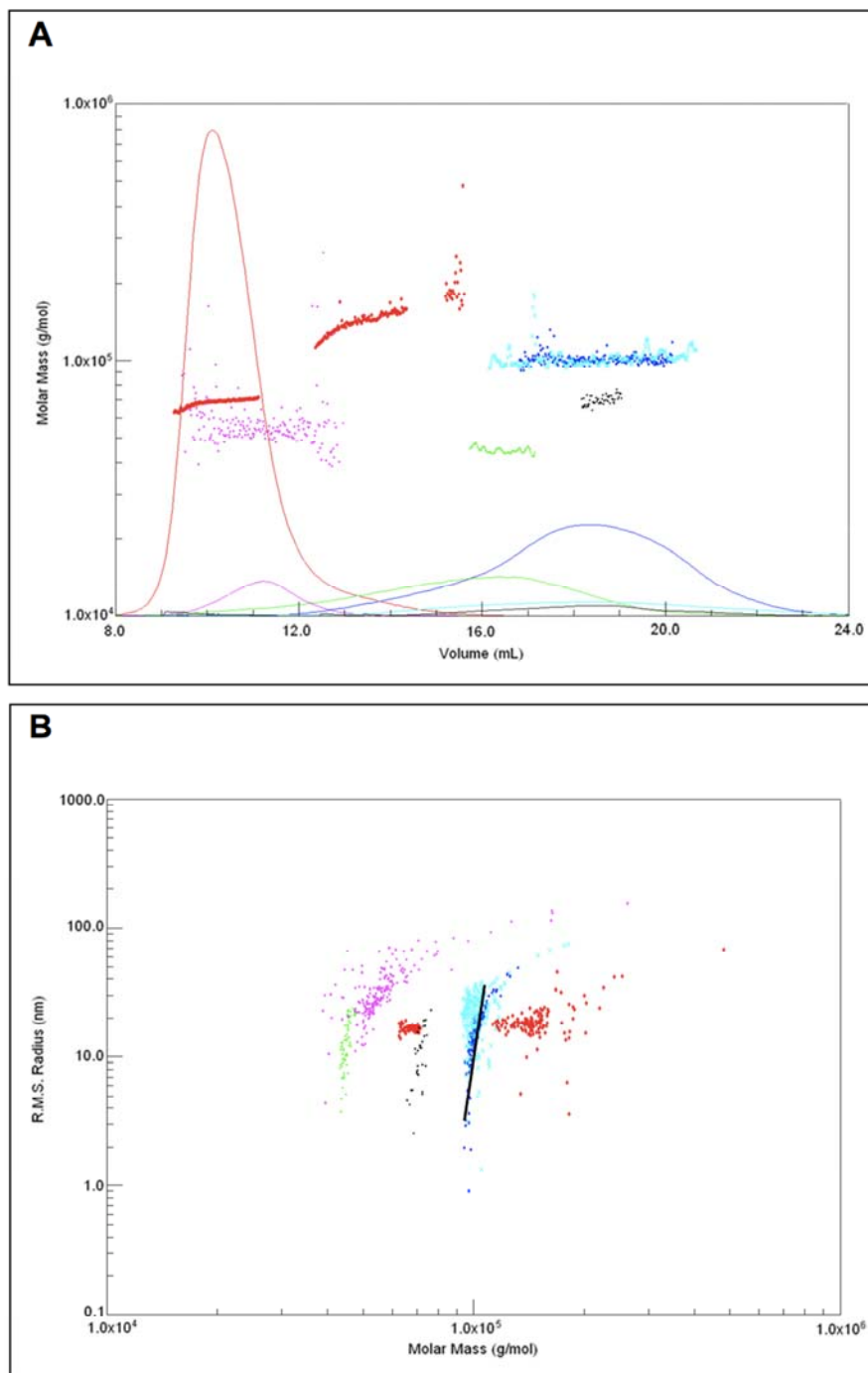


**Figure 25. (A)** Distribution of the Molar Mass [g/mol] *vs.* Volume [ml] of BSA and L10:L12 complexes from several bacteria. BSA (red): with a calculated mass of 68.69±1.6 (67) for the monomer, 136.3±12 (134) for the dimer and 198.4±77 (201) for the trimer states, respectively (the theoretical mass is shown in parentheses); *tma*L10:(L12)$_6$ (blue); *tma*L10:(L12 NTD)$_6$, (green); *tma*L10:(L12 NTD/hinge)$_6$ (pink); *aae*L10:(L12)$_6$ (cyan); *eco*L10:(L12)$_4$ (black). **(B)** Root Mean Square Radius [nm] *vs.* Molar Mass [g/mol] of BSA and L10:L12 complexes from several bacteria (color code as in (A)). One slope (black line) is drawn for the distributions of the RMS Radius *vs.* Molar Mass of the *tma*L10:(L12)$_6$ (blue), suggesting that no conformational changes occurred for this protein in solution.

By plotting the root mean square (RMS) radius *versus* molar mass of BSA and L10:L12 complexes (Figure 25B), it was possible to observe potential conformational changes in solution of the analyzed samples. A slope (Figure 25B, black line, exemplified for *tma*L10:(L12)$_6$) could be drawn for each of the distributions of RMS radius *versus* molar mass. The existence of a single slope for each of the samples instead of, e.g. two or more slopes separated by transition regions, suggests that there are no conformational changes in solution for either BSA or L10:L12 complexes. The steepness of the slope can easily be related to the conformation of the molecules, with extended structures giving larger slopes than compact molecules. As expected, monomer-state BSA is less extended than the dimer- and trimer-states. The least extended L10:L12 complexes seem to be *eco*L10:(L12)$_4$ and *tma*L10:(L12 NTD)$_6$, as compared to the *tma*L10:(L12 NTD/hinge)$_6$, *tma*L10:(L12)$_6$ and *aae*L10:(L12)$_6$ complexes.

Taken together, the multi-angle laser light scattering mass determinations were in agreement with the crystal structures showing a *tma*L10:(L12 NTD)$_6$ organization. Additionally, these results reconfirmed that in *E. coli* four copies of L12 can be accommodated by one L10 protein. Both *T. maritima* and *E. coli* L10 share a high degree of sequence conservation (approximately 65% identity (Wahl *et al.* 2000b)). Therefore it can be suggested that *E. coli* and *T. maritima* stalk proteins display a similar organization. The only difference is the absence of one of the three repetitive elements L10 helix α8-L12 NTD in *E. coli*, resulting in the accommodation of only two dimers of L12. Thus, it can be concluded that the length of L10 helix α8 determines the number of L12 copies per ribosome. The increased copy number of L12 found in some bacterial ribosomes emphasizes the importance of multiple L12 copies for the mechanism of translation.

# **Discussion**

## **I. The *tma*L10:(L12 NTD)$_6$ complex**

The crystal structure of the bacterial L10:(L12 NTD)$_6$ complex determined herein reconciles numerous previous structural and biochemical data. The present structures of L12 NTD molecules in complex with L10 are consistent with the observation that the N-terminal part of L12 is responsible for dimerization (Gudkov and Behlke 1978). The N-terminal dimerization mode of the L12 NTDs observed herein is in agreement with one of the dimerization modes found in the isolated *tma*L12 crystal structure (Wahl *et al.* 2000a). This dimerization mode was also described in *eco*L12 in solution (Bocharov *et al.* 2004) and *tma*L12 in solution (Moens *et al.* 2005). However, a compact, parallel dimerization mode in the *tma*L12 crystal structure, which was mediated by two helical hinges (Wahl *et al.* 2000a), is not seen in L10:(L12 NTD)$_6$ complexes. Indeed, the formation of such a dimer is obstructed in the *tma*L10:(L12 NTD)$_6$ complexes by the binding of L10 helix $\alpha$8 to the L12 NTD dimers at a position, which in the compact L12 dimer is occupied by a helical L12 hinge region. Displaced from their binding scaffold by L10 helix $\alpha$8, the L12 hinges are likely to be unstructured, as seen for *eco*L12 in solution (Bocharov *et al.* 2004; Mulder *et al.* 2004). Thus, the compact, parallel dimerization *via* helical L12 hinge regions is of no relevance to the ribosome-bound form of L12. These results refute a tentative model of the stalk in a 70S ribosome crystal structure (Yusupov *et al.* 2001), which was based on this compact L12 dimer structure.

In the present *tma*L10:(L12 NTD)$_6$ crystal structures, three L12 NTD dimers are found to bind to sequential segments on the C-terminal helix $\alpha$8 of L10. By deleting 20 to 33 C-terminal residues of *eco*L10, the binding of both *eco*L12 dimers was abolished, while the deletion of the terminal ten residues led to the loss of a single dimer (Griaznova and Traut 2000). An alignment of *eco*L10 with *tma*L10 (Figure 22) suggests that deletion of the terminal ten residues removes about one third of the predicted C-terminal L12 dimer binding region of *eco*L10 helix $\alpha$8. This deletion leaves the proximal L12 dimer binding site of helix $\alpha$8 intact, accounting for the loss of a single dimer. Deleting between 20 and 33 residues, which are predicted to encompass the entire helix $\alpha$8 in *eco*L10, accounts for the loss of both L12 dimers from the complex. These results, in conjunction with the

present crystal structures, underscore the modular design of the helix α8-L12 binding region, which consists of two (*E. coli*) or three (*T. maritima*) repetitive L12 NTD dimer-helix α8 elements. Notably, while the C-terminal deletion mutants of L10 lose their ability to bind L12, they remain unaffected in their binding activity to the ribosome (Griaznova and Traut 2000). These data are entirely in line with the assignment of the L10 NTD as a separate folding unit, which is necessary and sufficient for the interaction with the 23S rRNA. Furthermore, the analyses of *eco*L10 deletion mutants, which are in excellent agreement with the *tma*L10:(L12 NTD)$_6$ crystal structures, provide strong evidence that the fundamental structural principles in the L10:L12 complexes are conserved throughout the bacterial kingdom and that differences, e.g. between *E. coli* and *T. maritima*, are purely quantitative in nature (one additional modular element in the peripheral stalk region), but has most likely no fundamental functional consequences. The latter conclusion is corroborated by the fact that effects of a large number of mutations in the *eco*L10:L12 complex can be explained by the present crystal structures from *T. maritima*. F30 of *eco*L12 (F29 of *tma*L12) has been suggested to be crucial for the interaction with L10 (Gudkov *et al.* 1982). This hypothesis was confirmed by the crystal structure since in all six L12 molecules, F29 stacks on a hydrophobic L10 residue, which delineates the borders of helix α8 segments (Figure 18, Figure 22). Another point mutation S15F in *eco*L12 (T14F in *tma*L12) was shown to reduce the translational efficiency due to a reduced affinity for L10 (Nomura *et al.* 2003). However, the present crystal structure revealed that T14 is not engaged, as expected, in a direct contact to L10, and the effects of this mutation are most likely due to the role of this amino acid in the structural maintenance of the L12 NTD. Additionally, the crystal structure offers an explanation for the suggestion that in *E. coli*, one of the L12 dimers is more tightly bound to L10 than the other (Wiggers *et al.* 1997). Indeed, the proximal dimer of L12 in the *tma*L10:(L12 NTD)$_6$ structure engages in interactions with the L10 NTD, which are not observed for the other two dimers.

The localization of the *tma*L10:(L12 NTD)$_6$ on the large ribosomal subunit (Diaconu *et al.* 2005) revealed an extensive set of interactions between L10 NTD and 23S rRNA and only a small number of contacts to protein L11, which binds to the 23S rRNA in close vicinity to L10. Both L10 and L11 were previously shown to bind cooperatively to the ribosome (Dijk *et al.* 1979; Beauclerk *et al.* 1984; Egebjerg *et al.* 1990). However, the small number of direct interactions between L10 and L11 are not essential for L10 binding, because

L10:L12 complexes can bind to 23S rRNA also in the absence of L11 (Rosendahl and Douthwaite 1993). Therefore, the cooperative binding must be primarily an indirect effect. It is possible that the L10 NTD and L11 each stabilize the overall structure of the L10/L11 binding region of the 23S rRNA, thus facilitating a subsequent binding of the other protein. This notion is consistent with the observation that the L10 NTD presumably recognizes primarily the conserved fold but not the exact sequence of the rRNA.

# II. Beyond the L10:(L12 NTD)$_6$ crystal structure

In the present study, we determined crystal structures of an isolated bacterial L10:(L12 NTD)$_6$ complex. However, the important issue of how this complex is anchored to the 50S ribosomal subunit, remained to be addressed. Thus, combining the results of the L10:(L12 NTD)$_6$ crystal structure with cryo-electron microscopy and molecular model building, it was possible to elucidate the atomic structure of the L7/L12 stalk on the ribosome; additionally, rapid kinetic experiments were used to probe its factor-related functions (Diaconu *et al.* 2005). The data outlined in the following represented the result of a collaborative work with four laboratories.

## A. Placement of the *tma*L10:(L12 NTD)$_6$ structure on the 50S ribosomal subunit

A density modification procedure and a published diffraction data set of the *H. marismortui* 50S subunit (PDB accession code 1S72 (Klein *et al.* 2004); Suppl. Figure 3A, Appendices) allowed the tracing of the complete NTD of archaeal L10 (*hma*L10E) within the electron density of the large ribosomal subunit (Frank Schlünzen and Jörg M. Harms, Max-Planck Research Group, DESY, Hamburg). L10E NTD was found to engage in extensive contacts with the thiostrepton loop and in a small number of interactions with the neighboring CTD of protein L11E (Suppl. Figure 3B, Appendices). Interestingly, despite a lack of significant sequence identity, the superposition of the bacterial L10 NTD and archaeal L10E NTD, revealed a very similar overall fold. A similar observation was made for the other elements forming the base of the stalk (L11, L10/L11 binding region of rRNA).

These findings pointed to the notion that bacterial and archaeal L10 NTD interact in a similar fashion with the L10/L11 binding region of rRNA. Thus, the *tma*L10 NTD

could be placed on the 50S subunit. The fitting of this domain was further used to line up the entire L10:(L12 NTD)$_6$ structure (Suppl. Figure 3C, Appendices) on the ribosome (Suppl. Figure 3D, Appendices).

## B. Cryo-EM reconstructions of L7/L12 stalk elements

The reconstructed model of the stalk may account for the extended features previously observed in several cryo-EM maps of ribosomes in different phases of translation (Figure 6C). To prove this hypothesis, the resulting model of the stalk was positioned into a cryo-EM envelop of an *E. coli* 70S:EF-G:GDP:fusidic acid (Suppl. Figure 4, left, Appendices) and into various EM maps of ribosome-factor complexes available from public databases (performed by Niels Fischer and Holger Stark, Research Group of 3D Electron Cryo-Microscopy, MPI for Biophysical Chemistry, Göttingen). Convincing fits to a well-defined, extended density neighboring the thiostrepton loop were achieved by shortening the L10:(L12 NTD)$_6$ complex as envisioned for *E. coli* stalk and through a slight rotation of the L10 C-terminal α-helix in the flexible connector to its NTD (Suppl. Figure 4, right, Appendices). The L12 hinges and CTDs could not be located in the density of the *E. coli* 70S:EF-G:GDP:fusidic acid complex, probably due to their mobility.

## C. Active sites of the L7/L12 stalk and their factor-related functions

The L7/L12 stalk architecture displays an arrangement with three flexible regions: (i) the connection between the stalk base and the bulk of the 23S rRNA; (ii) the flexible region in L10; (iii) the highly mobile L12 hinges. This distribution of flexible regions suggests that the mobility progresses towards the extremity of the stalk. This prompted the hypothesis that L12 CTDs carried by highly flexible hinges might represent the active sites of the stalk, responsible for translation factor-related functions. To ascertain this notion, ribosomes lacking or containing mutant L12 CTDs were generated. By a specific ethanol/salt treatment, wild-type ribosomes were depleted of L12 and subsequently replaced with L12 that entirely lacked CTDs or exhibiting mutations in conserved surface residues of the CTDs. Using fast kinetic measurements it was then possible to differentiate effects on initial factor binding and on stimulation of GTP hydrolysis (Ute Kothe, Marina

V. Rodnina, Physical Biochemistry Department, University of Witten/Herdecke; A. Tonevitsky, Biological Department, MV Lomonosov Moscow State University). Ribosomes depleted in L12 CTD exhibited a decrease in the initial factor binding by more than one order of magnitude. In addition, their removal was found to induce a diminution of the rate of GTP hydrolysis on the ribosome by EF-Tu or EF-G of approximately 1000 times. The effects of removing the CTDs were comparable to cores depleted of entire L12 molecules. These results pinpointed L12 CTDs as active sites for initial factor binding and strong stimulators of GTPase reaction within the stalk. To identify the amino acids responsible for GTPase activation, point mutations of all conserved surface residues of L12 CTD were investigated by similar procedures. However, none of the point mutants abolished the GTPase activation, suggesting that none of the amino acid side chains of L12 is involved in catalysis. To further elucidate the stalk function in factor recruitment, the exchange between the ribosome-bound and factor-free L12 both in the presence and absence of EF-G was examined. Unlike its eukaryotic counterparts who appear to perform this exchange, bacterial L12 are found prevalently bound to the ribosome. Only a slow exchange between the free and ribosome-bound bacterial L12 was observed, independent of the presence or absence of EF-G. These findings disfavor models suggesting the recruitment of translation factors to the ribosome through the free L12 pool in bacteria.

# III. The L7/L12 stalk: structural model and function in translation

## A. Structural organization of the L7/L12 stalk

The placement of the *tma*L10:(L12 NTD)$_6$ crystal structure on the 50S subunit, subsequent localization of a L10:(L12 NTD)$_4$ element in cryo-EM reconstructions of *E. coli* 70S ribosomes, and additional guidelines provided by structures of *tma*L11-rRNA complex (Wimberly *et al.* 1999) and *eco*L12 in solution (Bocharov *et al.* 2004), allowed the devising of a complete atomic model of the L7/L12 stalk (Figure 26).

The stalk was divided into three structural and functional segments, delimited by flexible regions: (i) the *stalk base* comprising the entire L10/L11 binding region of 23S rRNA, L11 and the L10 NTD; it serves as an attachment site for the peripheral components of the stalk, positioning them in the neighborhood of the ribosomal factor

binding site; (ii) the _C-terminal α-helix of L10 in complex with the L12 NTDs_ that is flexibly attached to the stalk base, as seen in the three different crystal structures of _tma_L10:(L12 NTD)$_6$ and in the EM analysis; it can therefore be regarded as a moveable platform that carries remaining elements of L12 protein; (iii) highly mobile _L12 CTDs_ that are attached to the mobile platform _via_ the _hinge regions_; most likely the L12 hinges predominantly adopt random coil structures, as in isolated L12 (Bocharov _et al._ 2004), because they are displaced from the L12 NTD dimers by L10 helix α8, in agreement with recent NMR data on 70S ribosomes (Mulder _et al._ 2004). Additional evidence supporting the intrinsic flexibility of the L12 hinges derives from the R32 crystal structure of the L10:L12 complex from _T. maritima_. Attempts to solve the entire structure failed due to an unstructured region in L12 corresponding to the hinge domains.
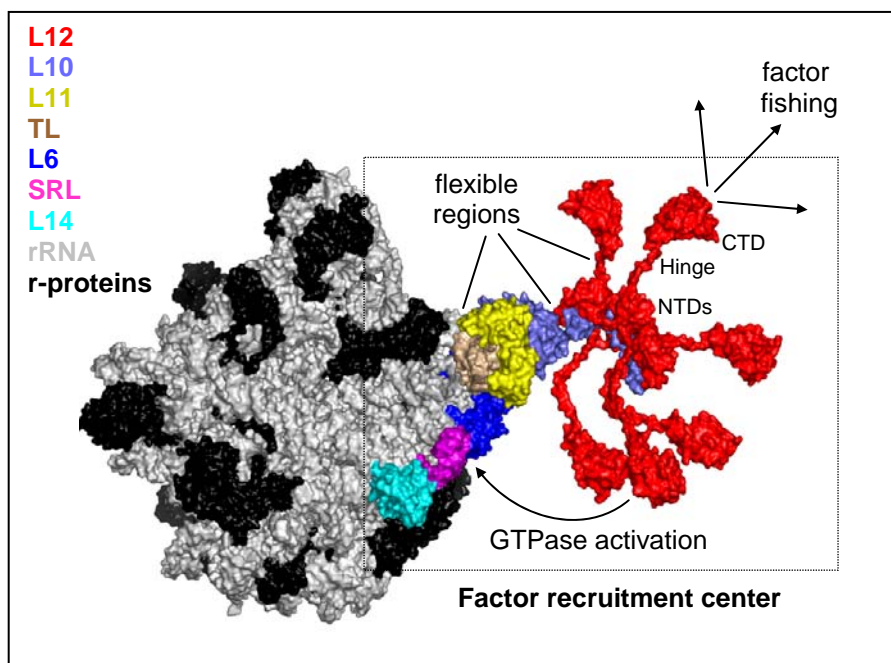


**Figure 26.** A complete structural model of the L7/L12 stalk comprising a L10:(L12)$_6$ complex on the 50S subunit. Proteins and rRNA regions are color-coded in the legend on the left.

Two flexible regions separate the stalk elements: the unstructured loop that connects the L10 NTD to helix α8 and the flexible hinge region intervening between the NTDs and CTDs of L12 and providing a high freedom of motion for the L12 CTDs. As documented by the above mentioned kinetic analysis, the L12 CTDs perform the functional interactions with the factors, and thus constitute the 'active sites' of the stalk. Restriction of L12 CTD mobility by hinge deletions inactivates the ribosome (Gudkov _et_

*al.* 1991; Oleinikov *et al.* 1993), indicating that the high degree of freedom of the L12 CTDs is crucial for the activity of the stalk.

## B. Dynamics of the stalk during translation

Cryo-EM analysis showed that the extended structural elements of the stalk neighboring the base undergo large rearrangements during translation (Agrawal *et al.* 1999) (Figure 6B, C). Previously, these mobile stalk elements were attributed to the hinge regions and CTDs of one L12 dimer (Dey *et al.* 1998). The present results suggest that the extended stalk elements revealed by cryo-EM rather represent the L10 helix $\alpha$8-L12 NTD portion of the stalk. According to the proposed model (Figure 26), L10 helix $\alpha$8-L12 NTD and the L12 CTDs can move relative to one another and relative to the stalk base (L10/L11-binding region of 23S rRNA, L11, L10 NTD). Cryo-EM reconstructions identified different preferred locations of the L10 helix $\alpha$8-L12 NTD part with respect to the stalk base, in 70S:EF-G:GDP:fusidic acid experimental density map and in numerous other EM structures form the database (e.g. 70S:RF2 complexes (data not shown) (Rawat *et al.* 2003)). Thus, EM provides suitable restrains to position portions of the present crystal structures reliably on the 50S subunit. Differences in the orientation of the helix $\alpha$8-(L12 NTD)$_4$ extension seen in complexes with EF-G and RF2 point that its position changes during translation. However, the electron density vanishes beyond helix $\alpha$8-(L12 NTD)$_4$ suggesting that remaining parts of L12 (hinges and CTDs) adopt multiple orientations with respect to the helix $\alpha$8-(L12 NTD)$_4$ segment and apparently are too mobile to be located.

In the EM structure of a 70S:EF-G complex in the GTP conformation (Agrawal *et al.* 1999), a bifurcated protrusion is visible at a similar position as in the 70S:EF:G:GDP-fusidic acid and 70S:RF2 complexes (Figure 6B). The bifurcated parts appear slimmer than the extended density seen in the 70S:EF-G:GDP:fusidic acid and 70S:RF2 structures but seem to have comparable lengths. One possibility is that they correspond to two populations of the helix $\alpha$8-(L12 NTD)$_4$ structure, which are not fully occupied. This structure could not be interpreted in more detail, since the EM density was not available from public databases at the time of this work. However, the mobility of the helix $\alpha$8-(L12 NTD)$_4$ part relative to the L10 NTD may be more extensive than suggested by the crystal structures, underlining its possible role in positioning L12 hinges and CTDs.

Two possibilities could be envisioned regarding the stabilization of the L10 helix α8-L12 NTD part in certain states. First, it has been proposed that upon binding of EF-G and during GTP hydrolysis the L11 NTD moves out independently of the remainder of the stalk base due to direct contacts to the factor (Agrawal *et al.* 2001). Our structures show that the L11 CTD maintains interactions to the L10 NTD. Thus, L11 may constitute a bridge between EF-G and L10 NTD. It is therefore conceivable that structural changes in L11 are communicated to the L10 NTD and could favor a particular interaction between the L10 NTD and the proximal L10 helix α8-L12 NTD dimer element. Examples for three different interaction modes between the latter two components can be seen in the different crystal structures of the L10:(L12 NTD)$_6$ complex (Figure 19B, C). Second, direct L12 CTD-ribosome or CTD-factor contacts could form in certain functional states, thereby restricting the mobility of L10 helix α8-L12 NTD. The possibility of direct L12 CTD-ribosome interactions has previously been suggested by crosslinking (Dey *et al.* 1998), NMR (Mulder *et al.* 2004) and EM studies (Montesano-Roditis *et al.* 2001).

## C. Mechanism of factor binding to the ribosome

The association of both EF-Tu:GTP:aminoacyl-tRNA and EF-G with the ribosome takes place more rapidly than expected for a random encounter of two particles of this size (Rodnina *et al.* 1996; Savelsbergh *et al.* 2003). Our data identify the L12 CTDs as interaction sites for the factors. Thus, the unexpectedly high rate of factors binding to the ribosome may be explained by an increase of the encounter frequency of the ternary complex or EF-G due to multiple copies of L12, leading to a higher association rate by introducing a favorable statistical factor (Rodnina *et al.* 1996). This suggestion is supported by the structural model of the stalk (Figure 26): the L12 CTDs can reach far out into solution, where they can 'catch' translation factors and 'hand them over' to the ribosomal factor binding site, thus efficiently restricting factor diffusion and leading to rapid recruitment. The long, unstructured L12 hinge regions and the flexible connection of the L10 helix α8-L12 NTD portion to the stalk base could allow the interaction of the translation factors with their ribosome binding site after initial capture by the L12 CTDs.

## D. Mechanism of GTPase stimulation

The L12 CTDs are responsible for an about 1000-fold stimulation of GTP hydrolysis by EF-Tu and EF-G. GTPase activation can be achieved either by promoting conformational rearrangements of the factors that correctly position their own catalytic groups in the active site or by donating additional catalytic groups in *trans.* The unique, highly conserved arginine residue in the CTD of L12 is not essential for the activation, excluding an 'arginine finger'-type mechanism (present data and (Savelsbergh *et al.* 2000)). Similarly, none of the other conserved, surface exposed amino acid residues in the CTD alone is responsible for the activation. These findings suggest that L12 facilitates GTP hydrolysis by stabilizing the GTPase transition state of the factors, rather than by providing residues involved in catalysis. This mechanism of activation resembles that of the regulators of G-protein signaling (RGS), which stimulate GTP hydrolysis in Gα proteins (for review see (Vetter and Wittinghofer 1999)).

Cryo-EM reconstructions showed extensive interactions of the G domains of both EF-Tu and EF-G with the SRL of 23S rRNA (Agrawal *et al.* 1998; Stark *et al.* 2002; Valle *et al.* 2003b), indicating that the SRL may stabilize the transition state conformation of the factors. Single-molecule fluorescence measurements indicated that cleavage of the SRL blocks EF-Tu in a state before GTP hydrolysis (Blanchard *et al.* 2004). Other contacts, which may contribute to GTP hydrolysis, include ribosomal protein L11 and the L11-binding region of 23S rRNA (Agrawal *et al.* 2001). L12 represents a third ribosomal element important for stimulation of GTP hydrolysis. *Via* its CTD it may both facilitate positioning the factors relative to other ribosomal components contributing to catalysis and stabilize the active conformation of the factors. Therefore, it can be envisaged that the L12 CTDs use their high freedom of motion to reach back towards the ribosome-bound factors to stimulate their GTPase activity. The requirement for additional signals for full stimulation of the GTPase activity, such as the interaction with SRL or L11, would help to avoid premature GTP hydrolysis during initial factor binding.

## E. Cross-kingdom similarities and differences in the stalk

The archaeal L10E NTD is structurally homologous to bacterial L10 NTD, consistent with a similar mode of binding to the 23S rRNA. Sequence conservation between archaeal and eukaryotic L10 orthologs (Figure 22) suggests that the eukaryotic P0

proteins are also similarly structured in the N-terminal part, and thus presumably bind to the 28S rRNA in a similar way. The notion of a structurally conserved rRNA binding module in L10 orthologs across the kingdoms, which seems to recognize a conserved fold in the rRNAs, explains why archaeal or eukaryotic orthologs of the L10:L12 complex can be attached to bacterial ribosomes and *vice versa* (Sanchez-Madrid *et al.* 1981; Stoffler-Meilicke and Stoffler 1991; Uchiumi *et al.* 1999; Uchiumi *et al.* 2002; Terasaki *et al.* 2004; Nomura *et al.* 2006). Eukaryotic P0:P1/P2 complexes transplanted onto *E. coli* ribosomes are functional, provided that eukaryotic translation factors are supplied.

However, beyond the rRNA binding domain, eukaryotic L10 orthologs differ from their bacterial counterparts in structure and in the mode of interaction with L12 orthologs (for a recent review see (Gonzalo and Reboud 2003)). E.g. eukaryotic P0 proteins are considerably longer than bacterial L10 (by some 150 residues) and the ultimate C-terminal part of L10 may encompass a P1/P2-like structure (Gonzalo and Reboud 2003). Eukaryotes maintain two (P1 and P2, some with subfamilies), plants possibly three (an additional P3) families of acidic phosphoproteins, which interact with P0. The more intricate organization of the P0:P1/P2(P3) complexes in higher organisms compared to the bacterial L10:L12 complexes may reflect additional functions in translation regulation (Gonzalo and Reboud 2003). The present results indicate that free bacterial L12 exchanges only very slowly with ribosome-bound L12. This situation seems to be decisively different in eukaryotes where exchange of P1/P2 and phosphorylation during translation were suggested to modify expression of some mRNAs (Gonzalo and Reboud 2003).

# **Outlook**

## I. L10$_{\Delta DBS}$:L12 complexes from *Thermotoga maritima*

Structures at 2.3, 2.1 and 1.9 Å resolution were determined for a bacterial L10:(L12 NTD)$_6$ complex. As previously described, their analysis demonstrated that the C-terminal domain of L10 carrying L12 NTDs is flexibly connected to its NTD *via* a short "hinge". Despite the certain degree of mobility of this complex, three well-diffracting crystal forms were easily obtained. Conversely, attempts to crystallize full-length L10:(L12)$_6$ complexes resulted in another truncated variant corresponding to L10:(L12 NTD)$_6$. The trimming occured in the hinge regions, which are most probably in an extended, random coil conformation and thereby susceptible to proteolysis. These results suggested that although the inherent flexibility of this complex is difficult to surmount, shorter complex variants could cope with some flexibility and result in well-resolved structures. In this view, terminal deletion variants of L10 were designed to carry either one or two full-length L12 dimers (L10$_{\Delta DBS}$:L12; DBS, dimer binding site). This approach was possible as the C-terminal α-helix of L10 is kinked in two positions, resulting in three almost equal segments, each of which accommodating one L12 dimer. The resulting L10$_{\Delta DBS}$:L12 complexes would reveal the structure of the full-length L12 molecules in the context of the L10:L12 complex. In addition, the placement of these truncated complexes on the ribosome would address the issue of whether L12 dimers attached to different sites in the L10 molecule perform different functions.

### A. Production of the *tma*L10$_{\Delta 2DBS}$:L12 complex

In order to generate a L10:L12 complex carrying one (*tma*L10$_{\Delta 2DBS}$:L12) or two (*tma*L10$_{\Delta 1DBS}$:L12) dimers of L12, stop codons were introduced after codon 153 and 163 respectively, in the plasmid used for *tma*L10 production (Table 8). *tma*L10$_{\Delta 2DBS}$ and *tma*L12$_{\Delta 1DBS}$ encoding plasmids were then co-transformed with the plasmid used for *tma*L12 production (Wahl *et al.* 2000b) and subsequently co-expressed in Rosetta(DE3) strain (Figure 27-1). So far, only the production of *tma*L10$_{\Delta 2DBS}$:L12 was carried out (Figure 27-2,3). The purification procedure was performed as described for *tma*L10:(L12

NTD)$_6$ (see section III.A.1., Results). Fractions containing the complex were combined, concentrated to 10 mg/ml and subjected to crystallization.
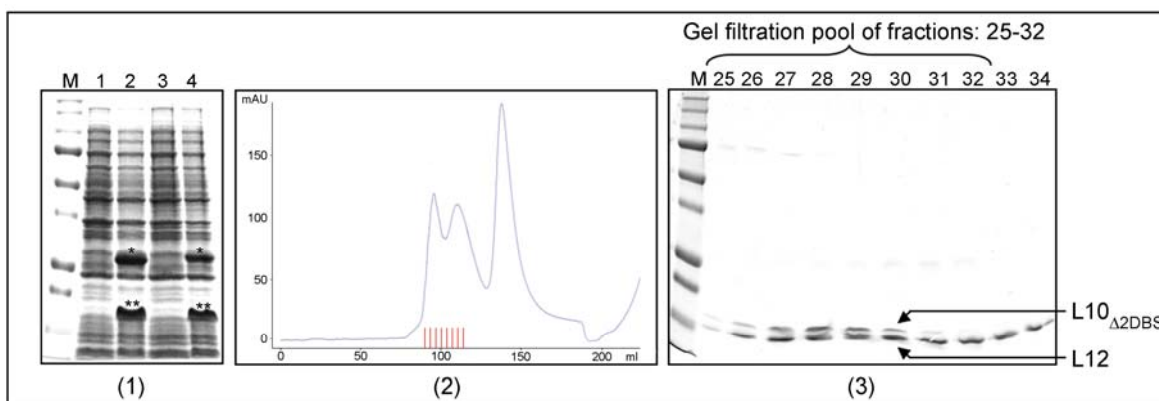


**Figure 27.** (1) Expression of *tma*L10$_{\Delta DBS}$:L12 complexes. Prior induction (lane 1) and post induction (lane 2) phases of *tma*L10$_{\Delta 2DBS}$:L12 complex expression; prior induction (lane 3) and post induction (lane 4) phases of *tma*L10$_{\Delta 1DBS}$:L12 complex expression; (*) overexpressed *tma*L10$_{\Delta 2DBS}$ and *tma*L10$_{\Delta 1DBS;}$ (**) overexpressed full-length L12. (2) Chromatogram representing the elution profile of the *tma*L10$_{\Delta 2DBS}$:L12 complex on the Superdex 75 gel filtration column, as the last step of purification. (3) Fractions containing the purified complex (25-32) were combined and concentrated to 10 mg/ml.

## B. Crystallization trials of the *tma*L10$_{\Delta 2DBS}$:L12 complex

A high-throughput crystallization experiment was initiated on the in-house vapor diffusion nano drop robot. 288 different conditions were screened for the *tma*L10$_{\Delta 2DBS}$:L12 complex using sparse matrix from Nextal Biotechnologies and Hampton Research. The outcome of these experiments is currently under investigation.

# II. *tma*L12 CTD and its interaction with elongation factors

Several lines of evidence indicated the involvement of L12 in various translation factor-related functions. The placement of the isolated *tma*L10:(L12 NTD)$_6$ structure on the large ribosomal subunit and the resulting model of the L7/L12 stalk, suggested that L12 CTDs represent the active sites of the stalk (Figure 26). Indeed, carefully designed fast kinetic experiments pinpointed L12 CTDs as primary interaction sites for factor GTPases and as active stimulators of their GTP hydrolysis (U. Kothe, M.V. Rodnina, see section II. C. and D., Discussion). As a mechanism of GTP hydrolysis, it was hypothesized that the L12 CTDs could either remain bound to the factors' G domain during movement of the factors to the ribosomal factor binding site or they could reach back towards the ribosome-bound

factor to stimulate their GTPase activities. Consequently, attempts to identify interactions between L12 CTD and the G domains of elongation factors (EF-Tu and EF-G) by means of X-ray crystallography and Biacore, using purified proteins from *T. maritima*, were made.

## A. Production of the *tma*L12 CTD and of *tma*EF-Tu(Gd)

Both L12 CTD and the G-domain of EF-Tu (EF-Tu(Gd)) were expressed from pETM-11 (Figure 28A-1) and pET22b(+) vectors in Rosetta(DE3) strain. The pETM-11 vector provide an N-terminal His$_6$-tag, whereas the pET22b(+) has no affinity tag (Table 5). In order to detect a potential interaction between L12 CTD and EF-Tu(Gd), a His$_6$-tag L12 CTD fusion protein from pETM-11 was co-transformed and subsequently co-expressed with EF-Tu(Gd) from pET22b(+) and *vice versa*. Only minute amounts of *tma*EF-Tu(Gd) protein were co-purified with His$_6$-*tma*L12 CTD on Ni-NTA affinity matrix (and *vice versa*), suggesting a very weak interaction between them (data not shown). Thus, for subsequent crystallographic and interaction studies, both proteins were produced individually from pETM-11 vector and combined in the end (Figure 28A-2, 3, 4, 5). The purification procedure used was as described previously for the *tma*L10:(L12 NTD)$_6$ (see section III.A.1., Results).
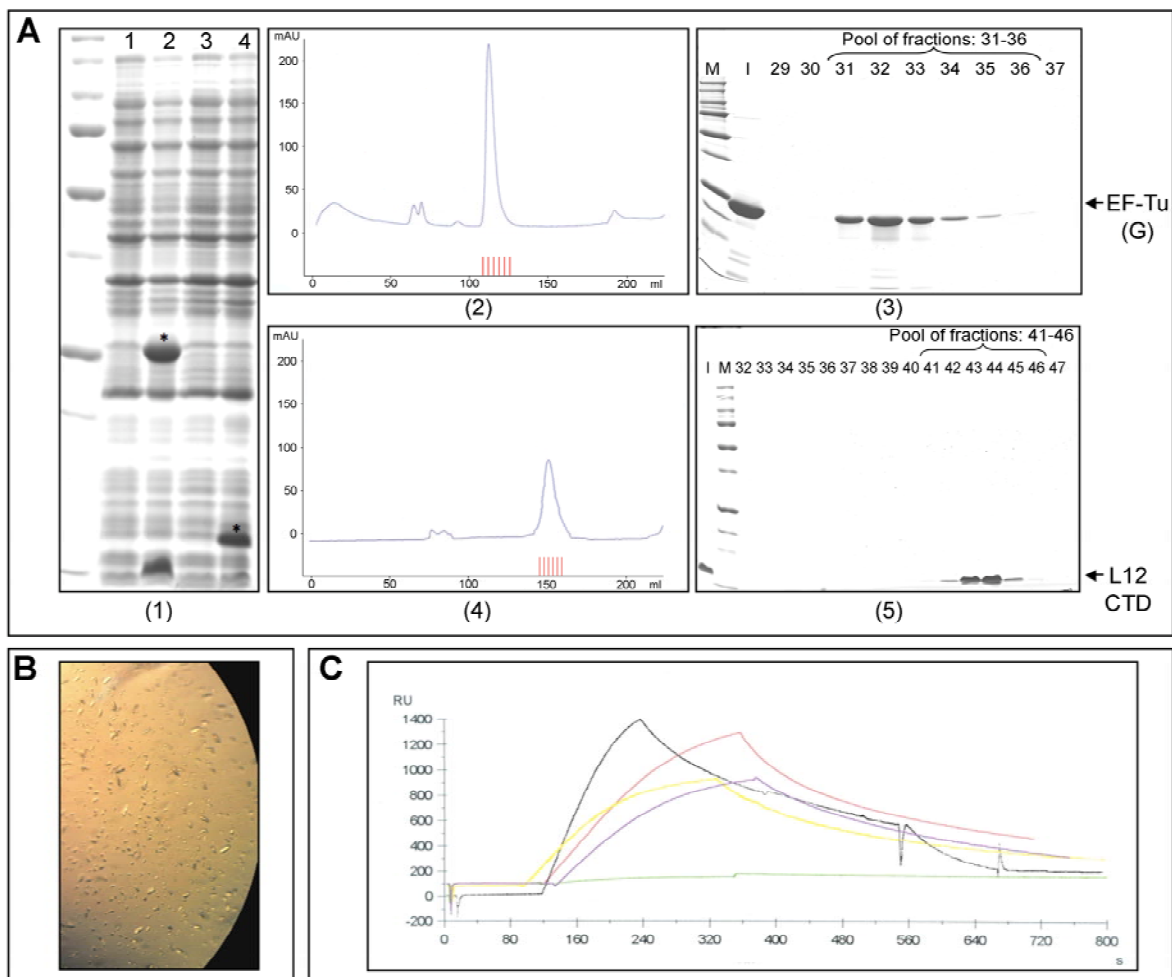
**Figure 28. (A)** (1) prior induction (lane 1) and post induction (lane 2) phases of His$_6$-*tma*EF-Tu(Gd) expression; prior induction (lane 3) and post induction (lane 4) phases of His$_6$-*tma*L12 CTD expression; (*) overexpressed proteins *tma*EF-Tu(Gd) and *tma*L12 CTD, respectively. (2) Chromatogram representing the elution profile of the *tma*EF-Tu(Gd) on a Superdex 75 gel filtration column, as a last step of the purification procedure. (3) Fractions (31-36) containing the purified protein were combined and concentrated to 10 mg/ml. (4) Chromatogram representing the elution profile of the *tma*L12 CTD on a Superdex 75 gel filtration column, as a last step of the purification procedure. (5) Fractions (41-46) containing the purified protein were combined and concentrated to 8 mg/ml. I, input sample, collected before the gel filtration chromatographic step. **(B)** *tma*L12 CTD:EF-Tu(Gd):GMPPNP putative crystals. **(C)** Sensorgram representing changes in the resonance signal [RU] over time [s] for the *tma*L12 CTD (yellow curve), *tma*L12 CTD:EF-Tu(Gd) (violet curve), *tma*L12 CTD:EF-Tu(Gd):GTP (black curve), *tma*EF-G (green curve), *tma*L12 CTF:EF-G (red curve). The sensorgram is a direct representation of the interaction between molecules in real time. 1000 RU (resonance units) represent a shift in the resonance angle of 0.1°. The Biacore measurements were performed together with Dr. Igor Agapov, Witten.

## B. Crystallization trials

672 different conditions (Nextal Biotechnologies) were set up at 20°C for each of the following complexes:

(1) *tma*L12 CTD:EF-Tu(Gd) :GDP in a molar ratio of 1 :1 :15

(2) *tma*L12 CTD:EF-Tu(Gd) :GMPPNP in a molar ratio of 1:1:20 (where GMPPNP is a non-hydrolysable GTP analogue)

(3) *tma*L12 CTD:EF-G :GMPPNP in a molar ratio of 1:1:20 ( full-length *tma*EF-G was kindly provided by A. Savelsbergh, Witten)

One condition belonging only to the L12 CTD:EF-Tu(Gd):GMPPNP yielded crystals represented in Figure 28B. Further screening and testing of these crystals are ongoing.

## C. Interaction studies of the *tma*L12 CTD and elongation factors by Biacore

In parallel with crystallization trials, the association ability of *tma*L12 CTD with either elongation factor was monitored using surface plasmon resonance (Biacore). A His$_6$-tagged *tma*L12 CTD fusion protein was produced for this purpose. After controlling that only this protein can bind onto the surface of the Ni-NTA sensor chip, samples containing *tma*L12 CTD together with *tma*EF-Tu(Gd) or *tma*EF-G were injected over this surface at a constant flow rate through a microfluidic channel system. His$_6$-*tma*L12 CTD alone bound to the Ni-NTA chip and produced a SPR signal of approximately 900 resonance units (RU) (Figure 28C, yellow curve). No variation in the SPR could be detected in the presence of *tma*EF-Tu(Gd) as compared to the sole *tma*L12 CTD (Figure 28C, violet curve). The latter result indicated that the binding between the two components is very weak or absent. The time-dependent dissociation was also found similar to the control sample. In the next approach, the addition of a complex of *tma*EF-Tu(Gd):GTP (with GTP incorporated in a pyruvate kinase-dependent reaction) had also no effect on the time-dependent dissociation of the His$_6$-*tma*L12 CTD (Figure 28C, black curve). The observed increase in the amplitude of the sensorgram is only related to almost doubly-concentrated ligand (His$_6$-*tma*L12 CTD) and analyte (*tma*EF-Tu(Gd):GTP) used in this experiment. To rule out any unspecific binding of *tma*EF-G to the Ni-NTA surface or to His$_6$-tagged *tma*L12 CTD,

*tma*EF-G was directly added onto the Ni-NTA chip (Figure 28C, green curve). No binding of *tma*EF-G onto the Ni-NTA chip was detected. Interestingly, when a premix of His$_6$-*tma*L12 CTD with *tma*EF-G was added onto the Ni-NTA chip, the SPR signal was found increased by a factor of 1.5 as compared to the sole His$_6$-*tma*L12 CTD, indicating a direct interaction between the two components (Figure 28C, red curve). Additionally, the dissociation of this complex was slower than for the control protein. Similar SPR data were reported for the eukaryotic counterparts, where eEF-2 was found to interact specifically *in vitro* with P proteins, however, with a higher affinity for P1 than for P2 (Bargis-Surgey *et al.* 1999).

Taken together, these results suggest that in isolation, EF-Tu(Gd) and L12 CTD molecules do not seem to associate or their association is very weak. The latter possibility is supported by the fact that small amounts of *tma*EF-Tu(Gd) were co-purified together with His$_6$-*tma*L12 CTD on Ni-NTA beads (data not shown). In contrast, EF-G and L12 CTD appear to associate in isolation. However, the relatively fast dissociation in time does not suggest a tight interaction between the two components. These results are in line with kinetic data regarding the effect of protein L12 on the GTP hydrolysis by EF-Tu and EF-G in isolation. L12 strongly stimulated GTP hydrolysis by EF-G (Savelsbergh *et al.* 2000), but not by EF-Tu, indicating that for the latter event additional ribosomal components are required (Piepenburg *et al.* 2000).

# III. L11:L12 CTD complexes from *Thermotoga maritima*

Highly mobile L12 CTDs promote the recruitment of translation factors to the ribosome and stimulate GTP hydrolysis by the ribosome-bound factors through stabilization of their active GTPase conformation. However, in the latter process, the involvement of additional elements, including protein L11 or sarcin-ricin loop seem to be required to prevent premature GTP hydrolysis during initial factor binding by L12 CTD. In order to identify a potential interaction between protein L11 and L12 CTD, a crystallographic experiment was initiated and a preliminary binding study by isothermal titration calorimetry was performed.

## A. Production of *tma*L11

L11 was expressed from pETM-11 and was found to preferentially require *E. coli* BL21(DE3) strain for propagation (Figure 29A-1). Following its expression, the $His_6$-L11 fusion protein was purified *via* Ni-NTA affinity chromatography. After removal of the $His_6$-tag, the protein was further purified by heat treatment and cation exchange chromatography. The final preparation was concentrated to 10 mg/ml (Figure 29A-2,3).
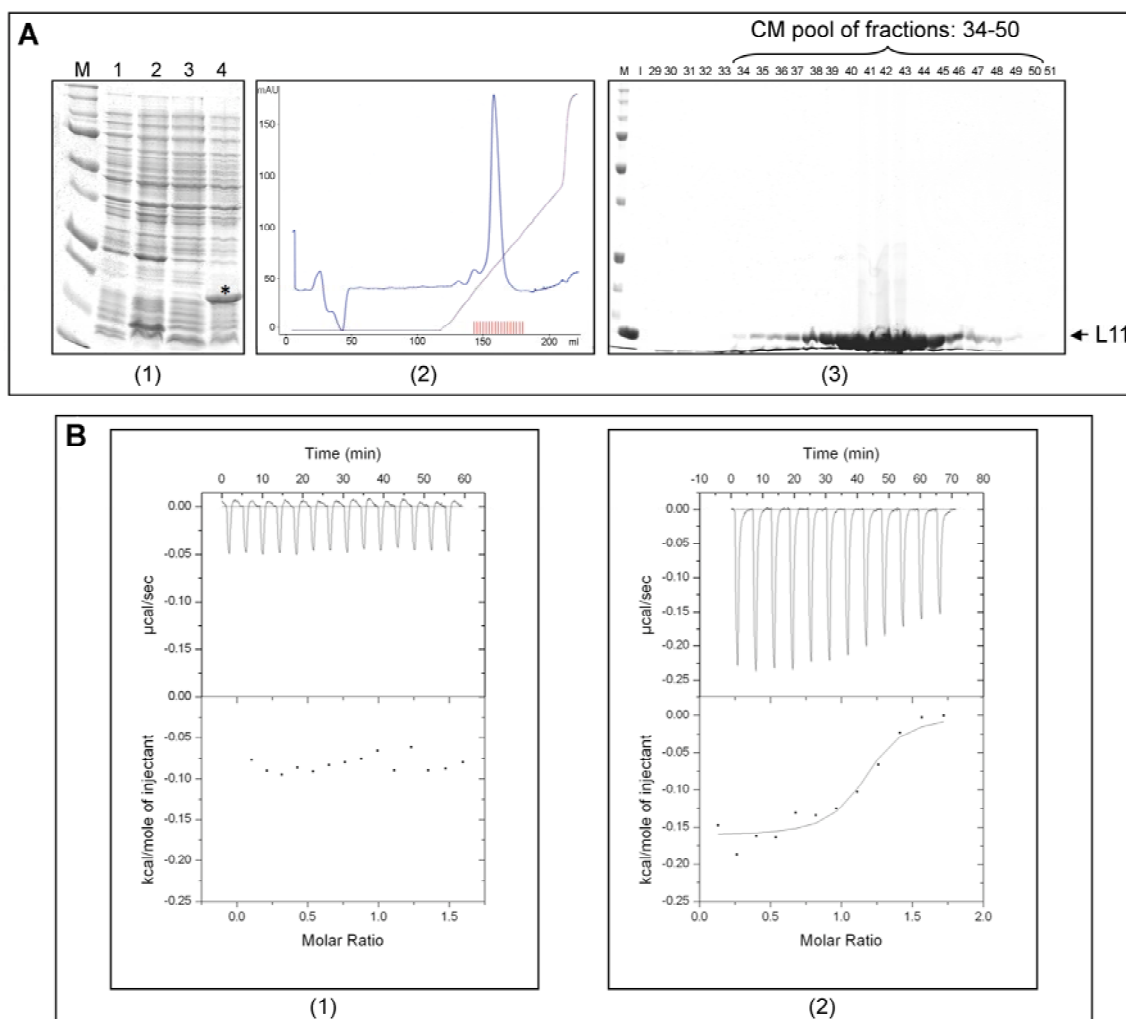


**Figure 29**. **(A)** Expression and purification of *tma*L11. (1) prior induction (lane 1) and post induction (lane 2) phases of *tma*L11 expression in Rosetta(DE3) strain, no expression was detected; prior induction (lane 3) and post induction (lane 4) phases of *tma*L11 expression in BL21(DE3) strain, (*) overexpressed protein. (2) Chromatogram representing the elution profile of the *tma*L11 on a CM cation exchange column, as the last step of the purification procedure. (3) Fractions (34-50) containing the purified protein were combined and concentrated to 10 mg/ml. **(B)** (1) ITC of the system's buffer as control, $\Delta H= -0.05$ kcal/mol. (2) ITC data for titration of 135 μM *tma*L12 CTD with 12 injections of 1mM *tma*L11. *Upper* panel: raw power (μcal/sec) *versus* time tracing. At each injection an exothermic spike is seen. The area under each spike is proportional to the heat of binding of *tma*L11 to *tma*L12 CTD; *lower* panel: amount of heat measured at each injection normalized to the number of moles of *tma*L11 injected (kcal/mol) versus molar ratio of cumulative *tma*L11 added to the *tma*L12 CTD in the cell. Data analysis indicated that the saturation will be reached at 2:1 molar ratio of *tma*L12 CTD:*tma*L11. A binding of $\Delta H= -0.16$ kcal/mol *tma*L11, and an equilibrium dissociation constant $k_d= 1.9$μM were obtained.

## B. Crystallization trials of *tma*L11:L12 CTD

*tma*L11 and *tma*L12 CTD proteins were mixed in a molar ratio of 1:1, at a final concentration of 9 mg/ml, incubated approximately 15 h at 4°C to allow complex formation and subjected to crystallization trials. 1152 different conditions (Nextal Biotechnologies) were next screened for the *tma*L11:L12 CTD, at 20°C, on the in-house vapor diffusion dispensing apparatus. These experiments are ongoing.

## C. Interaction study of the *tma*L11 and *tma*L12 CTD by isothermal titration calorimetry

A putative interaction between *tma*L12 CTD and *tma*L11 was assessed by microcalorimetry. Prior to this determination, a control sample representing the buffer of the sistem was analysed (Figure 29B-1). Subsequently, a titration of 135 µM *tma*L12 CTD (placed in a calorimetric cell) with 12 injections of 1 mM *tma*L11 was performed (Figure 29B-2). Increasing amounts of *tma*L11 were added to *tma*L12 CTD at the indicated molar ratios in a microcalorimeter, and the energy required to compensate for the binding enthalpy in order to reestablish thermal equilibrium after each addition, was measured and plotted in microcalories per second (Figure 29B-2, *upper* panel). From the plot of the binding enthalpies (Figure 29B-2, *lower* panel), transitions due to saturation appeared to be achieved for a stoichiometry of 1 mole of *tma*L11 to approximately 2 moles of *tma*L12 CTD. The dissociation equilibrium constant ($k_d$) was 1.9 µM, suggesting a weak interaction between the two components in isolation. Further testing of this interaction is currently under investigation. The accuracy of the above mentioned experiment needs to be ascertained by measurements with an increased amount of both cell and syringe reactants.

Despite the low affinity between these two components in isolation, several lines of evidence suggested an interaction between *tma*L12 CTD and *tma*L11 on the ribosome. Cryo-EM studies revealed that the G domains of factor GTPases (in their GDP bound conformation) form an arc-like connection with the base of the L7/L12 stalk (Stark *et al.* 1997a; Agrawal *et al.* 1998). Subsequently, the element at the base of the stalk implicated in the formation of this bridge was identified as L11 NTD (Agrawal *et al.* 2001). Recently, another cryo-EM analysis further delineated boundaries of the G' domain of EF-G and L11

NTD and tentatively positioned between them one copy of L12 CTD (Datta *et al.* 2005). This location of L12 CTD is in agreement with cross-linking (Dey *et al.* 1998) and EM (Montesano-Roditis *et al.* 2001) data that placed the L12 CTD in the vicinity of L11. In the present calorimetric study L11 and L12 CTD exhibit a low affinity for each other in isolation, suggesting that additional ribosomal elements or factor contacts are required for their proper association and function. Remarkably, in the above mentioned study of Datta and coworkers, the L12 CTD was seen near the L11 NTD lobe, both in the presence and absence of EF-G. During the course of EF-G-dependent reactions, L12 CTD underwent considerable conformational changes in association with L11 NTD. Furthermore, the L12 CTD was found slightly twisted toward the G' domain of EF-G upon GTP hydrolysis. The positioning of the L12 CTD was not close to the GTP catalysis center of EF-G, in agreement with our observation that L12 CTD activates GTP hydrolysis allosterically rather than catalytically. In addition to stimulating GTP hydrolysis by EF-G, the L12 CTD could also assist the release of the factor from the ribosome. Following GTP hydrolysis, the domain V of EF-G pushes outward the L11 NTD. This movement is transmitted to neighboring L12 CTD, which in turn would signal the dissociation of EF-G:GDP from the ribosome. Thus, L12 CTD is portrayed as a "multi-task" element, with dynamic and diverse role in the ribosome function, including the recognition and recruitment of various translational factors, the triggering of GTP hydrolysis-related events, and finally the removal of those factors from the ribosome.

# **References**

Ævarsson, A., Brazhnikov, E., Garber, M., Zheltonosova, J., Chirgadze, Y., al-Karadaghi, S., Svensson, L.A., and Liljas, A. 1994. Three-dimensional structure of the ribosomal translocase: elongation factor G from Thermus thermophilus. *Embo J* **13**(16): 3669-3677.

Agrawal, R.K., Heagle, A.B., Penczek, P., Grassucci, R.A., and Frank, J. 1999. EF-G-dependent GTP hydrolysis induces translocation accompanied by large conformational changes in the 70S ribosome. *Nat Struct Biol* **6**(7): 643-647.

Agrawal, R.K., Linde, J., Sengupta, J., Nierhaus, K.H., and Frank, J. 2001. Localization of L11 protein on the ribosome and elucidation of its involvement in EF-G-dependent translocation. *J Mol Biol* **311**(4): 777-787.

Agrawal, R.K., Penczek, P., Grassucci, R.A., and Frank, J. 1998. Visualization of elongation factor G on the Escherichia coli 70S ribosome: the mechanism of translocation. *Proc Natl Acad Sci U S A* **95**(11): 6134-6138.

Al-Karadaghi, S., Kristensen, O., and Liljas, A. 2000. A decade of progress in understanding the structural basis of protein synthesis. *Prog Biophys Mol Biol* **73**(2-4): 167-193.

Allen, G.S., Zavialov, A., Gursky, R., Ehrenberg, M., and Frank, J. 2005. The cryo-EM structure of a translation initiation complex from Escherichia coli. *Cell* **121**(5): 703-712.

Ban, N., Nissen, P., Hansen, J., Capel, M., Moore, P.B., and Steitz, T.A. 1999. Placement of protein and RNA structures into a 5 A-resolution map of the 50S ribosomal subunit. *Nature* **400**(6747): 841-847.

Ban, N., Nissen, P., Hansen, J., Moore, P.B., and Steitz, T.A. 2000. The complete atomic structure of the large ribosomal subunit at 2.4 A resolution. *Science* **289**(5481): 905-920.

Bargis-Surgey, P., Lavergne, J.P., Gonzalo, P., Vard, C., Filhol-Cochet, O., and Reboud, J.P. 1999. Interaction of elongation factor eEF-2 with ribosomal P proteins. *Eur J Biochem* **262**(2): 606-611.

Barton, G.J. 1993. ALSCRIPT: a tool to format multiple sequence alignments. *Protein Eng* **6**(1): 37-40.

Beauclerk, A.A., Cundliffe, E., and Dijk, J. 1984. The binding site for ribosomal protein complex L8 within 23 s ribosomal RNA of Escherichia coli. *J Biol Chem* **259**(10): 6559-6563.

Berchtold, H., Reshetnikova, L., Reiser, C.O., Schirmer, N.K., Sprinzl, M., and Hilgenfeld, R. 1993. Crystal structure of active elongation factor Tu reveals major domain rearrangements. *Nature* **365**(6442): 126-132.

Blanchard, S.C., Gonzalez, R.L., Kim, H.D., Chu, S., and Puglisi, J.D. 2004. tRNA selection and kinetic proofreading in translation. *Nat Struct Mol Biol* **11**(10): 1008-1014.

Bocharov, E.V., Gudkov, A.T., and Arseniev, A.S. 1996. Topology of the secondary structure elements of ribosomal protein L7/L12 from E. coli in solution. *FEBS Lett* **379**(3): 291-294.

Bocharov, E.V., Sobol, A.G., Pavlov, K.V., Korzhnev, D.M., Jaravine, V.A., Gudkov, A.T., and Arseniev, A.S. 2004. From structure and dynamics of protein L7/L12 to molecular switching in ribosome. *J Biol Chem* **279**(17): 17697-17706.

Boelens, R. and Gualerzi, C.O. 2002. Structure and function of bacterial initiation factors. *Curr Protein Pept Sci* **3**(1): 107-119.

Boublik, M., Hellmann, W., and Roth, H.E. 1976. Localization of ribosomal proteins L7L12 in the 50 S subunit of Escherichia coli Ribosomes by electron microscopy. *J Mol Biol* **107**(4): 479-490.

Bourne, H.R., Sanders, D.A., and McCormick, F. 1991. The GTPase superfamily: conserved structure and molecular mechanism. *Nature* **349**(6305): 117-127.

Bradford, M.M. 1976. A rapid and sensitive method for the quantitation of microgram quantities of protein utilizing the principle of protein-dye binding. *Anal Biochem* **72**: 248-254.

Brodersen, D.E., Clemons, W.M., Jr., Carter, A.P., Morgan-Warren, R.J., Wimberly, B.T., and Ramakrishnan, V. 2000. The structural basis for the action of the antibiotics tetracycline, pactamycin, and hygromycin B on the 30S ribosomal subunit. *Cell* **103**(7): 1143-1154.

Brodersen, D.E., Clemons, W.M., Jr., Carter, A.P., Wimberly, B.T., and Ramakrishnan, V. 2002. Crystal structure of the 30 S ribosomal subunit from Thermus thermophilus: structure of the proteins and their interactions with 16 S RNA. *J Mol Biol* **316**(3): 725-768.

Brosius, J., Dull, T.J., and Noller, H.F. 1980. Complete nucleotide sequence of a 23S ribosomal RNA gene from Escherichia coli. *Proc Natl Acad Sci U S A* **77**(1): 201-204.

Brot, N., Tate, W.P., Caskey, C.T., and Weissbach, H. 1974. The requirement for ribosomal proteins L7 and L12 in peptide-chain termination. *Proc Natl Acad Sci U S A* **71**(1): 89-92.

Brot, N. and Weissbach, H. 1981. Chemistry and biology of E. coli ribosomal protein L12. *Mol Cell Biochem* **36**(1): 47-63.

Brunger, A.T., Adams, P.D., Clore, G.M., DeLano, W.L., Gros, P., Grosse-Kunstleve, R.W., Jiang, J.S., Kuszewski, J., Nilges, M., Pannu, N.S., Read, R.J., Rice, L.M., Simonson, T., and Warren, G.L. 1998. Crystallography & NMR system: A new software suite for macromolecular structure determination. *Acta Crystallogr D Biol Crystallogr* **54**(Pt 5): 905-921.

Budisa, N., Steipe, B., Demange, P., Eckerskorn, C., Kellermann, J., and Huber, R. 1995. High-level biosynthetic substitution of methionine in proteins by its analogs 2-aminohexanoic acid, selenomethionine, telluromethionine and ethionine in Escherichia coli. *Eur J Biochem* **230**(2): 788-796.

Bushuev, V.N., Gudkov, A.T., Liljas, A., and Sepetov, N.F. 1989. The flexible region of protein L12 from bacterial ribosomes studied by proton nuclear magnetic resonance. *J Biol Chem* **264**(8): 4498-4505.

Cameron, D.M., Thompson, J., March, P.E., and Dahlberg, A.E. 2002. Initiation factor IF2, thiostrepton and micrococcin prevent the binding of elongation factor G to the Escherichia coli ribosome. *J Mol Biol* **319**(1): 27-35.

Carter, A.P., Clemons, W.M., Brodersen, D.E., Morgan-Warren, R.J., Wimberly, B.T., and Ramakrishnan, V. 2000. Functional insights from the structure of the 30S ribosomal subunit and its interactions with antibiotics. *Nature* **407**(6802): 340-348.

Carter, A.P., Clemons, W.M., Jr., Brodersen, D.E., Morgan-Warren, R.J., Hartsch, T., Wimberly, B.T., and Ramakrishnan, V. 2001. Crystal structure of an initiation factor bound to the 30S ribosomal subunit. *Science* **291**(5503): 498-501.

Casiano, C., Matheson, A.T., and Traut, R.R. 1990. Occurrence in the archaebacterium Sulfolobus solfataricus of a ribosomal protein complex corresponding to Escherichia coli (L7/L12)4.L10 and eukaryotic (P1)2/(P2)2.P0. *J Biol Chem* **265**(31): 18757-18761.

Cate, J.H., Yusupov, M.M., Yusupova, G.Z., Earnest, T.N., and Noller, H.F. 1999. X-ray crystal structures of 70S ribosome functional complexes. *Science* **285**(5436): 2095-2104.

Chandra Sanyal, S. and Liljas, A. 2000. The end of the beginning: structural studies of ribosomal proteins. *Curr Opin Struct Biol* **10**(6): 633-636.

References

Chinali, G. and Parmeggiani, A. 1982. Differential modulation of the elongation-factor-G GTPase activity by tRNA bound to the ribosomal A-site or P-site. *Eur J Biochem* **125**(2): 415-421.

Clemons, W.M., Jr., May, J.L., Wimberly, B.T., McCutcheon, J.P., Capel, M.S., and Ramakrishnan, V. 1999. Structure of a bacterial 30S ribosomal subunit at 5.5 A resolution. *Nature* **400**(6747): 833-840.

Correll, C.C., Munishkin, A., Chan, Y.L., Ren, Z., Wool, I.G., and Steitz, T.A. 1998. Crystal structure of the ribosomal RNA domain essential for binding elongation factors. *Proc Natl Acad Sci U S A* **95**(23): 13436-13441.

Cundliffe, E. and Thompson, J. 1981. Concerning the mode of action of micrococcin upon bacterial protein synthesis. *Eur J Biochem* **118**(1): 47-52.

Czworkowski, J., Wang, J., Steitz, T.A., and Moore, P.B. 1994. The crystal structure of elongation factor G complexed with GDP, at 2.7 A resolution. *Embo J* **13**(16): 3661-3668.

Datta, P.P., Sharma, M.R., Qi, L., Frank, J., and Agrawal, R.K. 2005. Interaction of the G' domain of elongation factor G and the C-terminal domain of ribosomal protein L7/L12 during translocation as revealed by cryo-EM. *Mol Cell* **20**(5): 723-731.

De Vendittis, E., Masullo, M., and Bocchini, V. 1986. The elongation factor G carries a catalytic site for GTP hydrolysis, which is revealed by using 2-propanol in the absence of ribosomes. *J Biol Chem* **261**(10): 4445-4450.

Dell, V.A., Miller, D.L., and Johnson, A.E. 1990. Effects of nucleotide- and aurodox-induced changes in elongation factor Tu conformation upon its interactions with aminoacyl transfer RNA. A fluorescence study. *Biochemistry* **29**(7): 1757-1763.

Deusser, E. 1972. Heterogeneity of ribosomal populations in Escherichia coli cells grown in different media. *Mol Gen Genet* **119**(3): 249-258.

Dey, D., Bochkariov, D.E., Jokhadze, G.G., and Traut, R.R. 1998. Cross-linking of selected residues in the N- and C-terminal domains of Escherichia coli protein L7/L12 to other ribosomal proteins and the effect of elongation factor Tu. *J Biol Chem* **273**(3): 1670-1676.

Dey, D., Oleinikov, A.V., and Traut, R.R. 1995. The hinge region of Escherichia coli ribosomal protein L7/L12 is required for factor binding and GTP hydrolysis. *Biochimie* **77**(12): 925-930.

Diaconu, M., Kothe, U., Schlunzen, F., Fischer, N., Harms, J.M., Tonevitsky, A.G., Stark, H., Rodnina, M.V., and Wahl, M.C. 2005. Structural basis for the function of the ribosomal L7/12 stalk in factor binding and GTPase activation. *Cell* **121**(7): 991-1004.

Dijk, J., Garrett, R.A., and Muller, R. 1979. Studies on the binding of the ribosomal protein complex L7/12-L10 and protein L11 to the 5'-one third of 23S RNA: a functional centre of the 50S subunit. *Nucleic Acids Res* **6**(8): 2717-2729.

Draper, D.E. and Reynaldo, L.P. 1999. RNA binding strategies of ribosomal proteins. *Nucleic Acids Res* **27**(2): 381-388.

Drenth, J. 1994. *Principles of protein X-ray crystallography*. Springer, New York.

Egebjerg, J., Douthwaite, S.R., Liljas, A., and Garrett, R.A. 1990. Characterization of the binding sites of protein L11 and the L10.(L12)4 pentameric complex in the GTPase domain of 23 S ribosomal RNA from Escherichia coli. *J Mol Biol* **213**(2): 275-288.

Endo, Y., Mitsui, K., Motizuki, M., and Tsurugi, K. 1987. The mechanism of action of ricin and related toxic lectins on eukaryotic ribosomes. The site and the characteristics of the modification in 28 S ribosomal RNA caused by the toxins. *J Biol Chem* **262**(12): 5908-5912.

Endo, Y. and Wool, I.G. 1982. The site of action of alpha-sarcin on eukaryotic ribosomes. The sequence at the alpha-sarcin cleavage site in 28 S ribosomal ribonucleic acid. *J Biol Chem* **257**(15): 9054-9060.

Fakunding, J.L., Traut, R.R., and Hershey, J.W. 1973. Dependence of initiation factor IF-2 activity on proteins L7 and L12 from Escherichia coli 50 S ribosomes. *J Biol Chem* **248**(24): 8555-8559.

Fernandez-Puentes, C. and Vazquez, D. 1977. Effects of some proteins that inactivate the eukaryotic ribosome. *FEBS Lett* **78**(1): 143-146.

Frank, J. and Agrawal, R.K. 2000. A ratchet-like inter-subunit reorganization of the ribosome during translocation. *Nature* **406**(6793): 318-322.

Gavrilova, L.P., Kostiashkina, O.E., Koteliansky, V.E., Rutkevitch, N.M., and Spirin, A.S. 1976. Factor-free ("non-enzymic") and factor-dependent systems of translation of polyuridylic acid by Escherichia coli ribosomes. *J Mol Biol* **101**(4): 537-552.

Goldberg, J. 1999. Structural and functional analysis of the ARF1-ARFGAP complex reveals a role for coatomer in GTP hydrolysis. *Cell* **96**(6): 893-902.

Gonzalo, P. and Reboud, J.P. 2003. The puzzling lateral flexible stalk of the ribosome. *Biol Cell* **95**(3-4): 179-193.

Griaznova, O. and Traut, R.R. 2000. Deletion of C-terminal residues of Escherichia coli ribosomal protein L10 causes the loss of binding of one L7/L12 dimer: ribosomes with one L7/L12 dimer are active. *Biochemistry* **39**(14): 4075-4081.

Gualerzi, C.O. and Pon, C.L. 1990. Initiation of mRNA translation in prokaryotes. *Biochemistry* **29**(25): 5881-5889.

Gudkov, A.T. 1997. The L7/L12 ribosomal domain of the ribosome: structural and functional studies. *FEBS Lett* **407**(3): 253-256.

Gudkov, A.T. and Behlke, J. 1978. The N-terminal sequence protein of L7/L 12 is responsible for its dimerization. *Eur J Biochem* **90**(2): 309-312.

Gudkov, A.T., Behlke, J., Vtiurin, N.N., and Lim, V.I. 1977. Tertiary and quaternary structure for ribosomal protein L7 in solution. *FEBS Lett* **82**(1): 125-129.

Gudkov, A.T., Bubunenko, M.G., and Gryaznova, O.I. 1991. Overexpression of L7/L12 protein with mutations in its flexible region. *Biochimie* **73**(11): 1387-1389.

Gudkov, A.T., Gongadze, G.M., Bushuev, V.N., and Okon, M.S. 1982. Proton nuclear magnetic resonance study of the ribosomal protein L7/L12 in situ. *FEBS Lett* **138**(2): 229-232.

Gudkov, A.T., Tumanova, L.G., Gongadze, G.M., and Bushuev, V.N. 1980. Role of different regions of ribosomal proteins L7 and L10 in their complex formation and in the interaction with the ribosomal 50 S subunit. *FEBS Lett* **109**(1): 34-38.

Gudkov, A.T., Tumanova, L.G., Venyaminov, S.Y., and Khechinashvilli, N.N. 1978. Stoichiometry and properties of the complex between ribosomal proteins L7 and L10 in solution. *FEBS Lett* **93**(2): 215-218.

Gutell, R.R. 1996. *Ribosomal RNA: Structure, Evolution, Processing and Function in Protein Biosynthesis*. CRC Press, Boca Raton, FL, 1996.

Hamel, E., Koka, M., and Nakamoto, T. 1972. Requirement of an Escherichia coli 50 S ribosomal protein component for effective interaction of the ribosome with T and G factors and with guanosine triphosphate. *J Biol Chem* **247**(3): 805-814.

Hanson, C.L., Fucini, P., Ilag, L.L., Nierhaus, K.H., and Robinson, C.V. 2003. Dissociation of intact Escherichia coli ribosomes in a mass spectrometer. Evidence for conformational change in a ribosome elongation factor G complex. *J Biol Chem* **278**(2): 1259-1267.

Hansson, S., Singh, R., Gudkov, A.T., Liljas, A., and Logan, D.T. 2005. Crystal structure of a mutant elongation factor G trapped with a GTP analogue. *FEBS Lett* **579**(20): 4492-4497.

Hardy, S.J. 1975. The stoichiometry of the ribosomal proteins of Escherichia coli. *Mol Gen Genet* **140**(3): 253-274.

Harms, J., Schluenzen, F., Zarivach, R., Bashan, A., Gat, S., Agmon, I., Bartels, H., Franceschi, F., and Yonath, A. 2001. High resolution structure of the large ribosomal subunit from a mesophilic eubacterium. *Cell* **107**(5): 679-688.

Hartz, D., McPheeters, D.S., and Gold, L. 1989. Selection of the initiator tRNA by Escherichia coli initiation factors. *Genes Dev* **3**(12A): 1899-1912.

Hensens, O.D., Albers-Schonberg, G., and Anderson, B.F. 1983. The solution conformation of the peptide antibiotic thiostrepton: a 1H NMR study. *J Antibiot (Tokyo)* **36**(7): 799-813.

Hunt, T.W., Fields, T.A., Casey, P.J., and Peralta, E.G. 1996. RGS10 is a selective activator of G alpha i GTPase activity. *Nature* **383**(6596): 175-177.

Ilag, L.L., Videler, H., McKay, A.R., Sobott, F., Fucini, P., Nierhaus, K.H., and Robinson, C.V. 2005. Heptameric (L12)6/L10 rather than canonical pentameric complexes are found by tandem MS of intact ribosomes from thermophilic bacteria. *Proc Natl Acad Sci U S A* **102**(23): 8192-8197.

Inoue-Yokosawa, N., Ishikawa, C., and Kaziro, Y. 1974. The role of guanosine triphosphate in translocation reaction catalyzed by elongation factor G. *J Biol Chem* **249**(13): 4321-4323.

Kaltschmidt, E. and Wittmann, H.G. 1970. Ribosomal proteins. VII. Two-dimensional polyacrylamide gel electrophoresis for fingerprinting of ribosomal proteins. *Anal Biochem* **36**(2): 401-412.

Karimi, R., Pavlov, M.Y., Buckingham, R.H., and Ehrenberg, M. 1999. Novel roles for classical factors at the interface between translation termination and initiation. *Mol Cell* **3**(5): 601-609.

Kastner, B., Stoffler-Meilicke, M., and Stoffler, G. 1981. Arrangement of the subunits in the ribosome of Escherichia coli: demonstration by immunoelectron microscopy. *Proc Natl Acad Sci U S A* **78**(11): 6652-6656.

Kawakita, M., Arai, K., and Kaziro, Y. 1974. Interactions between elongation factor tu-guanosine triphosphate and ribosomes and the role of ribosome-bound transfer RNA in guanosine triphosphatase reaction. *J Biochem (Tokyo)* **76**(4): 801-809.

Kaziro, Y. 1978. The role of guanosine 5'-triphosphate in polypeptide chain elongation. *Biochim Biophys Acta* **505**(1): 95-127.

Kischa, K., Moller, W., and Stoffler, G. 1971. Reconstitution of a GTPase activity by a 50S ribosomal protein and E. coli. *Nat New Biol* **233**(36): 62-63.

Kisselev, L.L. and Buckingham, R.H. 2000. Translational termination comes of age. *Trends Biochem Sci* **25**(11): 561-566.

Kjeldgaard, M., Nissen, P., Thirup, S., and Nyborg, J. 1993. The crystal structure of elongation factor EF-Tu from Thermus aquaticus in the GTP conformation. *Structure* **1**(1): 35-50.

Klaholz, B.P., Myasnikov, A.G., and Van Heel, M. 2004. Visualization of release factor 3 on the ribosome during termination of protein synthesis. *Nature* **427**(6977): 862-865.

Klein, D.J., Moore, P.B., and Steitz, T.A. 2004. The roles of ribosomal proteins in the structure assembly, and evolution of the large ribosomal subunit. *J Mol Biol* **340**(1): 141-177.

Klein, D.J., Schmeing, T.M., Moore, P.B., and Steitz, T.A. 2001. The kink-turn: a new RNA secondary structure motif. *Embo J* **20**(15): 4214-4221.

Kopke, A.K., Leggatt, P.A., and Matheson, A.T. 1992. Structure function relationships in the ribosomal stalk proteins of archaebacteria. *J Biol Chem* **267**(2): 1382-1390.

Kothe, U., Wieden, H.J., Mohr, D., and Rodnina, M.V. 2004. Interaction of helix D of elongation factor Tu with helices 4 and 5 of protein L7/12 on the ribosome. *J Mol Biol* **336**(5): 1011-1021.

Kristensen, O., Laurberg, M., Liljas, A., and Selmer, M. 2002. Is tRNA binding or tRNA mimicry mandatory for translation factors? *Curr Protein Pept Sci* **3**(1): 133-141.

## References

La Teana, A., Gualerzi, C.O., and Dahlberg, A.E. 2001. Initiation factor IF 2 binds to the alpha-sarcin loop and helix 89 of Escherichia coli 23S ribosomal RNA. *Rna* **7**(8): 1173-1179.

Laemmli, U.K. 1970. Cleavage of structural proteins during the assembly of the head of bacteriophage T4. *Nature* **227**(5259): 680-685.

Lake, J.A. 1976. Ribosome structure determined by electron microscopy of Escherichia coli small subunits, large subunits and monomeric ribosomes. *J Mol Biol* **105**(1): 131-139.

Laskowski, R.A., MacArthur, M.W., Moss, D.S., and Thornton, J.M. 1993. PROCHECK: a program to check the stereochemical quality of protein structures. *J Appl Cryst* **26**: 283-291.

Leffers, H., Egebjerg, J., Andersen, A., Christensen, T., and Garrett, R.A. 1988. Domain VI of Escherichia coli 23 S ribosomal RNA. Structure, assembly and function. *J Mol Biol* **204**(3): 507-522.

Leijonmarck, M., Eriksson, S., and Liljas, A. 1980. Crystal structure of a ribosomal component at 2.6 A resolution. *Nature* **286**(5775): 824-826.

Liao, D. and Dennis, P.P. 1994. Molecular phylogenies based on ribosomal protein L11, L1, L10, and L12 sequences. *J Mol Evol* **38**(4): 405-419.

Liljas, A. 1982. Structural studies of ribosomes. *Prog Biophys Mol Biol* **40**(3): 161-228.

Liljas, A. 1991. Comparative biochemistry and biophysics of ribosomal proteins. *Int Rev Cytol* **124**: 103-136.

Liljas, A., Erikssson, S., Donner, D., and Kurland, C.G. 1978. Isolation and crystallization of stable domains of the protein L7/L12 from Escherichia coli ribosomes. *FEBS Lett* **88**(2): 300-304.

Liljas, A. and Garber, M. 1995. Ribosomal proteins and elongation factors. *Curr Opin Struct Biol* **5**(6): 721-727.

Liljas, A. and Gudkov, A.T. 1987. The structure and dynamics of ribosomal protein L12. *Biochimie* **69**(10): 1043-1047.

Liljas, A. and Newcomer, M.E. 1981. Purification and crystallization of protein complex from Bacillus stearothermophilus ribosomes. *J Mol Biol* **153**(2): 393-398.

Littlefield, J.W., Keller, E.B., Gross, J., and Zamecnik, P.C. 1955. Studies on cytoplasmic ribonucleoprotein particles from the liver of the rat. *J Biol Chem* **217**(1): 111-123.

Lucas-Lenard, J. and Lipmann, F. 1966. Separation of three microbial amino acid polymerization factors. *Proc Natl Acad Sci U S A* **55**(6): 1562-1566.

Luer, C.A. and Wong, K.P. 1980. Conformational stability of ribosomal protein L7/L12: effects of pH, temperature, and guanidinium chloride. *Biochemistry* **19**(1): 176-183.

Maitra, U., Stringer, E.A., and Chaudhuri, A. 1982. Initiation factors in protein biosynthesis. *Annu Rev Biochem* **51**: 869-900.

Martemyanov, K.A., Liljas, A., and Gudkov, A.T. 2000. Extremely thermostable elongation factor G from Aquifex aeolicus: cloning, expression, purification, and characterization in a heterologous translation system. *Protein Expr Purif* **18**(3): 257-261.

Martemyanov, K.A., Liljas, A., Yarunin, A.S., and Gudkov, A.T. 2001. Mutations in the G-domain of elongation factor G from Thermus thermophilus affect both its interaction with GTP and fusidic acid. *J Biol Chem* **276**(31): 28774-28778.

Masullo, M., Parlato, G., De Vendittis, E., and Bocchini, V. 1989. Effect of propan-2-ol on enzymic and structural properties of elongation factor G. *Biochem J* **261**(3): 725-731.

Mesters, J.R., Potapov, A.P., de Graaf, J.M., and Kraal, B. 1994. Synergism between the GTPase activities of EF-Tu.GTP and EF-G.GTP on empty ribosomes. Elongation factors as stimulators of the ribosomal oscillation between two conformations. *J Mol Biol* **242**(5): 644-654.

Moazed, D., Robertson, J.M., and Noller, H.F. 1988. Interaction of elongation factors EF-G and EF-Tu with a conserved loop in 23S RNA. *Nature* **334**(6180): 362-364.

Moens, P.D., Wahl, M.C., and Jameson, D.M. 2005. Oligomeric state and mode of self-association of Thermotoga maritima ribosomal stalk protein L12 in solution. *Biochemistry* **44**(9): 3298-3305.

Moller, W., Groene, A., Terhorst, C., and Amons, R. 1972. 50-S ribosomal proteins. Purification and partial characterization of two acidic proteins, A 1 and A 2, isolated from 50-S ribosomes of Escherichia coli. *Eur J Biochem* **25**(1): 5-12.

Moller, W., Schrier, P.I., Maassen, J.A., Zantema, A., Schop, E., Reinalda, H., Cremers, A.F., and Mellema, J.E. 1983. Ribosomal proteins L7/L12 of Escherichia coli. Localization and possible molecular mechanism in translation. *J Mol Biol* **163**(4): 553-573.

Montanaro, L., Sperti, S., Mattioli, A., Testoni, G., and Stirpe, F. 1975. Inhibition by ricin of protein synthesis in vitro. Inhibition of the binding of elongation factor 2 and of adenosine diphosphate-ribosylated elongation factor 2 to ribosomes. *Biochem J* **146**(1): 127-131.

Montesano-Roditis, L., Glitz, D.G., Traut, R.R., and Stewart, P.L. 2001. Cryo-electron microscopic localization of protein L7/L12 within the Escherichia coli 70 S ribosome by difference mapping and Nanogold labeling. *J Biol Chem* **276**(17): 14117-14123.

Moreno, J.M., Drskjotersen, L., Kristensen, J.E., Mortensen, K.K., and Sperling-Petersen, H.U. 1999. Characterization of the domains of E. coli initiation factor IF2 responsible for recognition of the ribosome. *FEBS Lett* **455**(1-2): 130-134.

Morris, R.J., Perrakis, A., and Lamzin, V.S. 2003. ARP/wARP and automatic interpretation of protein electron density maps. *Methods Enzymol* **374**: 229-244.

Mulder, F.A., Bouakaz, L., Lundell, A., Venkataramana, M., Liljas, A., Akke, M., and Sanyal, S. 2004. Conformation and dynamics of ribosomal stalk protein L12 in solution and on the ribosome. *Biochemistry* **43**(20): 5930-5936.

Munishkin, A. and Wool, I.G. 1997. The ribosome-in-pieces: binding of elongation factor EF-G to oligoribonucleotides that mimic the sarcin/ricin and thiostrepton domains of 23S ribosomal RNA. *Proc Natl Acad Sci U S A* **94**(23): 12280-12284.

Myasnikov, A.G., Marzi, S., Simonetti, A., Giuliodori, A.M., Gualerzi, C.O., Yusupova, G., Yusupov, M., and Klaholz, B.P. 2005. Conformational transition of initiation factor 2 from the GTP- to GDP-bound state visualized on the ribosome. *Nat Struct Mol Biol* **12**(12): 1145-1149.

Nierhaus, K.H. and Dohme, F. 1974. Total reconstitution of functionally active 50S ribosomal subunits from Escherichia coli. *Proc Natl Acad Sci U S A* **71**(12): 4713-4717.

Nilsson, J. and Nissen, P. 2005. Elongation factors on the ribosome. *Curr Opin Struct Biol* **15**(3): 349-354.

Nissen, P., Hansen, J., Ban, N., Moore, P.B., and Steitz, T.A. 2000a. The structural basis of ribosome activity in peptide bond synthesis. *Science* **289**(5481): 920-930.

Nissen, P., Kjeldgaard, M., and Nyborg, J. 2000b. Macromolecular mimicry. *Embo J* **19**(4): 489-495.

Nissen, P., Kjeldgaard, M., Thirup, S., Polekhina, G., Reshetnikova, L., Clark, B.F., and Nyborg, J. 1995. Crystal structure of the ternary complex of Phe-tRNAPhe, EF-Tu, and a GTP analog. *Science* **270**(5241): 1464-1472.

Noel, J.P. 1997. Turning off the Ras switch with the flick of a finger. *Nat Struct Biol* **4**(9): 677-680.

Noller, H.F., Hoffarth, V., and Zimniak, L. 1992. Unusual resistance of peptidyl transferase to protein extraction procedures. *Science* **256**(5062): 1416-1419.

Nomura, T., Mochizuki, R., Dabbs, E.R., Shimizu, Y., Ueda, T., Hachimori, A., and Uchiumi, T. 2003. A point mutation in ribosomal protein L7/L12 reduces its ability to form a compact dimer structure and to assemble into the GTPase center. *Biochemistry* **42**(16): 4691-4698.

References

Nomura, T., Nakano, K., Maki, Y., Naganuma, T., Nakashima, T., Tanaka, I., Kimura, M., Hachimori, A., and Uchiumi, T. 2006. In vitro reconstitution of the GTPase-associated center of the archaebacterial ribosome: the functional features observed in a hybrid form with Escherichia coli 50S subunits. *Biochem J*.

Nyborg, J. 1998. Possible evolution of factors involved in protein biosynthesis. *Acta Biochim Pol* **45**(4): 883-894.

Ogle, J.M., Brodersen, D.E., Clemons, W.M., Jr., Tarry, M.J., Carter, A.P., and Ramakrishnan, V. 2001. Recognition of cognate transfer RNA by the 30S ribosomal subunit. *Science* **292**(5518): 897-902.

Ogle, J.M. and Ramakrishnan, V. 2005. Structural insights into translational fidelity. *Annu Rev Biochem* **74**: 129-177.

Oleinikov, A.V., Perroud, B., Wang, B., and Traut, R.R. 1993. Structural and functional domains of Escherichia coli ribosomal protein L7/L12. The hinge region is required for activity. *J Biol Chem* **268**(2): 917-922.

Otwinowski, Z. and Minor, W. 1996. Processing of x-ray diffraction data collected in the oscillation mode. *Methods enzymol* **276**: 307-326.

Palade, G.E. 1955. A small particulate component of the cytoplasm. *J Biophys Biochem Cytol* **1**(1): 59-68.

Pape, T., Wintermeyer, W., and Rodnina, M.V. 1998. Complete kinetic mechanism of elongation factor Tu-dependent binding of aminoacyl-tRNA to the A site of the E. coli ribosome. *Embo J* **17**(24): 7490-7497.

Pestka, S. 1970. Thiostrepton: a ribosomal inhibitor of translocation. *Biochem Biophys Res Commun* **40**(3): 667-674.

Pettersson, I. 1979. Studies on the RNA and protein binding sites of the E. coli ribosomal protein L10. *Nucleic Acids Res* **6**(7): 2637-2646.

Pettersson, I., Hardy, S.J., and Liljas, A. 1976. The ribosomal protein L8 is a complex L7/L12 and L10. *FEBS Lett* **64**(1): 135-138.

Pettersson, I. and Kurland, C.G. 1980. Ribosomal protein L7/L12 is required for optimal translation. *Proc Natl Acad Sci U S A* **77**(7): 4007-4010.

Pettersson, I. and Liljas, A. 1979. The stoichiometry and reconstitution of a stable protein complex from Escherichia coli ribosomes. *FEBS Lett* **98**(1): 139-144.

Piepenburg, O., Pape, T., Pleiss, J.A., Wintermeyer, W., Uhlenbeck, O.C., and Rodnina, M.V. 2000. Intact aminoacyl-tRNA is required to trigger GTP hydrolysis by elongation factor Tu on the ribosome. *Biochemistry* **39**(7): 1734-1738.

Pioletti, M., Schlunzen, F., Harms, J., Zarivach, R., Gluhmann, M., Avila, H., Bashan, A., Bartels, H., Auerbach, T., Jacobi, C., Hartsch, T., Yonath, A., and Franceschi, F. 2001. Crystal structures of complexes of the small ribosomal subunit with tetracycline, edeine and IF3. *Embo J* **20**(8): 1829-1839.

Polekhina, G., Thirup, S., Kjeldgaard, M., Nissen, P., Lippmann, C., and Nyborg, J. 1996. Helix unwinding in the effector region of elongation factor EF-Tu-GDP. *Structure* **4**(10): 1141-1151.

Ramakrishnan, V. 2002. Ribosome structure and the mechanism of translation. *Cell* **108**(4): 557-572.

Rawat, U., Gao, H., Zavialov, A., Gursky, R., Ehrenberg, M., and Frank, J. 2006. Interactions of the release factor RF1 with the ribosome as revealed by cryo-EM. *J Mol Biol* **357**(4): 1144-1153.

Rawat, U.B., Zavialov, A.V., Sengupta, J., Valle, M., Grassucci, R.A., Linde, J., Vestergaard, B., Ehrenberg, M., and Frank, J. 2003. A cryo-electron microscopic study of ribosome-bound termination factor RF2. *Nature* **421**(6918): 87-90.

Rodes, G. 2000. *Crystallography Made Crystal Clear: A Guide for Users of Macromolecular Models*. Academic Press, San Diego.

References

Rodnina, M.V., Daviter, T., Gromadski, K., and Wintermeyer, W. 2002. Structural dynamics of ribosomal RNA during decoding on the ribosome. *Biochimie* **84**(8): 745-754.

Rodnina, M.V., Pape, T., Fricke, R., Kuhn, L., and Wintermeyer, W. 1996. Initial binding of the elongation factor Tu.GTP.aminoacyl-tRNA complex preceding codon recognition on the ribosome. *J Biol Chem* **271**(2): 646-652.

Rodnina, M.V., Savelsbergh, A., Katunin, V.I., and Wintermeyer, W. 1997. Hydrolysis of GTP by elongation factor G drives tRNA movement on the ribosome. *Nature* **385**(6611): 37-41.

Rodnina, M.V., Savelsbergh, A., Matassova, N.B., Katunin, V.I., Semenkov, Y.P., and Wintermeyer, W. 1999. Thiostrepton inhibits the turnover but not the GTPase of elongation factor G on the ribosome. *Proc Natl Acad Sci U S A* **96**(17): 9586-9590.

Rodnina, M.V. and Wintermeyer, W. 1995. GTP consumption of elongation factor Tu during translation of heteropolymeric mRNAs. *Proc Natl Acad Sci U S A* **92**(6): 1945-1949.

Rosendahl, G. and Douthwaite, S. 1993. Ribosomal proteins L11 and L10.(L12)4 and the antibiotic thiostrepton interact with overlapping regions of the 23 S rRNA backbone in the ribosomal GTPase centre. *J Mol Biol* **234**(4): 1013-1020.

Sambrook, G., Fritsch, E.F., and Maniatis, T. 1989. *Molecular cloning: A laboratory manual, second edition.*, New York.

Sanchez-Madrid, F., Vidales, F.J., and Ballesta, J.P. 1981. Functional role of acidic ribosomal proteins. Interchangeability of proteins from bacterial and eukaryotic cells. *Biochemistry* **20**(11): 3263-3266.

Sanger, F., Nicklen, S., and Coulson, A.R. 1977. DNA sequencing with chain-terminating inhibitors. *Proc Natl Acad Sci U S A* **74**(12): 5463-5467.

Saraste, M., Sibbald, P.R., and Wittinghofer, A. 1990. The P-loop--a common motif in ATP- and GTP-binding proteins. *Trends Biochem Sci* **15**(11): 430-434.

Savelsbergh, A., Katunin, V.I., Mohr, D., Peske, F., Rodnina, M.V., and Wintermeyer, W. 2003. An elongation factor G-induced ribosome rearrangement precedes tRNA-mRNA translocation. *Mol Cell* **11**(6): 1517-1523.

Savelsbergh, A., Mohr, D., Wilden, B., Wintermeyer, W., and Rodnina, M.V. 2000. Stimulation of the GTPase activity of translation elongation factor G by ribosomal protein L7/12. *J Biol Chem* **275**(2): 890-894.

Schluenzen, F., Tocilj, A., Zarivach, R., Harms, J., Gluehmann, M., Janell, D., Bashan, A., Bartels, H., Agmon, I., Franceschi, F., and Yonath, A. 2000. Structure of functionally activated small ribosomal subunit at 3.3 angstroms resolution. *Cell* **102**(5): 615-623.

Schlunzen, F., Zarivach, R., Harms, J., Bashan, A., Tocilj, A., Albrecht, R., Yonath, A., and Franceschi, F. 2001. Structural basis for the interaction of antibiotics with the peptidyl transferase centre in eubacteria. *Nature* **413**(6858): 814-821.

Schmeing, T.M., Seila, A.C., Hansen, J.L., Freeborn, B., Soukup, J.K., Scaringe, S.A., Strobel, S.A., Moore, P.B., and Steitz, T.A. 2002. A pre-translocational intermediate in protein synthesis observed in crystals of enzymatically active 50S subunits. *Nat Struct Biol* **9**(3): 225-230.

Schmidt, F.J., Thompson, J., Lee, K., Dijk, J., and Cundliffe, E. 1981. The binding site for ribosomal protein L11 within 23 S ribosomal RNA of Escherichia coli. *J Biol Chem* **256**(23): 12301-12305.

Schneider, T.R. and Sheldrick, G.M. 2002. Substructure solution with SHELXD. *Acta Crystallogr D Biol Crystallogr* **58**(Pt 10 Pt 2): 1772-1779.

Schuwirth, B.S., Borovinskaya, M.A., Hau, C.W., Zhang, W., Vila-Sanjurjo, A., Holton, J.M., and Cate, J.H. 2005. Structures of the bacterial ribosome at 3.5 A resolution. *Science* **310**(5749): 827-834.

Shimmin, L.C., Newton, C.H., Ramirez, C., Yee, J., Downing, W.L., Louie, A., Matheson, A.T., and Dennis, P.P. 1989. Organization of genes encoding the L11, L1, L10, and

L12 equivalent ribosomal proteins in eubacteria, archaebacteria, and eucaryotes. *Can J Microbiol* **35**(1): 164-170.

Shine, J. and Dalgarno, L. 1974. The 3'-terminal sequence of Escherichia coli 16S ribosomal RNA: complementarity to nonsense triplets and ribosome binding sites. *Proc Natl Acad Sci U S A* **71**(4): 1342-1346.

Sievers, A., Beringer, M., Rodnina, M.V., and Wolfenden, R. 2004. The ribosome as an entropy trap. *Proc Natl Acad Sci U S A* **101**(21): 7897-7901.

Spirin, A.S. 1985. Ribosomal translocation: facts and models. *Prog Nucleic Acid Res Mol Biol* **32**: 75-114.

Sprang, S.R. 1997. G protein mechanisms: insights from structural analysis. *Annu Rev Biochem* **66**: 639-678.

Stark, H., Orlova, E.V., Rinke-Appel, J., Junke, N., Mueller, F., Rodnina, M., Wintermeyer, W., Brimacombe, R., and van Heel, M. 1997a. Arrangement of tRNAs in pre- and posttranslocational ribosomes revealed by electron cryomicroscopy. *Cell* **88**(1): 19-28.

Stark, H., Rodnina, M.V., Rinke-Appel, J., Brimacombe, R., Wintermeyer, W., and van Heel, M. 1997b. Visualization of elongation factor Tu on the Escherichia coli ribosome. *Nature* **389**(6649): 403-406.

Stark, H., Rodnina, M.V., Wieden, H.J., van Heel, M., and Wintermeyer, W. 2000. Large-scale movement of elongation factor G and extensive conformational change of the ribosome during translocation. *Cell* **100**(3): 301-309.

Stark, H., Rodnina, M.V., Wieden, H.J., Zemlin, F., Wintermeyer, W., and van Heel, M. 2002. Ribosome interactions of aminoacyl-tRNA and elongation factor Tu in the codon-recognition complex. *Nat Struct Biol* **9**(11): 849-854.

Steitz, T.A. and Moore, P.B. 2003. RNA, the first macromolecular catalyst: the ribosome is a ribozyme. *Trends Biochem Sci* **28**(8): 411-418.

Stoffler-Meilicke, M. and Stoffler, G. 1991. The binding site of ribosomal protein L10 in eubacteria and archaebacteria is conserved: reconstitution of chimeric 50S subunits. *Biochimie* **73**(6): 797-804.

Strycharz, W.A., Nomura, M., and Lake, J.A. 1978. Ribosomal proteins L7/L12 localized at a single region of the large subunit by immune electron microscopy. *J Mol Biol* **126**(2): 123-140.

Subramanian, A.R. 1975. Copies of proteins L7 and L12 and heterogeneity of the large subunit of Escherichia coli ribosome. *J Mol Biol* **95**(1): 1-8.

Szewczak, A.A. and Moore, P.B. 1995. The sarcin/ricin loop, a modular RNA. *J Mol Biol* **247**(1): 81-98.

Szick, K., Springer, M., and Bailey-Serres, J. 1998. Evolutionary analyses of the 12-kDa acidic ribosomal P-proteins reveal a distinct protein of higher plant ribosomes. *Proc Natl Acad Sci U S A* **95**(5): 2378-2383.

Tate, W.P., Dognin, M.J., Noah, M., Stoffler-Meilicke, M., and Stoffler, G. 1984. The NH2-terminal domain of Escherichia coli ribosomal protein L11. Its three-dimensional location and its role in the binding of release factors 1 and 2. *J Biol Chem* **259**(11): 7317-7324.

Taylor, M.M., Glasgow, J.E., and Storck, R. 1967. Sedimentation coefficients of RNA from 70S and 80S ribosomes. *Proc Natl Acad Sci U S A* **57**(1): 164-169.

Terasaki, M., Suzuki, T., Hanada, T., and Watanabe, K. 2004. Functional compatibility of elongation factors between mammalian mitochondrial and bacterial ribosomes: characterization of GTPase activity and translation elongation by hybrid ribosomes bearing heterologous L7/12 proteins. *J Mol Biol* **336**(2): 331-342.

Terhorst, C., Moller, W., Laursen, R., and Wittmann-Liebold, B. 1973. The primary structure of an acidic protein from 50-S ribosomes of Escherichia coli which is involved in GTP hydrolysis dependent on elongation factors G and T. *Eur J Biochem* **34**(1): 138-152.

References
_____

Thompson, J., Cundliffe, E., and Stark, M. 1979. Binding of thiostrepton to a complex of 23-S rRNA with ribosomal protein L11. *Eur J Biochem* **98**(1): 261-265.

Thompson, J.D., Gibson, T.J., Plewniak, F., Jeanmougin, F., and Higgins, D.G. 1997. The CLUSTAL_X windows interface: flexible strategies for multiple sequence alignment aided by quality analysis tools. *Nucleic Acids Res* **25**(24): 4876-4882.

Tocilj, A., Schlunzen, F., Janell, D., Gluhmann, M., Hansen, H.A., Harms, J., Bashan, A., Bartels, H., Agmon, I., Franceschi, F., and Yonath, A. 1999. The small ribosomal subunit from Thermus thermophilus at 4.5 A resolution: pattern fittings and the identification of a functional site. *Proc Natl Acad Sci U S A* **96**(25): 14252-14257.

Tokimatsu, H., Strycharz, W.A., and Dahlberg, A.E. 1981. Gel electrophoretic studies on ribosomal proteins L7/L12 and the Escherichia coli 50 S subunit. *J Mol Biol* **152**(2): 397-412.

Tomsic, J., Vitali, L.A., Daviter, T., Savelsbergh, A., Spurio, R., Striebeck, P., Wintermeyer, W., Rodnina, M.V., and Gualerzi, C.O. 2000. Late events of translation initiation in bacteria: a kinetic analysis. *Embo J* **19**(9): 2127-2136.

Traub, P. and Nomura, M. 1968. Structure and function of E. coli ribosomes. V. Reconstitution of functionally active 30S ribosomal particles from RNA and proteins. *Proc Natl Acad Sci U S A* **59**(3): 777-784.

Uchiumi, T., Honma, S., Nomura, T., Dabbs, E.R., and Hachimori, A. 2002. Translation elongation by a hybrid ribosome in which proteins at the GTPase center of the Escherichia coli ribosome are replaced with rat counterparts. *J Biol Chem* **277**(6): 3857-3862.

Uchiumi, T., Hori, K., Nomura, T., and Hachimori, A. 1999. Replacement of L7/L12.L10 protein complex in Escherichia coli ribosomes with the eukaryotic counterpart changes the specificity of elongation factor binding. *J Biol Chem* **274**(39): 27578-27582.

Urlaub, H., Kruft, V., Bischof, O., Muller, E.C., and Wittmann-Liebold, B. 1995. Protein-rRNA binding features and their structural and functional implications in ribosomes as determined by cross-linking studies. *Embo J* **14**(18): 4578-4588.

Valle, M., Gillet, R., Kaur, S., Henne, A., Ramakrishnan, V., and Frank, J. 2003a. Visualizing tmRNA entry into a stalled ribosome. *Science* **300**(5616): 127-130.

Valle, M., Sengupta, J., Swami, N.K., Grassucci, R.A., Burkhardt, N., Nierhaus, K.H., Agrawal, R.K., and Frank, J. 2002. Cryo-EM reveals an active role for aminoacyl-tRNA in the accommodation process. *Embo J* **21**(13): 3557-3567.

Valle, M., Zavialov, A., Li, W., Stagg, S.M., Sengupta, J., Nielsen, R.C., Nissen, P., Harvey, S.C., Ehrenberg, M., and Frank, J. 2003b. Incorporation of aminoacyl-tRNA into the ribosome as seen by cryo-electron microscopy. *Nat Struct Biol* **10**(11): 899-906.

Vetter, I.R. and Wittinghofer, A. 1999. Nucleoside triphosphate-binding proteins: different scaffolds to achieve phosphoryl transfer. *Q Rev Biophys* **32**(1): 1-56.

Vetter, I.R. and Wittinghofer, A. 2001. The guanine nucleotide-binding switch in three dimensions. *Science* **294**(5545): 1299-1304.

Vila-Sanjurjo, A., Ridgeway, W.K., Seymaner, V., Zhang, W., Santoso, S., Yu, K., and Cate, J.H. 2003. X-ray crystal structures of the WT and a hyper-accurate ribosome from Escherichia coli. *Proc Natl Acad Sci U S A* **100**(15): 8682-8687.

Wahl, M.C., Bourenkov, G.P., Bartunik, H.D., and Huber, R. 2000a. Flexibility, conformational diversity and two dimerization modes in complexes of ribosomal protein L12. *Embo J* **19**(2): 174-186.

Wahl, M.C., Huber, R., Marinkovic, S., Weyher-Stingl, E., and Ehlert, S. 2000b. Structural investigations of the highly flexible recombinant ribosomal protein L12 from Thermotoga maritima. *Biol Chem* **381**(3): 221-229.

Wahl, M.C. and Moller, W. 2002. Structure and function of the acidic ribosomal stalk proteins. *Curr Protein Pept Sci* **3**(1): 93-106.

Walleczek, J., Schuler, D., Stoffler-Meilicke, M., Brimacombe, R., and Stoffler, G. 1988. A model for the spatial arrangement of the proteins in the large subunit of the Escherichia coli ribosome. *Embo J* **7**(11): 3571-3576.

Watson, J.D. 1964. The Synthesis of Proteins Upon Ribosomes. *Bull Soc Chim Biol (Paris)* **46**: 1399-1425.

Weiel, J. and Hershey, J.W. 1982. The binding of fluorescein-labeled protein synthesis initiation factor 2 to Escherichia coli 30 S ribosomal subunits determined by fluorescence polarization. *J Biol Chem* **257**(3): 1215-1220.

Wieden, H.J., Wintermeyer, W., and Rodnina, M.V. 2001. A common structural motif in elongation factor Ts and ribosomal protein L7/12 may be involved in the interaction with elongation factor Tu. *J Mol Evol* **52**(2): 129-136.

Wiggers, R.J., Hadian, H., Traut, R.R., Oleinikov, A.V., and Glitz, D.G. 1997. Localization of two domains of a mutant form of Escherichia coli protein L7/L12 that binds the large ribosomal subunit as a single dimer. *Biochimie* **79**(6): 365-372.

Wilson, D.N., Harms, J.M., Nierhaus, K.H., Schlunzen, F., and Fucini, P. 2005. Species-specific antibiotic-ribosome interactions: implications for drug development. *Biol Chem* **386**(12): 1239-1252.

Wilson, D.N. and Nierhaus, K.H. 2005. Ribosomal proteins in the spotlight. *Crit Rev Biochem Mol Biol* **40**(5): 243-267.

Wilson, K.S. and Noller, H.F. 1998. Mapping the position of translational elongation factor EF-G in the ribosome by directed hydroxyl radical probing. *Cell* **92**(1): 131-139.

Wimberly, B.T., Brodersen, D.E., Clemons, W.M., Jr., Morgan-Warren, R.J., Carter, A.P., Vonrhein, C., Hartsch, T., and Ramakrishnan, V. 2000. Structure of the 30S ribosomal subunit. *Nature* **407**(6802): 327-339.

Wimberly, B.T., Guymon, R., McCutcheon, J.P., White, S.W., and Ramakrishnan, V. 1999. A detailed view of a ribosomal active site: the structure of the L11-RNA complex. *Cell* **97**(4): 491-502.

Wittmann, H.G., Mussig, J., Piefke, J., Gewitz, H.S., Rheinberger, H.J., and Yonath, A. 1982. Crystallization of Escherichia coli ribosomes. *FEBS Lett* **146**(1): 217-220.

Wood, P.N. 1991. The use of bonding between tRNAs to implement early peptide synthesis. *J Mol Evol* **33**(5): 464-469.

Wool, I.G. and Stöffler, G. 1974. *Ribosomes* Cold Spring Harbor Laboratory Press. Cold Spring Harbor, NY.

Wriggers, W., Agrawal, R.K., Drew, D.L., McCammon, A., and Frank, J. 2000. Domain motions of EF-G bound to the 70S ribosome: insights from a hand-shaking between multi-resolution structures. *Biophys J* **79**(3): 1670-1678.

Yonath, A.E., Muessig, J., and Tesche, B. 1980. Crystallization of the large ribosomal subunits from Bacillus stearothermophilus. *BIOCHEM INT* **1**(5): 428-435.

Yusupov, M.M., Yusupova, G.Z., Baucom, A., Lieberman, K., Earnest, T.N., Cate, J.H., and Noller, H.F. 2001. Crystal structure of the ribosome at 5.5 A resolution. *Science* **292**(5518): 883-896.

Yusupova, G.Z., Yusupov, M.M., Cate, J.H., and Noller, H.F. 2001. The path of messenger RNA through the ribosome. *Cell* **106**(2): 233-241.

Zavialov, A.V., Buckingham, R.H., and Ehrenberg, M. 2001. A posttermination ribosomal complex is the guanine nucleotide exchange factor for peptide release factor RF3. *Cell* **107**(1): 115-124.

Zavialov, A.V., Hauryliuk, V.V., and Ehrenberg, M. 2005. Guanine-nucleotide exchange on ribosome-bound elongation factor G initiates the translocation of tRNAs. *J Biol* **4**(2): 9.

# **Appendices**
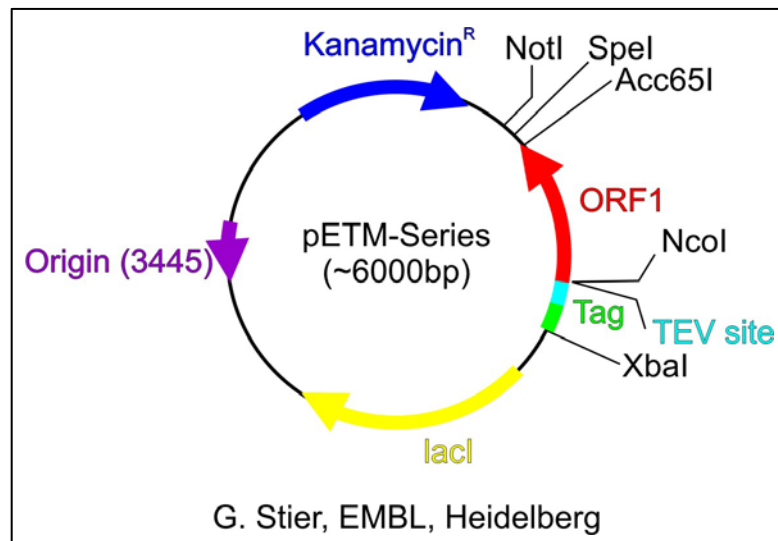


**Suppl. Figure 1.** The map of the pETM-Series vector.

| A | Ala | Alanine |
|---|-----|---------|
| R | Arg | Arginine |
| N | Asn | Asparagine |
| D | Asp | Aspartic acid |
| C | Cys | Cysteine |
| Q | Gln | Glutamine |
| E | Glu | Glutamic acid |
| G | Gly | Glycine |
| H | His | Histidine |
| I | Ile | Isoleucine |
| L | Leu | Leucine |
| K | Lys | Lysine |
| M | Met | Methionine |
| F | Phe | Phenylalanine |
| P | Pro | Proline |
| S | Ser | Serine |
| T | Thr | Threonine |
| W | Trp | Tryptophan |
| Y | Tyr | Tyrosine |
| V | Val | Valine |

**Suppl. Figure 2.** Amino acids: denominations and abbreviations (1 and 3 letters).
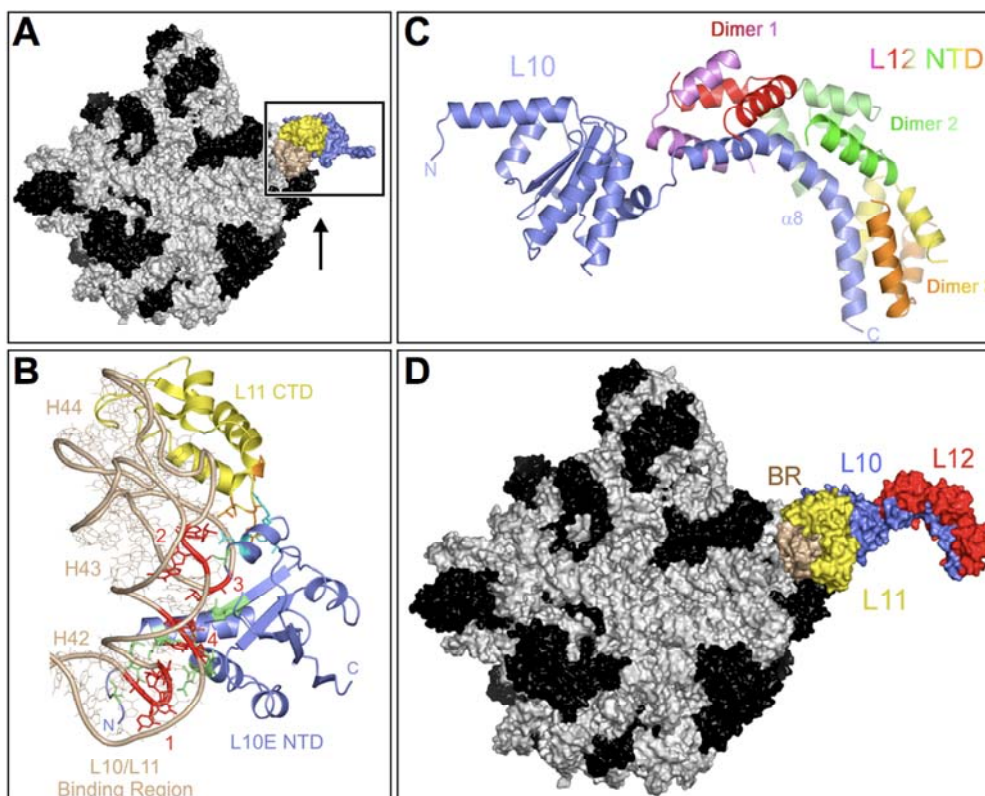
**Suppl. Figure 3. (A)** Surface view representation of a 50S ribosomal subunit from *H. marismortui* (PDB accession code 1S72 (Klein *et al.* 2004)) which was used for the tracing of the L10E NTD. The boxed region represents the L7/L12 stalk, lacking most of its peripheral elements. **(B)** The structure of the archaeal L10E NTD on the 50S subunit. A detailed view of the L10E NTD bound in the neighborhood of L11 to the L10/L11 binding region of the 23S rRNA is depicted. The L10E NTD (blue) contacts four non-consecutive regions of the rRNA (red). Regions of L10E NTD interacting with the rRNA are in green. A small number of contacts are observed with L11 (cyan and orange residues, respectively). **(C)** Structure of the *tma*L10:(L12 NTD)$_6$ complex. The C-terminal α-helix of L10 accommodates three L12 NTD dimers. **(D)** Reconstruction of a truncated L7/L12 stalk lacking both hinges and CTDs of L12, by lining up the isolated structure of *tma*L10:(L12 NTD)$_6$ according to the position of L10E NTD on the ribosome.
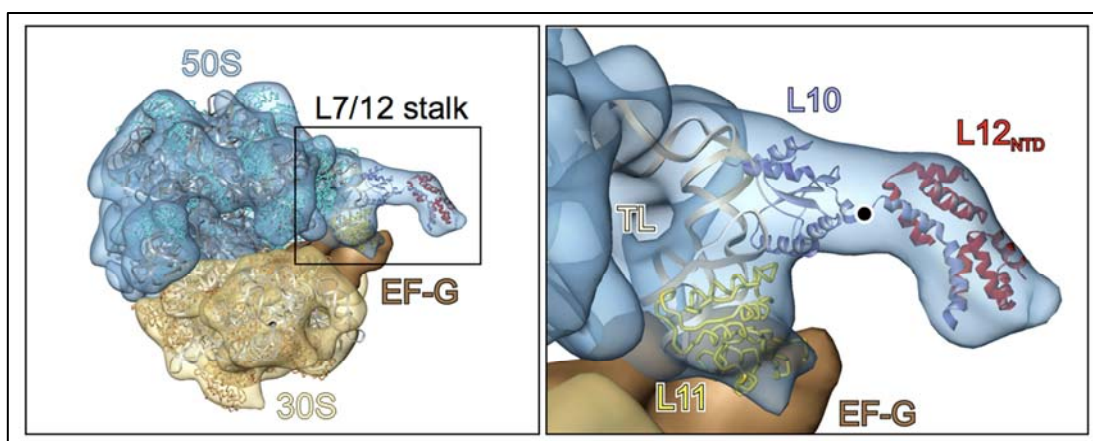


**Suppl. Figure 4.** (Left) 70S:EF-G:GDP:fusidic acid complex from *E. coli*, encompassing a truncated L7/L12 stalk that lacked the peripheral elements of L12, namely hinges and CTDs. (Right) The fit of the L10/L11 binding region, L11, and a shortened L10:(L12 NTD)$_4$ crystal structure in the electron density of the 70S:EF-G:GDP:fusidic acid complex.

# **Abbreviations**

| | |
|---|---|
| °C | degree Celsius |
| 3D | 3Dimentional |
| Å | Angstrom (1Å = $10^{-10}$ m) |
| aa | amino acid |
| *aae* | *Aquifex aeolicus* |
| ALC | Arc-Like Connection |
| BLAST | Basic Local Alignment Search Tool |
| bp | base pair |
| CC | Correlation Coefficient |
| CCD | Charged Coupled Device |
| CD | Circular Dichroism |
| CM | Carboxy Methyl |
| Cryo-EM | Cryo-Electron Microscopy |
| CTD | C-Terminal Domain |
| ddH2O | double distilled water |
| DEAE | Di-Ethyl Amino Ethyl |
| DESY | Deutsches Elektronen SYnchrotron |
| DMSO | DiMethylSulfOxide |
| DNA | DeoxyriboNucleic Acid |
| DTT | DiThioThreitol |
| *eco* | *Escherichia coli* |
| EDTA | Ethylene-Diamine-Tetraacidic Acid |
| EF | Elongation Factor |
| EF-G | Elongation Factor G |
| EF-Ts | Elongation Factor Ts |
| EF-Tu | Elongation Factor Tu |
| eIF | eukaryotic Initiation Factor |
| EMBL | European Molecular Biology Laboratory |
| F | structure Factor |
| fMet | formyl Methionine |
| FOM | Figure Of Merit |
| GAC | GTPase Associated Center |
| GAP | GTPase Activating Protein |
| GAR | GTPase Associated Region |
| GDP | Guanosine DiPhosphate |
| GEF | Guanosine Nucleotide Exchange Factor |
| GMPPNP | guanosine-5'-[β,γ-imido] triphosphate |
| GNBP | Guanosine Nucleotide Binding Protein |
| GST | Glutathione S-Transferase |
| GTP | Guanosine TriPhosphate |
| h | hour |

| | |
|---|---|
| HEPES | N-2-HydroxyEthylPiperazine-N'-2-EthaneSulfonic acid |
| *hma* | *Haloarcula marismortui* |
| I | Intensity |
| IF | Initiation Factor |
| IPTG | IsoPropyl-β-D-ThioGalactopyranoside |
| ITC | Isothermal Titration Calorimetry |
| K | Kelvin |
| kb | kilobase |
| kD | kilo Dalton |
| l | liter |
| LB | Luria Bertani medium |
| LiCl | Lithium Chloride |
| M | Molarity |
| MAD | Multi-wavelength Anomalous Dispersion |
| MALLS | Multi-Angle Laser Light Scattering |
| mAU | milli-Absorption Unit |
| MES | 2-(N-Morpholino)-EthaneSulfonic acid |
| min | minute |
| MIR | Multiple Isomorphous Replacement |
| MPD | 2-methyl 2,4-pentanediol |
| MR | Molecular Replacement |
| mRNA | messenger RNA |
| NaCl | Natrium Chloride |
| Ni-NTA | Nickel-NitriloTriAcetate |
| nm | nanometer |
| NMR | Nuclear Magnetic Resonance |
| NTD | N-Terminal Domain |
| OD | Optical Density |
| P | Phosphate |
| PBS | Phosphate-Buffered Saline |
| PCR | Polymerase Chain Reaction |
| PDB | Protein Data Bank |
| PEG | PolyEthylene Glycol |
| PMSF | phenylmethylsulfonyl fluoride |
| PTC | Peptidyl Transferase Center |
| r.m.s.d. | residual mean-square deviation |
| RF | Release Factor |
| RGS | Regulator of G protein Signaling |
| RMS | Root Mean Square |
| RNA | RiboNucleic Acid |
| rpm | revolutions per minute |
| r-protein | ribosomal protein |
| RRF | Ribosome Recycling Factor |
| RRM | RNA Recognition Motif |
| rRNA | ribosomal RNA |

| | |
|---|---|
| RT | Room Temperature |
| RU | Resonance Unit |
| s | second |
| S | Svedberg |
| SAD | Single-wavelength Anomalous Diffraction |
| SDS-PAGE | Sodium Dodecyl Sulfate-PolyacrylAmide Gel Electrophoresis |
| SeMet | SelenoMethionine |
| SIR | Single Isomorphous Replacement |
| SIRAS | Single Isomorphous Replacement Anomalous Scattering |
| SLS | Swiss Light Source |
| SPR | Surface Plasmon Resonance |
| SRL | Sarcin-Ricin Loop |
| T°C | Temperature in degree Celsius |
| Taq | *Thermus aquaticus* |
| TEV | Tobacco Etch Virus protease |
| TL | Thiostrepton Loop |
| *tma* | *Thermotoga maritima* |
| Tris | Tris-(hydroxymethyl)aminomethane |
| tRNA | transfer RNA |
| *tth* | *Thermus thermophilus* |
| U | Unit |
| UV | UltraViolet |
| V | Volume |
| x g | times gravity |

# **Acknowledgements**

# **Curriculum Vitae**

**Mihaela Ştefania Diaconu**, born on August 20th 1977 in Bucharest, Romania

**Education and professional experience**

1992-1996   "Grigore Moisil" High School, Bucharest, Romania, Baccalaureate
1996-2000   B. Sc. in Biochemistry, University of Bucharest, Romania
                    *Project*: Analysis of the biochemical properties of glucose transporters
                    *Advisor*: Prof. Dr. Dana Iordachescu
2000-2001   Research assistant, Institute of Cellular Biology and Pathology, Bucharest,
                    Romania
                    *Project*: Endothelial nitric oxide synthase gene polymorphism is common
                          to both Fabry disease and atherosclerosis
                    *Advisors*: Dr. Constantina Heltianu, Dr. Maya Simionescu
2000-2002   M. Sc. in Biochemistry and Molecular Biology, Institute of Human  Genetics,
                    Göttingen, Germany/Faculty of Biology, University of Bucharest, Romania
                    *Project*: The PHGPx gene in oligoasthenozoospermia and its expression in
                          murine tissue
                    *Advisors*: Prof. Dr. med. Wolfgang Engel, Dr. Karim Nayernia/Prof. Dr.
                          Dana  Iordachescu, Dr. Otilia Zarnescu
2003-2006   Ph. D. studies, Cellular Biochemistry/X-Ray Crystallography Department,
                    Max-Planck Institute for Biophysical Chemistry, Göttingen, Germany
                    *Project*: Structural and functional characterization of the L7/L12 ribosomal
                          stalk
                    *Advisor*: Priv.-Doz. Dr. Markus C. Wahl

  **Publications**

- Nayernia K, Diaconu M, Aumuller G, Wennemuth G, Schwandt I, Kleene K, Kühn H, Engel W. *Phospholipid hydroperoxide glutathione peroxidase: expression pattern during testicular development in mouse and evolutionary conservation in spermatozoa*. **Mol Reprod Dev** 2004; 67(4): 458-464
- Heltianu C, Costache G, Gafencu A, Diaconu M, Bodeanu M, Cristea C, Azibi K, Poenaru L, Simionescu M. *Relationship of eNOS gene variants to diseases that have in common an endothelial cell dysfunction*. **J Cell Mol Med** 2005; 9(1): 135-142
- Diaconu M, Kothe U, Schlünzen F, Fischer N, Harms JM, Tonevitsky AG, Stark H, Rodnina MV, Wahl MC. *Structural basis for the function of the ribosomal L7/L12 stalk in factor binding and GTPase activation*. **Cell** 2005; 121(7): 991-1004
- Diaconu M, Wahl MC. *Filling a gap in the ribosomal GAP*. **MPIbpc News,** 10/2005:1-7
- Diaconu M, Tangat Y, Kühn H, Michelmann HW, Schreiber G, Haidl G, Glander H, Müller C, Engel W, Nayernia K. *Failure of phospholipid hydroperoxide glutathione peroxidase expression in oligoasthenozoospermia and mutations in the PHGPx gene*  (in press)